The cover illustration is the natural vegetation of the Earth, simulated by the BIOME4 global vegetation model.

Geophysical Applications of Vegetation Modeling

Dissertation
Jed O. Kaplan

2001

LUND UNIVERSITY

Jed O. Kaplan
Max Planck Institute for Biogeochemistry
Postfach 10 01 64
D-07701 Jena
Germany
jed.kaplan@bgc-jena.mpg.de

isbn 91-7874-089-4 Lund University Lund Sweden

Lund University Cataloging Data, Dokumentdatablad, enl. SIS 61 41 21

Organization:	Lund University, Dept. of Ecology, Plant Ecology
Address:	Ecology Building, S-223 62 Lund, Sweden
Document name:	Doctoral dissertation
Date of Issue:	February 2001
CODEN:	SE-LUNBDS/NBBE-01/1062+128pp
Author:	Kaplan, Jed Oliver, 1972-
Title:	Geophysical Applications of Vegetation Modeling
Key words:	Vegetation model, biogeochemistry, biogeography, biome, LGM, ice age, tundra, mammoths, Holocene, methane, ice core, wetland, carbon cycle, stable isotopes, CO_2, CH_4
Language:	English with Swedish summary
ISBN:	9178740894
Number of pages:	128
Distribution by:	See above

printed in Germany

Preface

A doctoral thesis at a university in Sweden is produced either as a monograph or as a collection of papers. In the latter case, the introductory part constitutes the formal thesis, which summarizes the accompanying papers. These have already been published or are manuscripts at various stages (in press, submitted, or manuscript).

This thesis describes the development and selected applications of a global vegetation model. The model is applied to problems in vegetation distribution and climate, isotope biogeochemistry, and trace gas production. It demonstrates how a modeling approach, based on principles of plant physiology and ecology, can be applied to interdisciplinary problems that cannot be adequately addressed by direct observations or experiments.

The work is relevant to understanding the potential effects of climate change on the biosphere. Today's focus on anthropogenic climate change makes it all the more important to understand the role of the biosphere in the natural operation of the climate system. This thesis therefore deals not only with modeling the contemporary state of the biosphere, but also with modeling aspects of the recent geological past, and (in Paper I) an attempt to look a century ahead, to assess the changes that could be in store if atmospheric greenhouse gases continue to build up at there present rate.

Paper I describes the Pan-Arctic INitiative, a groundbreaking attempt to develop, validate and apply a large-scale vegetation model to the problem of understanding high-latitude vegetation and how it reacts to changes in the physical climate system.

Paper II describes the development and application of a global model for the simulation of natural wetland areas and their methane emissions. The model is applied in the context of the climate of the Last Glacial Maximum, to investigate the possible importance of variation in the terrestrial source of atmospheric methane in determining the large natural variations in atmospheric methane that are recorded in polar ice cores.

Paper III deals with the problem of Carbon-13 in the biosphere. Atmospheric ^{13}C has been used by geophysicists to partition the uptake of anthropogenic CO_2 in the atmosphere between terrestrial and oceanic components. However, in order to make a reliable partitioning, the ^{13}C signatures of CO_2 sources and sinks in the terrestrial biosphere must be characterized. This requires the application of a global vegetation model with the ability to represent the physiological and ecological processes that determine the fractionation of carbon isotopes during photosynthesis.

The ideas for paper I were conceived jointly by the PAIN project members, a group of vegetation ecologists, paleoecologists, and modelers who assembled for

the first time in May 1998. I implemented the BIOME4 model for Arctic vegetation, assembled the driver datasets, and generated all of the biome model output. The members of the PAIN organizing committee (Sandy Harrison, Wolfgang Cramer, Linda Brubaker, Mary Edwards, Colin Prentice, Nancy Bigelow, and myself) oversaw the process. I wrote the text of the paper as it stands now, with input from Sandy Harrison and Colin Prentice. The text may yet be modified based on input from the whole group of PAIN participants.

I conceived the ideas for paper II at the PAGES Open Science Conference in 1998. I implemented all of the modeling, assembled the driver datasets and analyzed the output. The manuscript is wholly written by me, though not without a great deal of useful commentary from Colin Prentice, Sander Houweling, and Sandy Harrison.

Paper III was conceived by me and Colin Prentice over the course of several years. Nina Buchmann provided ideas and data during later stages of the project. I implemented all of the modeling, assembled the driver dataset and the databases of Δ_{leaf} and troposphere $\delta^{13}C$ measurements, and wrote the manuscript. Nina Buchman provided the Δ_e dataset and commented on the text. Colin Prentice assisted with the data analysis and commented on the manuscript. Martin Heimann provided the HAMOCC3 ocean flux data, helped me solve the non-trivial task of actually using it, and assisted in analyzing the results.

When I arrived in Europe in September 1994 as a teacher at a nature school in the Bernese Alps, many of the ideas developed here regarding plant geography, biogeochemistry, and paleoclimatology were already in my head. For that introduction I must thank my Dartmouth College professors: especially Laura Conkey who introduced me to most of the subjects that have been the focus of my scientific career, and Xiahong Feng, Page Chamberlain, and Joel Blum who got me interested in stable isotopes.

Colin Prentice took me on as his student in Lund shortly afterwards, and gave me the freedom to discover for myself, through reading, travels, courses, and contact with many other colleagues that there was a scientific agenda I could develop from my interests. The contacts that I made under Colin's promotion led to valuable collaborations with Nina Buchmann, Nancy Bigelow, Martin Heimann, Sandy Harrison, Mary Edwards, and Linda Brubaker, all of whom have contributed helpfully to this dissertation. For these opportunities, and for all of Colin's helpful and patient advice over the years, I am very grateful.

I must also thank many other scientists I have met over the last five years, and in some cases had the chance to work with, for good scientific discussion, ideas, and support: especially Pat Bartlein, Arnoud Boom, Harald Bugmann, Wolfgang Cramer, Torben Christensen, Basil Davis, Jim Ehleringer, Louis François, Joël Guiot, Willow Hallgren, Alex Haxeltine, Erik Hobbie, Steve Jackson, Dominique Jolly, Dave Kicklighter, Rob Marchant, Dave McGuire, Bengt Nihlgård, Lennart Olsson, Andy Pitman, Steve Running, Andy Ridgwell, Jonathan Seaquist, Sarah Shafer, Stephen Sitch, Ben Smith, Martin Sykes, Henrik Søgaard, Pavel Tarasov, Bob Thompson, Paul Valdes, and Jack Williams.

I am very grateful to Anna Joabsson for translating the thesis summary into Swedish.

One cannot become a plant ecologist without going in the field: I thank Torben Christensen, Bo Wallén, and Honor Prentice for providing me with the opportunity to work in some incredible places, on interesting projects, and with great colleagues.

The wide spectrum of friends I have made as a doctoral student had enriched my life in more ways than I could have imagined; I thank Stephen Sitch, Eric Stein, Ursula Malm, Wolfgang Knorr, Anna Joabsson, Karin Nadrowski, Basil Davis, Harri Moora, Chris Day, Alex Haxeltine, Jonathan Seaquist, Ann-Mari Fransson, Gunnar Thelin, André Klose, Pete Harvey, Troy Baisden, Annette Davies, Bernd Kaufmann, Liz Pickett, Ulli Seibt, and Johanna Lindberg for the great companionship and adventures around the world. I especially thank Ed Watson who kept me going early on, and despite the distance, has always been a great friend.

Finally, I dedicate this dissertation to my loving, supportive, dynamic, and ever-interesting family: Anita and Steve Kaplan, Zoë Kaplan and Helga Vanthournout for being there for me always and being who they are.

Jena, January 2001 Jed O. Kaplan

Abstract

This thesis describes the development and selected applications of a global vegetation model, BIOME4. The model is applied to problems in high-latitude vegetation distribution and climate, trace gas production, and isotope biogeochemistry. It demonstrates how a modeling approach, based on principles of plant physiology and ecology, can be applied to interdisciplinary problems that cannot be adequately addressed by direct observations or experiments. The work is relevant to understanding the potential effects of climate change on the terrestrial biosphere and the feedbacks between the biosphere and climate.

BIOME4 simulates the distribution of 15 high-latitude biomes, including five tundra vegetation types, for the present day using observed climate, and the LGM, mid-Holocene, and a "greenhouse" scenario for 2100 using the output of GCMs. In the LGM simulations, the high-latitudes show a marked increase in the area of graminoid and forb tundra, which is also the predominant feature in the paleodata. This vegetation has no widespread modern analog; it was favored by the cold, dry climate, and supported large mammoth populations. Mid-Holocene simulations indicate a modest, asymmetrical northward advance of the Arctic treeline compared to present, with greatest extension in central Siberia (up to 300 km), and little to no change in the Western Hemisphere. This result is in good agreement with pollen and megafossil data from the same period. Differential warming of the continents in response to increased high-latitude solar radiation is hypothesized to account for the asymmetry. Vegetation changes in the 2100 projection, which assumes a continued exponential increase in atmospheric GHG concentrations, are more radical than those simulated for the mid-Holocene. The year-round forcing due to GHGs increases both summertime and annual temperatures in the high latitudes by up to double the mid-Holocene anomaly. However the potential treeline advances and biome shifts in our simulation are unlikely to be realized within 100 years, because of the time required for migration and establishment of new vegetation types.

Potential natural wetland area for the present day was simulated by BIOME4 as $11.0 \times 10^6 km^2$. This value is higher than other estimates but includes small ($<50 km^2$) and seasonal wetlands which have not been included in previous surveys. The wetland CH_4 source was simulated as $140 Tg yr^{-1}$. At the LGM, simulated wetland area was increased by 15% but CH_4 emissions were 24% less than the present-day. The simulated reduction in the CH_4 source is due to substrate limitation induced by low atmospheric CO_2 concentrations at the LGM. The 100% increase in atmospheric CH_4 concentrations measured in ice cores between the

LGM and the preindustrial Holocene may not be due to changes in CH_4 source strength alone, as other trace gases influence the atmospheric CH_4 sink.

The stable carbon isotope composition of the terrestrial biosphere was simulated by BIOME4 and compared to measurements at the leaf, ecosystem and troposphere scales. Model simulations are correlated within one standard deviation to measured means at the PFT and biome scales, and at six Northern Hemisphere CO_2 monitoring stations. Global carbon isotope discrimination in the terrestrial biosphere averaged 18.6‰ for potential natural vegetation and 18.1‰ when an agricultural land-use mask was applied. These simulated values are slightly higher than previous estimates, but consistent with measurements. This information is important for the interpretation of contemporary atmospheric observations in terms of carbon sources and sinks on land and in the ocean.

Populärvetenskaplig sammanfattning på svenska

Avhandlingen beskriver utvecklingen och utvalda tillämpningar av en global vegetationsmodell, BIOME4. Modellen kan appliceras på frågeställningar kring vegetationsfördelning och klimat på höga latituder, produktion av spårgaser, och isotopers biogeokemi. Den demonstrerar hur en teoretisk modell, baserad på växtfysiologins och ekologins principer, kan tillämpas på interdisciplinära problem vilka inte kan angripas på ett adekvat sätt genom direkta observationer eller experiment. Arbetet är relevant för förståelsen av återkopplingsmekanismer mellan biosfären och klimatet samt för hur den terrestra biosfären potentiellt kan reagera på förändringar i klimatet.

BIOME4 simulerar fördelningen av 15 biom på höga latituder, inklusive fem olika typer av tundravegetation. För nutiden används observerat klimat i simuleringarna och för den senaste istiden (LGM, Last Glacial Maximum, ca. 21000 år före idag), mitten av Holocene (ca. 6000 år före idag) och ett "växthusscenario" för år 2100 används resultat från generella cirkulationsmodeller av klimatet (GCM, General Circulation Model). Simuleringarna av LGM visar en markant ökning av områden med graminoid och örtdominerad tundravegetation, vilket även är den dominerande tendensen i paleodata. Denna vegetationstyp har ingen utbredd modern motsvarighet; den gynnades av det kalla, torra klimatet och kunde underhålla stora populationer av mammutar. Simuleringar av en period i mitten av Holocene indikerar att den Arktiska trädgränsen försköts asymmetrisk något mot norr jämfört med dagens förhållanden, med störst utvidgning i de centrala delarna av Sibirien (upp till 300 km), och liten till ingen förändring på den Västra Hemisfären. Detta resultat stämmer väl överens med pollen- och megafossildata från samma tidsperiod. Skillnader i uppvärmning av kontinenterna, som ett resultat av ökad solinstrålning på höga latituder, antas vara orsaken till denna asymmetri. Vegetationsförändringarna i 2100-projektionen, vilken antar att koncentrationen av växthusgaser i atmosfären fortsätter att öka exponentiellt, är mer radikala än de simulerade förändringarna under Holocene. Den årliga globala uppvärmningspotentialen orsakad av GHGs leder till en ökning av både sommartemperaturerna och de årliga temperaturerna på höga latituder med upp till den dubbla avvikelsen för Holocene. Den potentiella förskjutningen av trädgränsen och biomförändringarna i vår simulering blir dock troligtvis inte realiserade inom 100 år, på grund av den tid som behövs för migration och etablering av nya vegetationstyper.

Den nutida potentiella arealen av naturliga våtmarker simulerades av BIOME4 till $11.0 \times 10^6 \text{km}^2$. Detta värde är högre än andra uppskattningar, men det inkluderar även små ($< 50 \text{km}^2$) och säsongsberoende våtmarker som inte har inkluderats

i tidigare undersökningar. Våtmarkerna simulerades till att vara en källa till methan (CH_4) motsvarande 140 $Tgyr^{-1}$. Under LGM ökade den simulerade våtmarksarealen med 15%, men CH_4-emissionen var 24% lägre än idag. Denna simulerade reduktion av CH_4-källan beror på substratbegränsning orsakad av låg atmosfärskoncentration av CO_2 under LGM. Den i iskärnor uppmätta 100-procentiga ökningen av koncentrationen av CH_4 i atmosfären mellan LGM och det förindustriella Holocene är inte nödvändigtvis enbart ett resultat av förändringar i CH_4-källans styrka, eftersom andra spårgaser påverkar den atmosfäriska CH_4-sänkan.

Sammansättningen av stabila isotoper av kol i den terrestra biosfären simulerades av BIOME4 och jämfördes med mätningar på blad- ekosystem- och troposfärsnivå. Modellens simuleringar korrelerar inom en standardavvikelse mot uppmätta medelvärden på en skala av vegetationens funktionella grupper (PFT, Plant Functional Type) och på biomnivå, samt även för sex stycken stationer på Norra Hemisfären där koldioxid (CO_2) moniterats. Global diskriminering av kolisotoper i den terrestra biosfären var i medeltal 18.6‰ för potentiellt naturlig vegetation och 18.1‰ då hänsyn togs till agrikulturell markanvändning. Dessa simulerade värden är något högre än tidigare uppskattningar, men de är förenliga med uppmätta värden. Denna information är viktig för tolkningen av nutida atmosfäriska observationer av kolkällor och kolsänkor på land och i oceanerna.

Contents

1 Geophysical applications of vegetation modeling
The global vegetation model as a tool for plant ecologists

1.1 Introduction

This thesis centers around a new model of the Earth's vegetation. BIOME4 was developed – as an extension of the BIOME3 global vegetation model [*Haxeltine and Prentice*, 1996] – to address several problems on the interface between plant ecology /biogeography and the geophysical aspects of climate change. BIOME4 is also more generally applicable to problems in vegetation science, paleoecology, biosphere-atmosphere interaction, and biogeochemistry. BIOME4 uses long-term climatic data and basic information on soil properties to simulate vegetation distribution, productivity, isotopic composition, and other biogeochemical variables.

Here, BIOME4 is used first to simulate the distribution of vegetation in high northern latitudes. Results are tested against a modern botanical vegetation classification and paleoecological information from pollen assemblages (paper I). BIOME4 is also applied to simulate the global distribution of wetlands and their methane emissions; the modeling approach allowed mechanistic simulation of the primary global methane source at the Last Glacial Maximum, when both climate and atmospheric methane concentrations were drastically different from today (paper II). Finally BIOME4 is made to simulate the stable isotopic signature of carbon in the terrestrial biosphere, an exercise critical for the reliable observational partitioning of CO_2 sources and sinks between the oceans and land (paper III).

As a sub-discipline of plant ecology, vegetation modeling is central to understanding the role that plants have played in shaping the Earth's atmospheric composition and climate in the past and the potential responses and feedbacks of vegetation to future climates. Vegetation models can be used to assess the relative importance of climate, soil, nutrients and other edaphic features, and plant functional traits on plant distribution, productivity, and resilience to changing conditions and the relationship between plants and other aspects of the climate system and global biogeochemical cycles. Vegetation models synthesize relationships made in field and laboratory studies into a globally applicable framework. A global vegetation model is a valuable tool for the investigation of phenomena that would otherwise be impossible to study because of spatial or temporal constraints. Vegetation models may also help the interdisciplinary scientist explore the interaction between humans and their environment, both past and present.

1.2 History

Through its origins in plant geography, plant ecology, and plant physiology, vegetation modeling has evolved into an interdisciplinary field with a wide spectrum of applications. Scientific study of global patterns in plant geography began with the expeditions of Alexander von Humboldt and Charles Darwin in the 19th century, who recognized the influence of climate on the form and composition of plant communities [*Darwin*, 1845; *von Humboldt*, 1850]. Half a century later, Schimper [1903] made a systematic study of the Earth's vegetation and concluded that climate, through plant physiology, controls the distribution of plant species and overall ecosystem function. These observations led directly to the development of classification schemes, based on functional rather than taxonomic grouping of plants, that linked plant distribution to climate [*Holdridge*, 1947; *Köppen*, 1936; *Küchler*, 1949]. Most recently, computer models with a basis in the physiological mechanisms controlling global plant distribution have appeared [*Box*, 1981; *Prentice et al.*, 1992; *Woodward and Williams*, 1987]. Simultaneously, plant physiologists developed conceptual models of plant growth based on processes at the leaf level [*Collatz et al.*, 1992; *Farquhar et al.*, 1980; *Larcher*, 1995]. The new field of biogeochemistry developed out of studies on the complete cycles of elements through terrestrial ecosystems both in the field and with models [*Gorham*, 1991; *Likens et al.*, 1977].

Syntheses of global vegetation distribution from an ecophysiological perspective provided the foundation for global vegetation modeling [*Walter*, 1973; *Walter et al.*, 1975; *Woodward*, 1987]. The concept of the Plant Functional Type (PFT) was developed, wherein plants exhibiting certain fundamental characteristics (i.e. growth form, phenology, rooting depth) can be grouped together into a framework that made vegetation modeling at the global scale possible. Improvements in technology and the compilation of a gridded global climatology [*Leemans and Cramer*, 1991] culminated in the development of computerized vegetation models. These models could simulate, at a global scale, vegetation distribution (biogeography) or the cycles of carbon and water through plants (biogeochemistry) [e.g. *Prentice et al.*, 1992; *Running and Hunt*, 1993; *VEMAP members*, 1995]. Models that coupled both biogeography and biogeochemistry components appeared shortly thereafter [*Foley et al.*, 1996; *Haxeltine and Prentice*, 1996; *Neilson*, 1995]. Global vegetation modeling has evolved a latest generation of Dynamic Global Vegetation Models, (DGVM) which incorporate the ecologically dynamic effects of fire, land-use and change, and ecosystem history with biogeography and biogeochemistry with the initial aim of more accurately simulating the fluxes of CO_2 through the terrestrial biosphere [*Sitch*, 2000]. Further development of vegetation models has proceeded at a rapid rate and models have been used in an increasingly broad array of applications, validation exercises and sensitivity tests to answer questions related to the impacts of anthropogenic climate change and the global carbon cycle [e.g. *Cramer et al.*, in press; *Schimel et al.*, 2000; *VEMAP*, 1995].

1.3 Problems addressed

The Pan Arctic INitiative (PAIN, Paper I) was a first-time effort to fuse the botanical, paleoecological, and modeling branches of vegetation science in order to develop a new paradigm for the description, identification, and simulation of northern high-latitude vegetation. The global significance of the project lies in the sensitivity of high-latitude vegetation to potential future climate changes and the strong feedbacks that are present in the vegetation-atmosphere system at high latitudes. The project has provided the most detailed description and modeling framework of northern high-latitude vegetation developed to date. The PAIN group began by developing a comprehensive description of northern high-latitude vegetation using an approach based on plant functional types (PFTs). Plant ecologists and systematists, working in the field and familiar with the present day vegetation, developed a unified classification and map of modern potential natural vegetation for the region. Pollen analysts and paleoecologists contributed to the development of the vegetation classification in light of which vegetation characteristics are identifiable in the paleo-record. Vegetation modelers assembled physiological and biogeochemical data on northern high-latitude plants and ecosystems and built a model that could simulate the vegetation types observed both in the past and present. The model was used to investigate the extent to which "observed" changes in vegetation between the Last Glacial Maximum (LGM), mid-Holocene, and present could be reproduced – and then to assess the implied sensitivity of northern high-latitude vegetation to anthropogenic changes in atmospheric greenhouse-gas concentration and climate.

Methane (CH_4), together with water and CO_2, is one of the three most important radiatively active trace gases in the Earth's atmosphere today. Understanding the natural sources and sinks for methane is critical to an understanding of the controls on atmospheric composition and climate. Wetlands are the single greatest natural source of methane to the atmosphere, accounting for more than half of the total flux (other non-anthropogenic methane sources include grazing animals, termites, wildfire, and the ocean). Atmospheric methane concentrations more closely parallel the higher-frequency component of polar ice-core temperature records of the past 100 ka than any other measured trace gas (Fig. 1.1) [*Chappellaz et al.*, 2000]. The sensitivity of methane source area and magnitude to climate and the related feedbacks between methane and climate have been controversial. Changes in the wetland methane source and the atmospheric methane sink (i.e. the concentration of OH radicals in the atmosphere), and catastrophic releases of methane from ocean sediments, have all been proposed as the primary reason for the close relationship between atmospheric methane concentrations and polar temperature records [*Brook et al.*, 2000; *Dällenbach et al.*, 2000; *Kennett et al.*, 2000; *Nisbet*, 1990]. Using BIOME4, the modeling approach first developed using BIOME3 by Christensen *et al.* [1996] was extended to simulate changing global wetland areas as well as the associated methane emissions (paper II). This extension allows the prog-

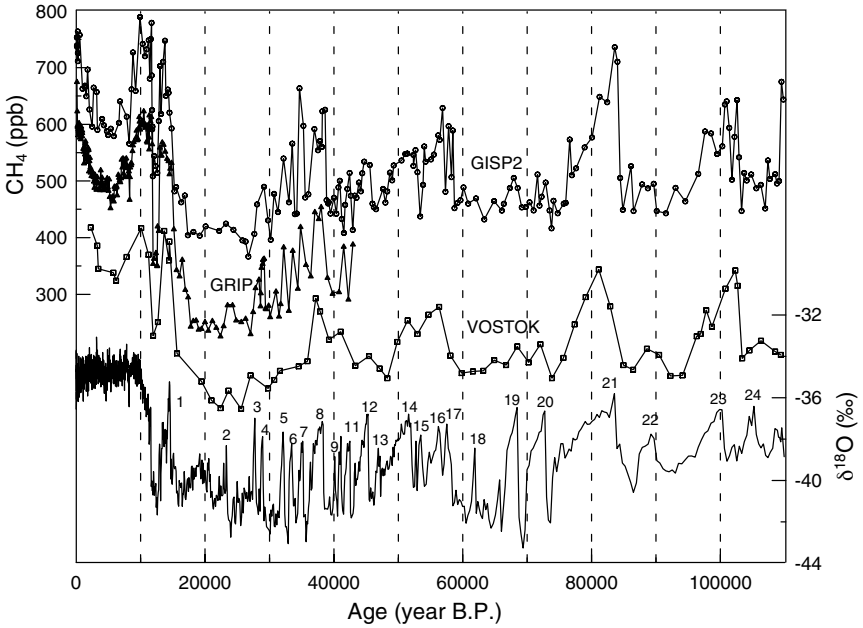

Fig. 1.1. Polar temperature and atmospheric CH_4 concentrations during the last 110 000 years from the GISP2 [*Brook et al.* 1996], GRIP [*Chappellaz et al.* 1993] and Vostok [*Chappellaz et al.* 1990] ice cores. The time scale for all three CH_4 profiles is from Brook et al. [1996] and Chappellaz et al. [2000]. The GRIP and Vostok profiles are reduced by 120 and 250 ppb, for clarity. The GISP2 ^{18}O profile, which is related to Greenland temperature, is shown for comparison [*Grootes et al.* 1993]. Numbers 1 to 24 indicate the Dansgaard-Oeschger events. Adapted with permission from Chappellaz et al. [2000].

nostic simulation of global wetland methane emissions under changed climates. Paper II presents such a simulation for natural wetland emissions in the present and for the Last Glacial Maximum, taking into account changes in atmospheric CO_2, climate, and sea-level.

To investigate the impact of anthropogenic CO_2 emissions on potential future climate change, a thorough understanding of the global carbon cycle in necessary [*Schimel et al.*, 1996]. Carbon has seasonally variable sources and sinks in both the terrestrial biosphere and ocean which can in principle be distinguished by measuring the concentration and stable isotopic composition (ratio of $^{13}C/^{12}C$) of atmospheric CO_2. However, a 10% inaccuracy in the assumed isotopic composition of the terrestrial biosphere will produce a change in the inferred terrestrial C sink equal to the entire magnitude of the sink. Furthermore, the carbon isotopic signature of the terrestrial biosphere may change from year to year as vegetation responds to short-term climatic variability. Here, BIOME4 is used to simulate the isotopic signature of the terrestrial biosphere. The model result is compared to measurements at three scales, from the leaf to the atmospheric level. This modeling

strategy is generally applicable to other investigations of the carbon cycle and will later be used in a full dynamic simulation of the terrestrial carbon cycle.

These three applications demonstrate the usefulness of a global vegetation model where other methods leave the investigator lacking information, either spatially, temporally or both. Pollen data can be used to infer vegetation history at a point, but extrapolation is difficult given the sensitivity of vegetation to climatic and edaphic factors beyond the catchment of the pollen source. The source areas for methane emissions from wetlands cannot be constrained at the present-day using available data; for times in the past the problem is even more uncertain. Point measurements of ^{13}C in different ecosystems have demonstrated the spatial and temporal heterogeneity of the isotopic signature of the terrestrial biosphere source. The global carbon isotopic signature cannot be adequately constrained by current measurement networks. BIOME4 provides a spatially and temporally resolved simulation of the metabolism of the biosphere including ^{13}C, validated to a dataset of measurements at three scales, and provides a tool required for analysis of the global cycles of carbon, CH_4 and ^{13}C.

1.4 The BIOME4 Global Vegetation Model

BIOME4 is an equilibrium terrestrial biosphere model developed from the BIOME3 model of Haxeltine and Prentice [1996]. BIOME4's main differences from its predecessor include the addition of a module to calculate isotopic discrimination during photosynthesis, the re-parameterization of the original Plant Functional Types (PFTs), and the addition of several new PFTs to reflect poorly represented vegetation types especially in the Arctic and the arid subtropics. BIOME4 simulates the vegetation of the Earth in 27 biomes which represent broad amalgamations of plant communities based on composition, phenology and climate regime (Fig. 1.2). The biomes are defined so as to be downwards compatible with the classification used in the BIOME 6000 dataset of reconstructed past vegetation [*Prentice and Webb*, 1998; *Prentice et al.* 2000].

BIOME4 is a coupled carbon and water flux model that predicts global vegetation distribution, structure, and biogeochemistry. The model is driven by monthly averages of temperature, precipitation, cloudiness and absolute minimum temperature. In addition the model uses information on soil texture and soil depth and a recently available global survey of rooting depth [*Canadell et al.*, 1996; *FAO*, 1995; *Haxeltine and Prentice*, 1996; *Jackson et al.*, 1996]. The model is run globally at a 0.5° resolution. Model operation is based on 12 PFTs representing physiologically distinct classes, from arctic/alpine cushion forbs to tropical evergreen trees. Each PFT is assigned absolute bioclimatic limits (Table 1.1) which determine whether or not its net primary productivity (NPP) is calculated for a given grid cell. The annual computational core of the model is a coupled carbon and water flux scheme, which determines the leaf area index (LAI) that maximizes NPP for any given PFT

Table 1.1. Absolute bioclimatic limits

Plant Functional Type	T_c min (°C)	T_c max (°C)	T_{min} min (°C)	T_{min} max (°C)	GDD_5 min	GDD_0 min	T_{wm} min (°C)	T_{wm} max (°C)	Snow min (cm)
Trees									
tropical broadleaf			0				10		
temperate broadleaf evergreen			-10	5	1200		10		
temperate broadleaf summergreen	5			-10	1200				
temperate needleleaf evergreen	-2			10	900		10		
cold evergreen	-32.5	-2						21	
cold deciduous		5		-10				21	
Non-trees									
temperate grass				0	550				
tropical grass			-3				10		
desert woody shrub			-45		500		10		
tundra woody shrub						50		15	15
cold herbaceous						50		15	
cushion-forb								15	

T_c, mean temperature of the coldest month; T_{min}, absolute minimum temperature; GDD_5, growing-degree-days on a 5 °C base; GDD_0, growing-degree-days on a 0 °C base; T_{wm}, temperature of the warmest month; *Snow*, minimum survivable winter snowpack

based on a daily time-step simulation of soil water balance, canopy conductance, photosynthesis, and respiration. Environmental factors affecting this calculation include variable soil texture with depth and seasonal patterns in precipitation, as well as the ambient concentration of atmospheric CO_2. PFT-specific parameters determine the sensitivity of each PFT to changes in environment (Tables 1.3 and 1.4). Photosynthetic pathway is PFT-specific: all trees and cold-climate herbaceous plants are C_3, tropical grasses are C_4. Temperate grasses and desert woody shrubs may have either pathway; the dominant pathway is selected seasonally on the basis of maximizing seasonal NPP. This convention does not imply that individual plants change pathway (which is rare), but rather that dominance shifts seasonally between taxa with different pathways (which is well documented).

The woody PFT which achieves the maximum annual NPP (at its optimized LAI) is generally considered the dominant PFT except in cases where grass or mixtures of grass and trees would be expected to dominate because of an implied disturbance regime or soil moisture constraints; thus, semi-empirical rules based on inferred fire risk and the balance of NPP between trees and grasses are used to assign the boundaries between forests, savannas, and grasslands (Table 1.2). Biogeochemical fluxes calculated by the model generally represent the dominant PFT for a each grid-cell. However, in the case of tropical savannas and other mixed tree-grass plant communities, certain output variables are assigned an NPP-weighted average of grass and tree types. To choose the biome for a given grid cell, the model orders the tree and non-tree of the PFTs that were calculated in that grid cell in terms of NPP, LAI and mean annual soil mositure and uses the semi-empirical rule base to assign each grid cell to one of 27 biomes.

Table 1.2. Schematic rule base for determining dominant vegetation in BIOME4

Dominant PFT	Rules
All tree PFTs	NPP < 140 g m^{-2} yr^{-1} then tree PFT not sustainable (grass, shrub, and tundra biomes)
Tropical and temperate broadleaf trees	LAI < 2.0 or firedays > 190 then non-tree PFT is dominant (grass and shrub biomes)
	2.0 < tree LAI < 3.0 then woodland/savanna biomes
Temperate and cold needleleaf trees	LAI < 1.0 or firedays > 90 then non-tree pft is dominant
Temperate needleleaf tree only	LAI < 1.2 then woodland biome
Cold deciduous trees	LAI < 1.0 or firedays > 60 then woodland biome
Herbaceous and shrub pfts	Ranked in order of NPP
No dominant PFT (all PFTs have 0 NPP)	Barren

Table 1.3. PFT-specific physiological parameters I

Plant Functional Type	P	G_{min}	E_{max}	S_l leafout	S_l leafdrop	R_{30}	L_m	GDD_5	GDD_0	R_s
		(mm s^{-1})	(mm d^{-1})	(%)	(%)	(%)	(month)			
Trees										
tropical broadleaf	rg	0.5	10	60	50	70	9			yes
temperate broadleaf evergreen	eg	0.2	4.8			67	18			yes
temperate broadleaf summergreen	sg	0.8	10			65	7	200		yes
temperate needleleaf evergreen	eg	0.2	4.8			52	30			yes
cold evergreen	eg	0.5	4.5			83	24			yes
cold deciduous	sg	0.8	10			83	6	200		yes
Non-trees										
temperate grass	rg	0.8	6.5	30	20	83	8		100	no
tropical grass	rg	0.8	8	30	20	57	10			no
desert woody shrub	eg	0.1	1			53	12			yes
tundra woody shrub	eg	0.8	1			93	8			yes
cold herbaceous	sg	0.8	1			93	8		25	no
cushion-forb	eg	0.8	1			93	8			yes

P, phenological type (rg, raingreen; eg, evergreen; sg, summergreen); G_{min}, minimum canopy conductance; E_{max}, maximum daily transpiration rate; S_l, soil moisture threshold for leaf-out and leaf-drop of the raingreen phenology expressed as a percent of field capacity; R_{30}, proportion of plant roots in the top layer (≤30cm) of soil; L_m, relative leaf longevity; GDD_5, number of GDD_5 required to grow a full canopy; GDD_0, number of GDD_0 required to grow a full canopy; R_s, presence of sapwood respiration

Table 1.4. PFT-specific physiological parameters II

Plant Functional Type	C_4	optratio	kk	T_{pC3} (°C)	T_{pC4} (°C)	T_{curve}	R_{fact}	Alloc	Fire (%)
Trees									
tropical broadleaf	no	0.9	0.7	10		1	0.8	1	20
temperate broadleaf evergreen	no	0.8	0.6	5		1	1.4	1.2	40
temperate broadleaf summergreen	no	0.8	0.6	4		1	1.6	1.2	50
temperate needleleaf evergreen	no	0.9	0.5	3		0.9	0.8	1.2	40
cold evergreen	no	0.8	0.5	0		0.8	4	1.2	33
cold deciduous	no	0.9	0.4	0		0.8	4	1.2	33
Non-trees									
temperate grass	yes	0.65	0.4	4.5	10	1	1.6	1	40
tropical grass	yes	0.65	0.4	10	10	1	0.8	1	40
desert woody shrub	yes	0.7	0.3	5	10	1	1.4	1	33
tundra woody shrub	no	0.9	0.5	-7		0.6	4	1	33
cold herbaceous	no	0.75	0.3	-7		0.6	4	1	33
cushion-forb	no	0.8	0.6	-12		0.5	4	1.5	33

C_4, presence of the C_4 photosynthetic pathway; *optratio*, the maximum acheivable c_i/c_a ratio; *kk*, the Beer's Law extinction coefficient; T_{pC3}, minimum monthly temperature for C_3 photosynthesis; T_{pC4}, minimum monthly temperature for C_4 photosynthesis; T_{curve}, relative response of photosynthesis to temperature; R_{fact}, relative response of maintence respiration to temperature; *Alloc*, relative minimum allocation; *Fire*, soil moisture percent of field capacity at which a fire day may be counted

BIOME4 and BIOME3 (or its prototype BIOME2) have been applied to a variety of studies which demonstrate the versatility and usefulness of the modeling approach. BIOME3 has been used in biogeochemical applications to investigate global- and continental-scale carbon cycling [*Heimann et al.*, 1998; *Kicklighter et al.*, 1999; *VEMAP*, 1995] and methane emissions from northern wetlands [*Christensen et al.*, 1996]. BIOME3 was applied to study the effect of low CO_2 concentrations on ecosystem structure and biome distribution [*Cowling*, 1999; *Jolly and Haxeltine*, 1997]. Both models have been used to investigate climate-biosphere interactions in the past, including the problem of glacial inception [*de Noblet et al.*, 1996], Pliocene vegetation on Antarctica [*Haywood et al.*, in press], and sources of atmospheric dust [*Mahowald et al.*, 1999]. BIOME3 and BIOME4 have been used to assess the impact of future climate change on regional vegetation [*Neilson et al.*, 1998; *Rathgeber et al.*, submitted; *Shafer*, 2000]. Finally BIOME4 has been recently applied to paleovegetation model-data comparison [*Williams et al.*, 1998] and in inverse modeling of paleoclimates [*Guiot et al.*, 1999].

1.4.1 Equilibrium versus dynamic global vegetation models

Despite the recent focus on developing dynamic global vegetation models (DGVMs) for carbon cycle research [*Sitch*, 2000; *Cox et al.*, 2000], "snapshot" models like BIOME4 remain important tools in plant ecology, biogeochemistry, and climate modeling. Equilibrium vegetation models are currently far more detailed and precise than DGVMs in their ability to simulate biogeographic patterns. Nor is a DGVM appropriate for addressing every research problem. A DGVM requires 10 to 100 times more overhead in terms of the size of input and output datasets and computing power to run than BIOME4. Equilibrium vegetation models thus provide an efficient method to investigate global ecosystem theory and a required test-bed for developing methods for simulating the behavior of vegetation that may later be applied in a DGVM context. A DGVM is required to study periods of rapidly changing climate where ecosystem "memory" is important, e.g. biogeochemical feedbacks in the anthropogenically modified environment of the present and the near future. Equilibrium models are more suited to analyses of "time slices" where an equilibrium approximation is adequate and interest focuses on regional phenomena that are not as well simulated with current DGVMs.

1.4.2 Arctic vegetation types in BIOME4

BIOME4 was expressly developed with several "new" PFTs to better represent high-latitude and alpine vegetation (Paper I). The three PFTs cold woody shrub, cold herbaceous, and cushion-forbs were defined to represent the most widespread, dominant forms of tundra plants. Values of parameters were assigned based on available physiological information and limits inferred in comparisons of habitat

Table 1.5. Tundra biomes simulated by BIOME4

Biome	Definition	Typical taxa
Low- and high-shrub tundra	Continuous shrubland, 50 cm to 2 m tall, deciduous or evergreen, sometimes with tussock-forming graminoids and true mosses, bog mosses and lichens	*Alnus*, *Betula*, *Salix*, *Pinus pumila* (in eastern Siberia), *Eriophorum*, *Sphagnum*
Erect dwarf-shrub tundra	Continuous shrubland 2 to 50 cm tall, deciduous or evergreen, with graminoids, true mosses, and lichens	*Betula*, *Cassiope*, *Empetrum*, *Salix*, *Vaccinium*, Gramineae, Cyperaceae
Prostrate dwarf-shrub tundra	Discontinuous shrubland of prostrate deciduous shrubs 0 to 2 cm tall	*Salix*, *Dryas*, *Pedicularis*, *Asteraceae*, *Caryophyllaceae*, Gramineae, true mosses
Cushion forb, lichen, and moss tundra	Discontinuous cover of rosette plants or cushion forbs with lichens and mosses	*Saxifragaceae*, *Caryophyllaceae*, *Papaver*, *Draba*, lichens, true mosses
Graminoid and forb tundra	Predominantly herbaceous vegetation dominated by forbs, graminoids, true mosses, and lichens	*Artemisia*, *Kobresia*, *Brassicaceae*, *Asteraceae*, *Caryophyllaceae*, Gramineae, true mosses

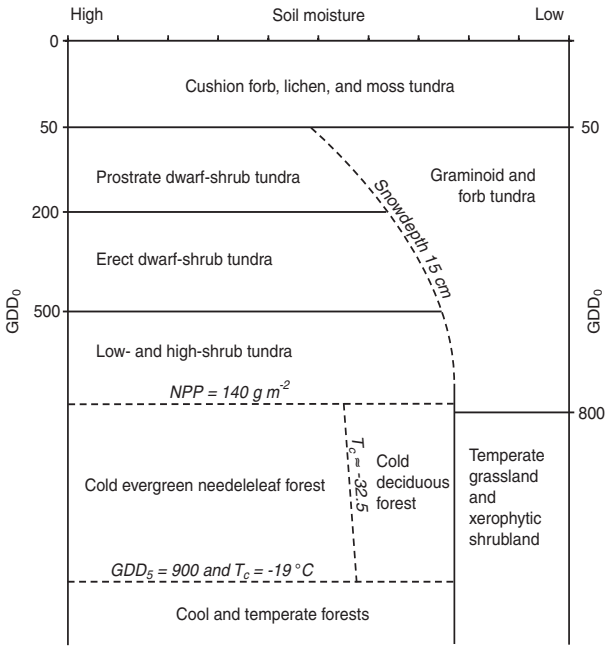

Fig. 1.3. Climate space occupied by the Arctic biomes defined in BIOME4

ranges with climate data (see Tables 1.1, 1.3, and 1.4). Five new biomes represent tundra (Table 1.5, Fig. 1.3). The new biomes allow direct comparison with a new map of potential natural vegetation in northern high-latitudes, developed for the PAIN project, and with paleovegetation data based on pollen and macrofossil counts.

1.4.3 Wetland area and methane emissions in BIOME4

BIOME4 was used to simulate global wetland area and associated methane (CH_4) emissions (Paper II). Simulated soil moisture, vegetation type, productivity, and heterotrophic respiration (R_h) are combined with a global digital terrain model to identify areas both wet and flat enough to form wetlands (Fig. 1.4). Vegetation productivity constrains the annual rate of CH_4 evolution through its control of the size of the pool of material available for heterotrophic respiration. The fraction of R_h that is released as CH_4 depends on the extents to which the CH_4 is oxidized on its way to the atmosphere through the soil, roots, and aboveground vegetation. The model simply assigns a differential in-situ oxidation rate for CH_4 based on the biome that is simulated in the wetland area. BIOME4 is then combined with the terrestrial dry-soil CH_4 sink model of Ridgwell *et al.* [1999], applied across all non-wetland areas, to simulate a global terrestrial source-sink balance.

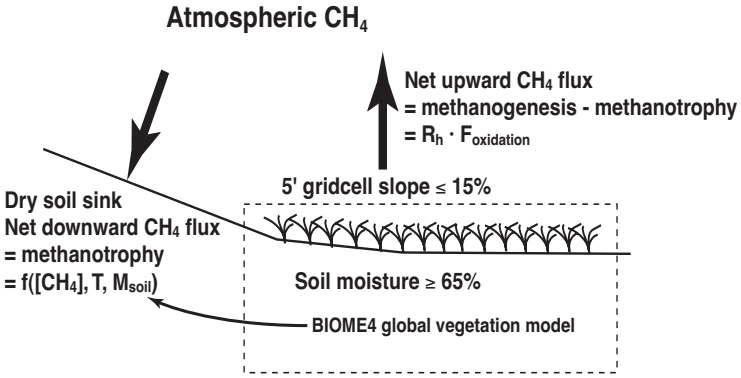

Fig. 1.4. Schematic diagram of the wetland and methane model

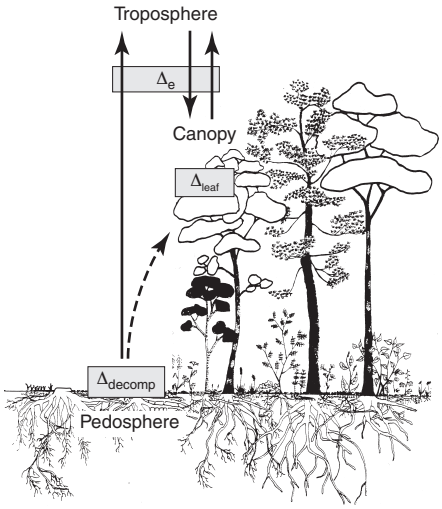

Fig. 1.5. Conceptual diagram of ecosystem discrimination in a forest. Important CO_2 fluxes are represented as arrows; carbon isotope discrimination Δ is represented in the boxes.

1.4.4 Carbon isotope discrimination in BIOME4

BIOME4 calculates the isotopic discrimination against ^{13}C in CO_2 during photosynthesis (Δ_{leaf}), and total ecosystem "discrimination" (Δ_e) which is the difference between atmospheric and total terrestrial ecosystem $\delta^{13}C$ (Fig. 1.5) (Paper III). Carbon isotope ratios are expressed in $\delta^{13}C$ notation with is calculated as:

$$\delta^{13}C = \frac{R_{sample}}{R_{std}} - 1 \tag{1.1}$$

where R_{sample} and R_{std} are the $^{13}C/^{12}C$ ratios of the sample and the standard, respectively. Conventionally, $\delta^{13}C$ and Δ are expressed in units of per mil (‰). Isotopic discrimination Δ is defined as the difference in δ between two pools such that

$$\Delta = \frac{\delta_a - \delta_b}{1 + \delta_b} \tag{1.2}$$

where δ_a and δ_b represent the average isotopic composition of pools *a* and *b* [*Buchmann et al.* 1998].

The photosynthetic discrimination model is conceptually related to other models of leaf carbon isotope discrimination [*Beerling*, 1994; *Lloyd and Farquhar*, 1994]. However, BIOME4 explicitly simulates the concentration of CO_2 in the chloroplast through the optimization calculations balancing carbon gain with water stress. Only a maximum ratio of $[CO_2]$ inside the leaf to $[CO_2]$ outside the leaf (c_i/c_a) is

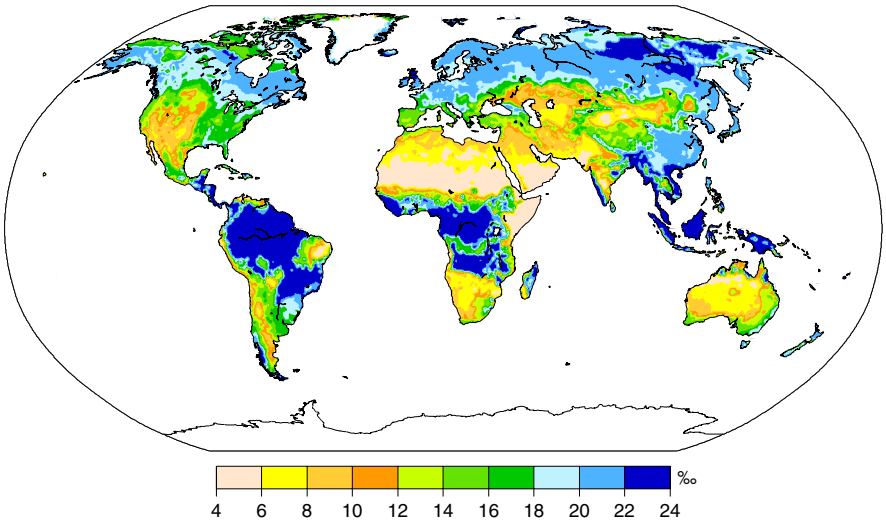

Fig. 1.6. Global ecosystem discrimination Δ_e of potential natural vegetation simulated by BIOME4 with 20th century mean climatology

prescribed for each PFT. The actual c_i/c_a is subsequently calculated though iterative optimization [*Haxeltine and Prentice*, 1996]. Maximum c_i/c_a ratios were compiled from direct measurements in laboratory studies [*Farquhar*, 1983; *Farquhar et al.*, 1982] and inferred from maximum measured values of $\delta^{13}C$ in leaf material from samples of all PFTs [see e.g. *Brooks et al.*, 1997; *Donovan and Ehleringer*, 1994; *Ehleringer et al.*, 1987; *Guehl et al.*, 1998; *Hattersley*, 1983; *Kloeppel et al.*, 1998; *Körner et al.*, 1991; *Larcher*, 1995; *Michelsen et al.*, 1996; *Osmond et al.*, 1975; *Schulze et al.*, 1996; *Schulze et al.*, 1998].

Total ecosystem discrimination, Δ_e [*Brooks et al.*, 1997; *Buchmann et al.*, 1998; *Buchmann and Kaplan*, in press; *Flanagan and Ehleringer*, 1998] was also modeled (Fig. 1.6). Monthly Δ_e is estimated as the flux-weighted difference in discrimination against ^{13}C from NPP and heterotrophic respiration (R_h). Photosynthate, with a specific ^{13}C content determined by the Δ_{leaf}, is incorporated into the plant on an integrated flux-weighted basis. A simple model for R_h determines the monthly flux of respired CO_2 and $^{13}CO_2$ to the atmosphere [*Foley*, 1994; *Lloyd and Taylor*, 1994; *Sitch*, 2000]. The source of respired CO_2 is the aggregated annual NPP for the dominant vegetation type in a grid cell. This carbon stock is divided into three pools according to the scheme of Foley [1994]. Each pool is subjected to a degree of isotopic fractionation during respiration based upon the assumed decay rate of the pool.

1.5 Three Applications of BIOME4

1.5.1 The Pan-Arctic INitiative

Of all the Earth's vegetation, Arctic tundra is perhaps the most acutely sensitive to climate change and at the same time has a significant potential for feedbacks, both physical and chemical, which could in turn affect the climate [*Bonan et al.*, 1995; *Chapin et al.*, 1995; *Christensen et al.*, 1999; *Foley et al.*, 1994; *Kutzbach et al.*, 1998; *Oechel et al.*, 1993]. The goals of the Pan-Arctic INitiative (PAIN) included the simulation of northern high-latitude vegetation in a globally consistent manner. The simulated vegetation was systematically reconciled to the modern potential natural vegetation map developed by PAIN. Driven by the output of several general circulation models (GCMs), the vegetation of the mid-Holocene and the Last Glacial Maximum (LGM) was also simulated and compared with spatially extensive paleovegetation data derived from pollen records (which also formed a component of the PAIN project). The impact of a future climate scenario was finally simulated using a GCM simulation of the next 100 years based on the assumption of a continuing exponential increase in atmospheric greenhouse gas concentrations.

Spatially extensive paleovegetation data can be used as a benchmark for coupled climate-vegetation model simulations [*Prentice and Webb*, 1998]. The time slices of the mid-Holocene (6000 yr BP) and LGM (21 000 yr BP; approximately equivalent to 18 000 yr BP by ^{14}C-dating) are considered important test-periods in the recent geological past where the Earth's climate was considerably different from the present due to well-known changes in boundary conditions: orbital variations between the mid-Holocene and present, and at the LGM low CO_2 and other greenhouse gas concentrations, low sea level, and extensive ice sheets. These time slices have been the main focus of the Paleoclimate Modelling Intercomparison Project (PMIP) [*Joussaume*, 1999; *Pinot et al.*, 1999]. Paleo-vegetation distribution can be estimated from pollen data using a PFT-based method called biomization [*Prentice et al.*, 1996]. The biomization method has been applied to continuous pollen records to investigate vegetation change [*Tarasov et al.*, 1997]. Biomization is currently being used to generate global paleovegetation maps for the mid-Holocene and LGM using a uniform set of biomes as part of the BIOME 6000 project [*Kohfeld and Harrison*, 2000; *Prentice et al.*, 2000; *Prentice and Webb*, 1998]. Mid-Holocene paleo data indicate that, although caused by a longitudinally uniform forcing around the Arctic, warming was not spatially uniform compared to the present [*Bigelow et al.*, submitted; *MacDonald et al.*, 2000; *Prentice et al.*, 2000; *TEMPO members*, 1996]. LGM paleo data indicate a radical difference from present with a dramatic retreat of the forest limit and widespread occurrence of graminoid-forb tundra, which does not cover large, continuous areas of the high northern latitudes in today's climate.

The Arctic vegetation simulated by BIOME4 has been validated against a map of present potential natural vegetation (Fig. 1.7) and at the mid-Holocene and the

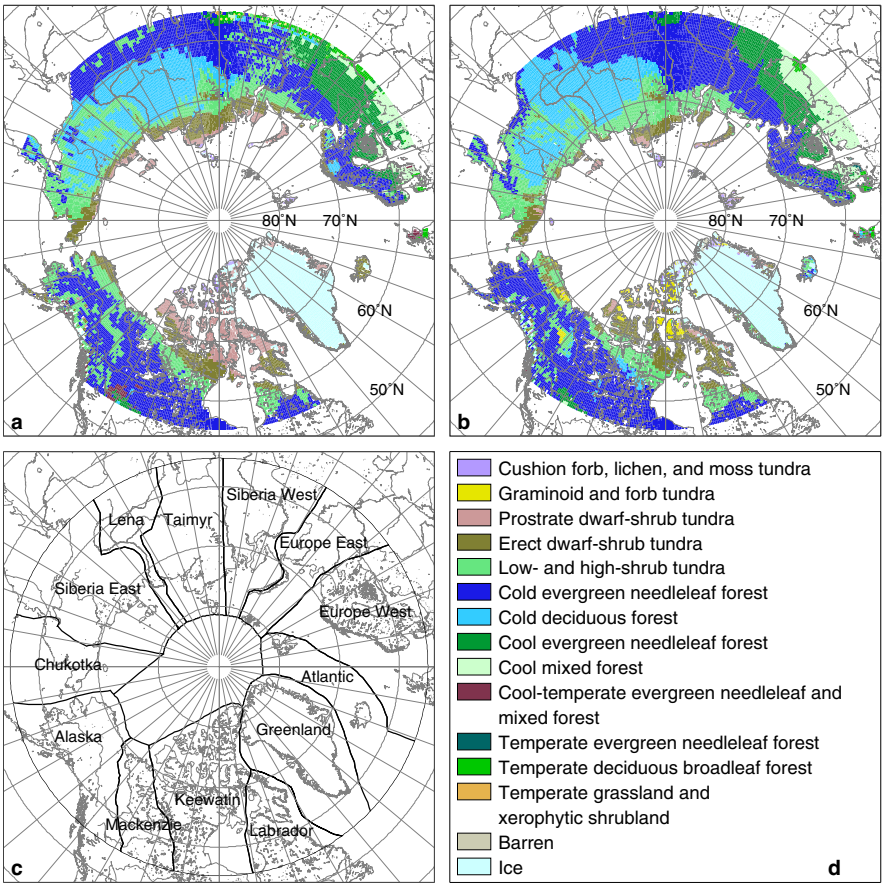

Fig. 1.7. Present-day potential natural vegetation of the Arctic from floristic surveys **a**, and simulated by BIOME4 **b** with 20th century mean climatology. Sectors used in calculating treeline changes **c** and legend **d** for this figure and figures 1.8 and 1.9

LGM using biomized pollen data (Figs. 1.8, 1.9) [*Bigelow et al.*, submitted]. Simulated vegetation matches the map of potential natural vegetation well, with a few exceptions. For example, the oceanic tundra landscapes of southwestern Alaska and Iceland are not simulated correctly by BIOME4. The effect of extreme cloudiness combined with low sun angles at high latitudes may be the cause of the mismatch.

To simulate vegetation distribution at the mid-Holocene and the LGM, BIOME4 was run using the climate simulations of a series of AGCMs. PMIP simulations with prescribed sea-surface temperatures, ice sheets and atmospheric CO_2 concentration (200 ppm) show a large range of high-latitude cooling on unglaciated land at the LGM. The observed prevalence of dwarf-shrub and graminoid-forb tundra and extreme restriction of low and high shrub tundra were nevertheless reproduced successfully in a qualitative sense (Fig. 1.8). The simulated graminoid-forb tundra

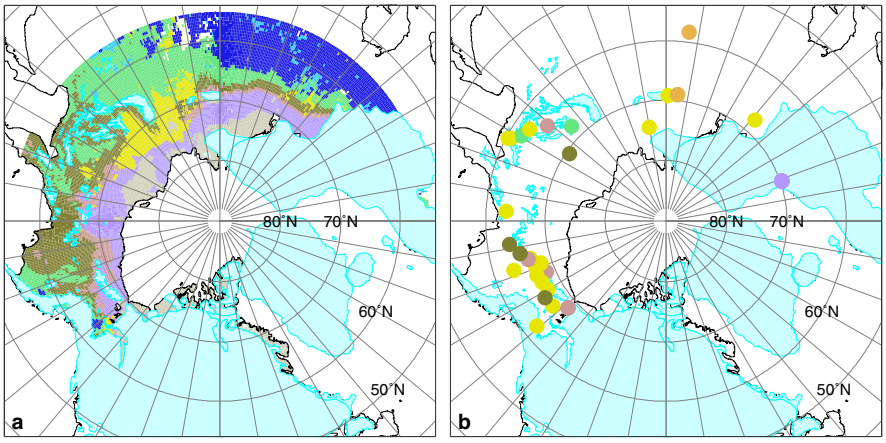

Fig. 1.8. Simulated **a** and observed **b** vegetation at the Last Glacial Maximum. LGM climate data is from the MRI2 GCM; observed vegetation is based on pollen reconstructions

was about twice as productive as its spatially restricted modern equivalents, due to lower latitude and less cloudiness.

Changes in the orbital configuration of the Earth produced a substantial, zonally uniform increase in summer and annual insolation in the Arctic during the early and mid-Holocene relative to the present day. Results obtained with two coupled atmosphere-ocean models (AOGCMs, HADCM2 and IPSL) for 6000 yr BP indicate that mid-Holocene tree line extension was modest (0-300 km) and longitudinally asymmetrical, with maximal extension in central Siberia and little or no change in Alaska (Table 1.6). This model result is supported by pollen-based vegetation reconstruction and megafossil distributions which also indicate a heterogeneous change in the tree line latitude compared to the present [*Bigelow et al.*, submitted; *MacDonald et al.*, 2000]. That the tree line was further south than present in Labrador is assumed to be due to local effects of residual ice sheets still present in the mid-Holocene [*Clark et al.*, 2000], which were not represented in the simulations. Models and data also agree in showing a 100-300 km northward displacement of shrub tundra types (Fig. 1.9).

Projections of the effect of increasing atmospheric greenhouse gas concentration based on a HADCM2 simulation suggest a potential for larger changes in Arctic ecosystems during the 21st century than have occurred between the mid-Holocene and present. This is because greenhouse gases produce a large, year-round climate forcing with major consequences for the distribution of sea ice, thus removing the steep thermal gradient towards the Arctic coast. Ecosystem effects of the CO_2 increase (to >700 ppm) were slight compared with the effects of the simulated change in climate (Table 1.6). It should be noted however that this is a hypothetical scenario based on the IS92a projection of an approximately 1% per year exponential increase in CO_2 emissions throughout the 21st century; lesser emissions would

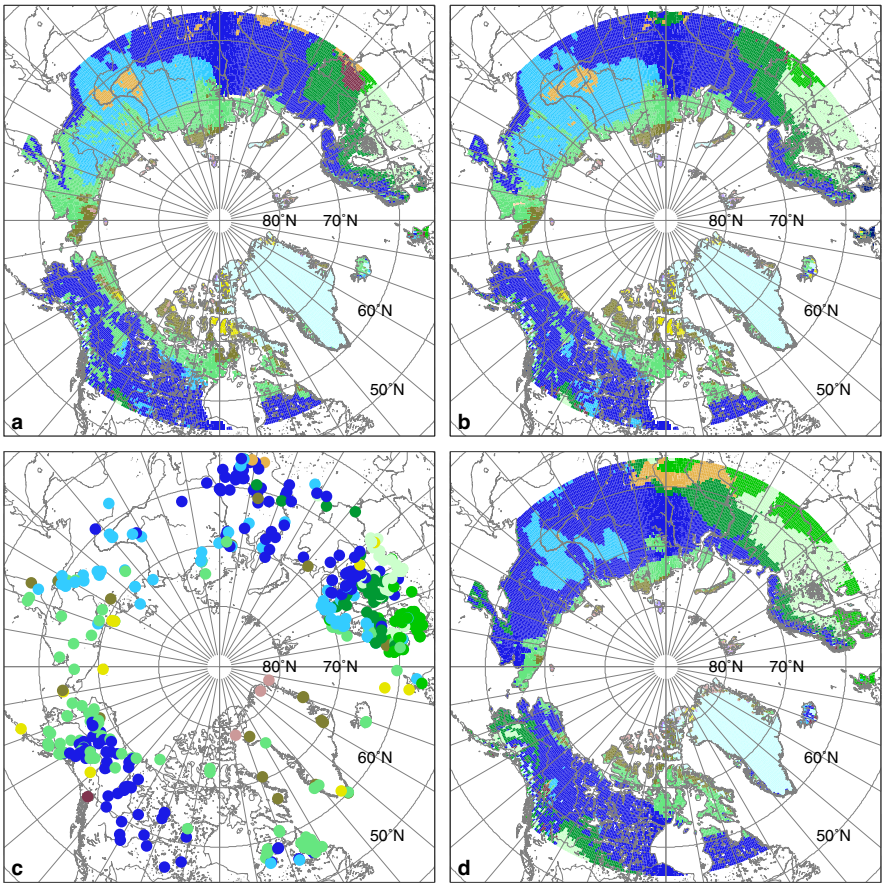

Fig. 1.9. Simulated Arctic vegetation at the mid-Holocene with **a** the IPSL-CM1 AOGCM and with **b** the HADCM2 AOGCM. Observed vegetation at the mid-Holocene **c** from pollen data. Simulated potential vegetation for 2090 to 2100 **d** with the HADCM2-SUL GCM using the IS92a greenhouse-gas scenario.

lead to a smaller climatic and vegetational impact. In contrast, physical vegetation feedback to climate, which was not included in this study, is likely to compound the effect of warming [*Betts et al.*, 2000].

1.5.2 Wetlands and methane emissions

Before industrialization (including the use of natural gas for fuel) and the great expansion of rice cultivation in recent centuries, natural wetlands exerted the primary control on the global terrestrial CH_4 source. CH_4 is an important trace gas in the atmosphere, 20.6 times more insulating than CO_2, and accounting for about

Table 1.6. Changes in the position of Arctic treeline

Sector	6k - present-day			Future - present-day
	HADCM2	IPSL-CM1	Pollen	HADCM2-S IS92a scenario
Alaska	ø	ø	ø	+++
Mackenzie	ø	-	ø	+
Keewatin	+	+	-	++++
Labrador	+	++	------	+++
Greenland	ø	ø	ø	++++++++
Atlantic	----	-	ø	ø
Europe West	ø	ø	+	+
Europe East	ø	ø	ø	++
Siberia West	+	+	++	+++
Taimyr	++	ø	+++	++++
Lena	ø	ø	ø	+
Siberia East	ø	ø	++	+++
Chukotka	ø	ø	ø	+++++

The tree line position in each sector is defined as the maximum latitude band where ≥50% of the gridcells are a forest biome. Each + or - symbol represents a difference of 1° (ca. 110 km), a ø represents no change. The sectors were defined to represent climatically contiguous regions within which local topographic influence (e.g. deep river valleys) and regional circulation effects (e.g. ocean currents and ice sheets) on the location of treeline are minimized.

17% of the total present-day trace-gas induced atmospheric radiative forcing. Changes in the natural sources and sinks of CH_4 may have had a significant impact on global climate. Changes in the atmospheric concentration of CH_4 over the last glacial-interglacial cycle measured in ice cores indicate that CH_4 concentrations closely paralleled polar temperatures. However, the cause of the changing CH_4 concentrations is not well constrained by observations.

Based on present-day knowledge of the CH_4 budget, qualitative explanations for the relationship between atmospheric CH_4 concentrations and climate have been based on the CH_4 emission from natural wetlands and CH_4 oxidation by OH radicals in the troposphere. OH, the primary sink for CH_4, is produced in the atmosphere by the reaction of O_2 with high-energy solar radiation and H_2O; OH abundances are strongly controlled by the abundances of other reactive trace gases including CO and NO_x [*Houweling et al.*, 2000; *Thompson et al.*, 1993]. Other sources of CH_4 (including termites, ruminant animals, wildfires, and ocean sediments), as well as the dry-soil CH_4 sink, are a small part of the current global CH_4 budget, and would probably not have contributed significantly to changes observed in the past [*Chappellaz et al.*, 2000]. The role of CH_4 hydrates in ocean sediments in influencing short-term global climate fluctuations is controversial. Evidence for rapid degassing and corresponding climate fluctuations have been reported from the marine record [*Kennett et al.*, 2000], but high-resolution sampling of ice cores

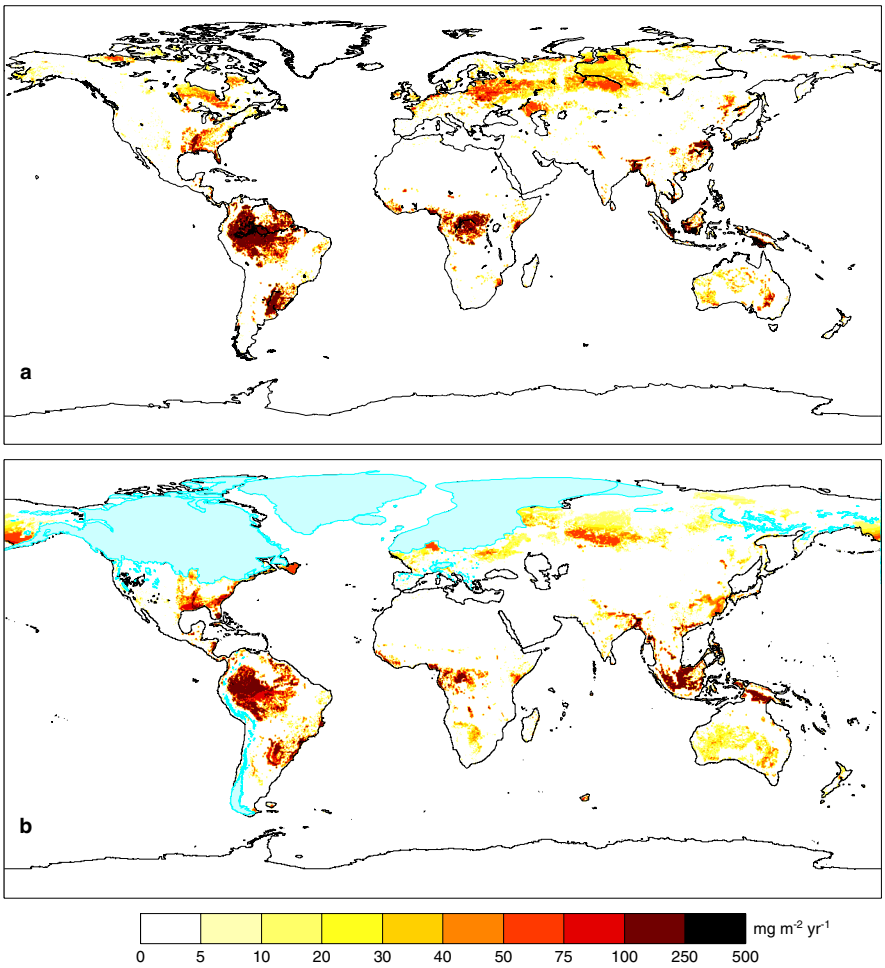

Fig. 1.10. Potential natural wetlands and CH_4 emission simulated for **a** the present-day and **b** the LGM

have failed to show the very rapid increases in CH_4 concentrations required by this hypothesis [*Chappellaz et al.*, 2000].

BIOME4 has been used to simulate potential natural wetland area and CH_4 emissions for the present-day and for the LGM (Fig. 1.10). Simulated potential natural wetland area is nearly 50% greater than earlier estimates largely because BIOME4 simulates seasonal wetlands which, because of the methods used to assess wetland area, could not be detected in other studies (Fig. 1.10). Simulated CH_4 emissions for the present-day are however comparable to other estimates. At the LGM, simulated area of wetlands was 15% larger than present but their total CH_4 emissions were 24% less. Extensive wetlands were simulated on the wide, flat conti-

nental shelves, a result supported by paleoecological evidence from the tropics and Arctic [*Edwards et al.*, in press; *Hanebuth et al.*, 2000; *Webb et al.*, 1993]. However, peak CH_4 emission rates were reduced because of low temperatures and low CO_2 concentration, both leading to lower rates of substrate formation for methanogenic organisms. Simulated global wetland CH_4 emissions, 140 Tg per year at the present and 107 Tg at the LGM, are within the range of previous estimates. The soil sink for CH_4 was simulated as 14 Tg at present and less than 0.5 Tg at the LGM, i.e., ambient atmospheric CH_4 concentration at the LGM was too low to sustain methanotrophy in dry soils. A sensitivity test simulating vegetation, wetland area, and CH_4 emission with the glacial climate but with mid-20th century CO_2 concentration produced a wetland CH_4 source of 140 Tg, i.e. similar to present. The simulated increase in natural CH_4 emissions since the LGM is therefore largely due to the increase in substrate availability from changes in wetland productivity, which in turn is strongly linked to CO_2 concentrations in the model. Field studies disagree in their assessment of the real importance of atmospheric CO_2 concentration to CH_4 production [*Chapman and Thurlow*, 1996; *Hutchin et al.*, 1995; *Whiting and Chanton*, 1993]. However, no experiment on CH_4 production has considered explicitly the low CO_2 concentrations present at the LGM, despite evidence for a strong nonlinear response of vegetation productivity and structure at sub-ambient [CO_2] [*Cowling*, 2000].

Changes in the atmospheric OH sink may need to be postulated to explain the full magnitude of the increase in atmospheric CH_4 since the LGM. CH_4 concentrations increased from 350 to 700 ppb from the LGM to pre-industrial time; this 100% increase in concentration is larger than could likely be accounted for by the simulated increase in source strength of only 24%. This result is in contrast to earlier studies which suggested that the long-term increases in atmospheric CH_4 concentration were largely or entirely due to the effect of changing temperature and precipitation patterns on wetlands [*Chappellaz et al.*, 1993; *Crutzen and Bruhl*, 1993; *Martinerie et al.*, 1995; *Petit-Maire et al.*, 1991; *Pinto and Khalil*, 1991; *Thompson et al.*, 1993]. Atmospheric OH concentrations are strongly regulated by the concentration of CO and NO_x as well as by the extent of saturation by CH_4 itself. It is expected that source strength and emission patterns of these gases were different at the LGM, as these too are strongly dependent on vegetation processes, including fire, which were evidently very different at the LGM. To better constrain LGM OH concentrations requires further research towards building a comprehensive model of trace gas sources in the biosphere and linking to atmospheric chemistry models.

While the location of wetlands since the Last Glacial Maximum has changed greatly, neither the global total simulated wetland area (15% increase) nor consequent simulated CH_4 emissions (24% decrease) changed in proportion with the observed changes in atmospheric CH_4 recorded in ice cores. CH_4 emissions are strongly controlled by substrate availability, which at the LGM was limited strongly by atmospheric CO_2 concentrations, according to these model results. These results place the close co-variance of the ice-core derived polar temperatures and atmo-

spheric CH_4 concentration into a new light, as it appears that the mechanisms controlling the global CH_4 source are less sensitive to climate change on glacial-interglacial time-scales than previously thought. However, on shorter timescales, CH_4 from boreal wetlands may respond rapidly to climate change, as recent work has suggested [*Worthy et al.*, 2000].

1.5.3 Carbon isotopic composition of the terrestrial biosphere

Because the terrestrial biosphere discriminates strongly against ^{13}C during photosynthesis, the $^{13}C/^{12}C$ ratio of CO_2 in the atmosphere has been used to partition the sources and sinks of atmospheric CO_2 between oceanic and biospheric components [*Bakwin et al.*, 1998; *Battle et al.*, 2000; *Bousquet et al.*, 1999; *Ciais et al.*, 1995a; *Ciais et al.*, 1995b]. This partitioning of CO_2 sources and sinks is critical for understanding how the global carbon budget is affected by climate, and in turn, how CO_2, the atmosphere's second most important greenhouse gas after water vapor, feeds back to the climate system. However, in order to clearly define the CO_2 sources and sinks using CO_2 and $\delta^{13}C$ the isotopic composition of the principal components in the system must be known. Further complicating the problem is that the isotopic signatures of the components, especially the terrestrial biosphere, are not homogenous through space and time. Measurements of the isotopic composition of the biosphere, while they exist at a variety of scales, are limited in spatial and temporal coverage. Thus, a global vegetation model can be used to provide an approximation of the global signature of ^{13}C in the biosphere. Measured $\delta^{13}C$ at the leaf, ecosystem,

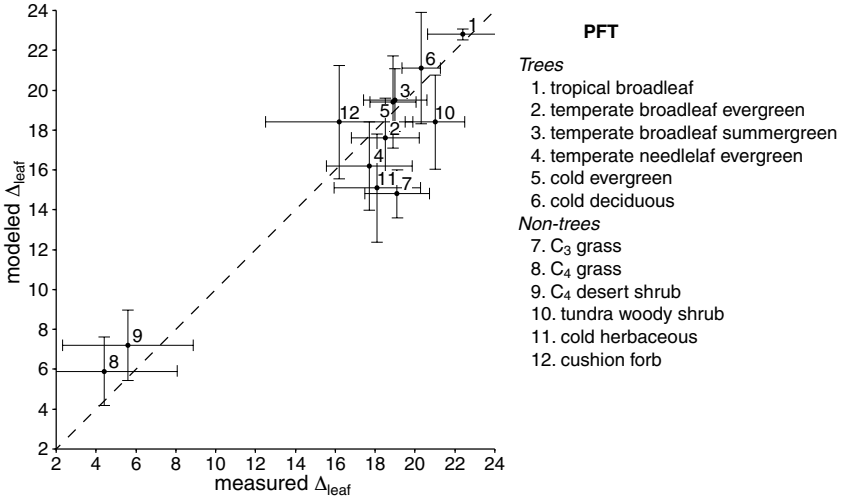

Fig. 1.11. Modeled and measured leaf carbon isotope discrimination Δ_{leaf}. Error bars represent one standard deviation around the mean.

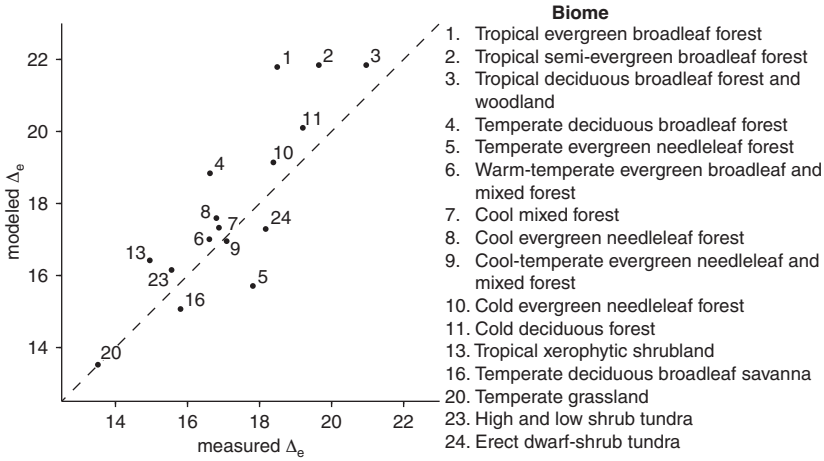

Fig. 1.12. Measured and modeled Δ_e. Flask samples of canopy and neighboring troposphere air were used to measure Δ_e. Modeled values are simulated by BIOME4 using 20th century climatology.

and troposphere levels may all be used to make a robust validation of the model result.

Carbon isotope discrimination of the terrestrial biosphere was compared to measurements at the leaf, canopy, and free-atmosphere scales. The simulated leaf-level discrimination (Δ_{leaf}) was compared to estimates from leaf $\delta^{13}C$ measurements (Fig. 1.11) and simulated total ecosystem discrimination Δ_e was compared to canopy-level measurements (Figs. 1.12, 1.13). To test the model at the whole atmosphere scale, the seasonal cycle of tropospheric CO_2 and ^{13}C was simulated by combining BIOME4 with an ocean biogeochemistry model and coupling the resultant flux field to an atmospheric tracer transport matrix. The simulated CO_2 concentration and ^{13}C were compared to measurements of free troposphere air at various locations around the world (Fig. 1.14).

Measurements of Δ_{leaf} were classified into 12 PFTs simulated by BIOME4. In total the dataset of Δ_{leaf} represents more than 1000 measurements from samples taken on vegetation growing in natural habitats. Modeled Δ_{leaf} was summarized from the present-day potential natural vegetation simulation of BIOME4 (Fig. 1.11).

At the whole ecosystem level BIOME4 simulates Δ_e, incorporating the effects of isotopic discrimination during photosynthesis and in soil decomposition processes. Buchmann and Kaplan [in press] have compiled a dataset of measurements on ecosystem-level validation which uses the "Keeling plot" technique to estimate isotopic signature from samples of canopy air. The Keeling plot is based on the fact that CO_2 concentration and ^{13}C co-vary in a predictable manner. When $1/[CO_2]$ is plotted against $\delta^{13}C$, the intercept of a linear regression line through the points indicates the flux-integrated ^{13}C signature of the CO_2 source [*Buchmann et al.*, 1998; *Keeling*, 1961]. For the ecosystem level measurements, the diurnal cycle of CO_2 was used to

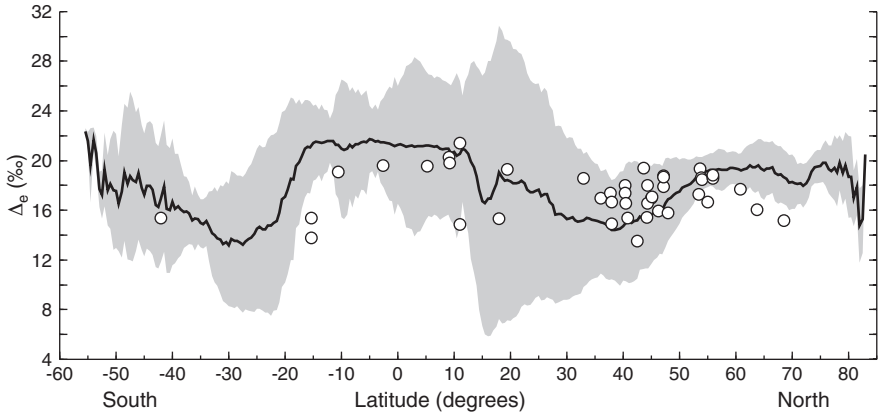

Fig. 1.13. Simulated flux-weighted latitudinal distribution of ecosystem discrimination **solid line** and measured ecosystem discrimination **open circles**. The shaded area represents 1 standard deviation around the simulated mean.

create the Keeling plot. Ecosystem level Δ_e simulations compared closely to measurements made on canopy flask air both at the biome level and on global latitude bands (Figs. 1.12, 1.13).

Changes in CO_2 concentration over the seasonal cycle can also be used to estimate source ^{13}C signatures. At the troposphere level, a global flux field of CO_2 and ^{13}C was generated by combining BIOME4 outputs with an ocean biogeochemistry model simulation [*Six and Maier-Reimer*, 1996]. The seasonal cycle of CO_2 and ^{13}C at specific free-troposphere measuring stations were then simulated with the flux field as input to an adjoint tracer transport matrix [*Kaminski et al.*, 1996]. The model-simulated signature of the ^{13}C source was close to the measured value at six

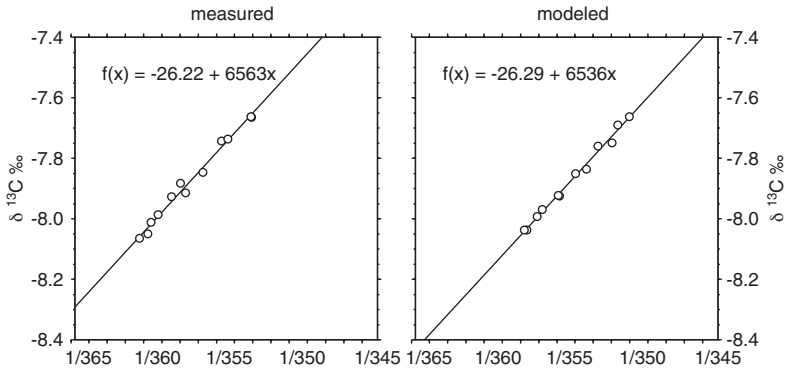

Fig. 1.14. Keeling plots of measured and modeled CO_2 concentration and $\delta^{13}C$ in CO_2 in the free troposphere at Niwot Ridge, Colorado, USA. The intercept of the fit line indicates the $\delta^{13}C$ of the source CO_2

medium- to high-latitude stations in the northern hemisphere and reflected the observed latitudinal gradient.

To test the importance of short-term climatic variability on global isotopic discrimination, I developed a transient version of BIOME4 called BIODYNE [*J.O. Kaplan*, unpublished results]. BIODYNE simulates the carbon and isotopic fluxes of all of the plant functional types included in BIOME4. The dynamic simulation is driven by the same soils data as BIOME4 and a variable climatology. Results of a fifteen-year simulation (1980-1995) with BIODYNE indicate that the interannual variability of global Δ_e may be as high as 1‰ (Fig. 1.15). This variability, along with the range of uncertainty in Δ_e currently predicted by this and other global models of Δ_e, is important because a mis-estimate in global Δ_e of 3‰ can produce a 20% change in the inferred strength of the terrestrial carbon sink. A global Δ_e that overemphasizes the importance of C_3 vegetation leads to the too-strong inference of oceanic sink [*Fung et al.*, 1997]. Therefore, the spatial and temporal patterns of vegetation in the tropics and agricultural land use are particularly important to better constrain the carbon budget using ^{13}C. Future plans include investigating the dynamics of ^{13}C using the Lund-PIK-Jena (LPJ) DGVM [*M. Scholze, J.O. Kaplan, W. Knorr, M. Heimann, and S. Sitch*, unpublished results].

Fig. 1.15. Global NPP and Δ_{leaf} simulated by BIODYNE

1.6 Conclusions

Vegetation models are powerful tools for the investigation of questions in plant ecology that are impossible to assess directly in the field or laboratory because of spatial or temporal sampling limitations and the impossibility of performing very large-scale experiments. This thesis describes three applications of a global vegetation model to problems that cannot be solved using observations or experiments alone but are nonetheless highly relevant to contemporary global change issues because of the important role vegetation plays in land-atmosphere climate feedbacks; the budget of CH_4, an important greenhouse gas; and the global cycle of carbon, which determines the fate of anthropogenic CO_2.

The BIOME4 global vegetation model has achieved the most detailed and accurate simulation of global potential natural vegetation to date. The model successfully simulates the distribution of Arctic vegetation both in the present day and, when combined with a climate model, in the past, where it is validated against pollen-based vegetation reconstructions. BIOME4 simulates the global distribution of natural wetlands at a higher resolution and with more temporal information than previously accomplished. CH_4 emissions from natural wetlands are simulated for the present day and are within the range of other estimates. At the LGM, CH_4 emissions from wetlands are not simulated as low as previously thought because the model indicates that areas suitable for wetland development were more extensive (especially taking into account the exposure of large, flat continental shelf areas) than previous reconstructions have assumed. A complete explanation of the glacial CH_4 cycle may require a full simulation of reactive trace gases and a new analysis of LGM atmospheric chemistry. Simulations of the isotopic composition of the biosphere indicate that ^{13}C is more variable spatially and temporally than has generally been assumed in geophysical analyses of the contemporary carbon cycle. The accuracy of the model was confirmed by validation at the leaf, ecosystem, and whole-atmosphere level.

Further research should integrate the new plant ecological information from field studies, especially those using new micrometerological techniques, into existing model frameworks. A comprehensive sensitivity test by Hallgren and Pitman [2000] showed that the greatest changes in vegetation distribution simulated by BIOME3 could be affected by changing the root distribution of the different model PFTs. These results point to the general sensitivity of the vegetation model, and its successors, to hydrology. Recent studies point to the importance of tropical vegetation to interannual variability in the global carbon cycle [*McGuire et al.*, in press]. Given the known variability of the hydrologic cycle at the interannual to decadal scale, especially in the tropics, further research must also focus on improving hydrology in vegetation models.

As a means of exploring the importance of particular processes in the functioning of ecosystems, vegetation modeling provides plant ecologists with a new perspective. Vegetation models can be used to explore phenomena that are impossible

to measure directly. The future will bring improvements to BIOME4 and its descendant models that assimilate new advances in plant ecology and at the same time allow the assessment of the importance of plant ecological processes at a variety of spatial and temporal scales. BIOME4 has already proven its usefulness in several applications and will continue to be useful for studying states of the Earth in other periods of geologic time; as a baseline to help in understanding causes and effects of major climate changes observed in the past; and as a tool to help in the assessment of anthropogenic climate changes, now and in the future.

I thank I.C. Prentice, K.E. Kohfeld, and S. Sitch for their comments, which improved this manuscript.

References

Bakwin, P.S., P.P. Tans, J.W.C. White, and R.J. Andres, Determination of the isotopic ($^{13}C/^{12}C$) discrimination by terrestrial biology from a global network of observations, *Global Biogeochemical Cycles*, *12* (3), 555-562, 1998.

Battle, M., M.L. Bender, P.P. Tans, J.W.C. White, J.T. Ellis, T. Conway, and R.J. Francey, Global carbon sinks and their variability inferred from atmospheric O_2 and $\delta^{13}C$, *Science*, *287* (5462), 2467-2470, 2000.

Beerling, D.J., Predicting leaf gas exchange and $\delta^{13}C$ responses to the past 30 000 years of global environmental change, *New Phytologist*, *127*, 1-9, 1994.

Betts, R.A., Offset of the potential carbon sink from boreal forestation by decreases in surface albedo, *Nature*, *408* (6809), 187-190, 2000.

Bigelow, N.H., L.B. Brubaker, M.E. Edwards, S.P. Harrison, I.C. Prentice, P.M. Anderson, A.A. Andreev, P.J. Bartlein, T.R. Christensen, W. Cramer, J.O. Kaplan, A.V. Lozhkin, N.V. Matveyeva, D.F. Murray, A.D. McGuire, V.Y. Razzhivin, J.C. Ritchie, B. Smith, D.A. Walker, S.L. Clayden, T. Ebel, K. Gajewski, J. Hahne, B.H. Holmqvist, Y. Igarashi, J.W. Jordan, K.V. Kremenetskii, M. Melles, W.W. Oswald, A. Paus, M.F.J. Pisaric, G.N. Shilova, C. Siegert, V.S. Volkova, and V.G. Wolf, Climate change and Arctic ecosystems I: Biome reconstruction of tundra vegetation types at 0, 6, and 18 radiocarbon kyr in the Arctic, *Climate Dynamics*, submitted.

Bonan, G.B., F.S. Chapin, and S.L. Thompson, Boreal forest and tundra ecosystems as components of the climate system, *Climatic Change*, *29* (2), 145-167, 1995.

Bousquet, P., P. Peylin, P. Ciais, M. Ramonet, and P. Monfray, Inverse modeling of annual atmospheric CO_2 sources and sinks 2. Sensitivity study, *Journal of Geophysical Research-Atmospheres*, *104* (D21), 26179-26193, 1999.

Box, E.O., Predicting physiognomic vegetation types with climate variables, *Vegetatio*, *45* (2), 127-139, 1981.

Brook, E.J., S. Harder, J. Severinghaus, E.J. Steig, and C.M. Sucher, On the origin and timing of rapid changes in atmospheric methane during the last glacial period, *Global Biogeochemical Cycles*, *14* (2), 559-572, 2000.

Brooks, J.R., L.B. Flanagan, N. Buchmann, and J.R. Ehleringer, Carbon isotope composition of boreal plants: Functional grouping of life forms, *Oecologia*, *110* (3), 301-311, 1997.

Buchmann, N., R.J. Brooks, L.B. Flanagan, and J.R. Ehleringer, Carbon isotope discrimination of terrestrial ecosystems, in *Stable Isotopes*, edited by H. Griffiths, BIOS Scientific Publishers, Oxford, 1998.

Buchmann, N., and J.O. Kaplan, Carbon isotope discrimination of terrestrial ecosystems - how well do observed and modeled results match?, in *Global Biogeochemical Cycles in the Climate System*, edited by E.-D. Schulze, D.S. Schimel, and I.C. Prentice, Academic Press, in press.

Canadell, J., R.B. Jackson, J.R. Ehleringer, H.A. Mooney, O.E. Sala, and E.D. Schulze, Maximum rooting depth of vegetation types at the global scale, *Oecologia*, *108* (4), 583-595, 1996.

Chapin, F.I., M. Bret-Harte, S. Hobbie, and H. Zhong, Plant functional types as predictors of transient responses of Arctic vegetation to global change, *Journal of Vegetation Science*, *7* (3), 347-358, 1995.

Chapman, S.J., and M. Thurlow, The influence of climate on CO_2 and CH_4 emissions from organic soils, *Agricultural and Forest Meteorology*, *79* (4), 205-217, 1996.

Chappellaz, J., D. Raynaud, T. Blunier, and B. Stauffer, The ice core record of atmospheric methane, in *Atmospheric Methane*, edited by M.A.K. Khalil, pp. 9-24, Springer-Verlag, Berlin, 2000.

Chappellaz, J.A., I.Y. Fung, and A.M. Thompson, The atmospheric CH_4 increase since the Last Glacial Maximum (1). Source estimates, *Tellus Series B-Chemical and Physical Meteorology*, *45* (3), 228-241, 1993.

Christensen, T.R., S. Jonasson, T.V. Callaghan, and M. Havstrom, On the potential CO_2 release from tundra soils in a changing climate, *Applied Soil Ecology*, *11* (2-3), 127-134, 1999.

Christensen, T.R., I.C. Prentice, J. Kaplan, A. Haxeltine, and S. Sitch, Methane flux from northern wetlands and tundra - An ecosystem source modelling approach, *Tellus Series B-Chemical and Physical Meteorology*, *48* (5), 652-661, 1996.

Ciais, P., P.P. Tans, M. Trolier, J.W.C. White, and R.J. Francey, A large northern hemisphere terrestrial CO_2 sink indicated by the $^{13}C/^{12}C$ ratio of atmospheric CO_2, *Science*, *269* (5227), 1098-1102, 1995a.

Ciais, P., P.P. Tans, J.W.C. White, M. Trolier, R.J. Francey, J.A. Berry, D.R. Randall, P.J. Sellers, J.G. Collatz, and D.S. Schimel, Partitioning of ocean and land uptake of CO_2 as inferred by $\delta^{13}C$ measurements from the NOAA Climate Monitoring and Diagnostics Laboratory Global Air Sampling Network, *Journal of Geophysical Research-Atmospheres*, *100* (D3), 5051-5070, 1995b.

Clark, C.D., J.K. Knight, and J.T. Gray, Geomorphological reconstruction of the Labrador Sector of the Laurentide Ice Sheet, *Quaternary Science Reviews*, *19* (13), 1343-1366, 2000.

Collatz, G.J., M. Ribas-Carbo, and J.A. Berry, Coupled photosynthesis stomatal conductance model for leaves of C_4 plants, *Australian Journal of Plant Physiology*, *19* (5), 519-538, 1992.

Cowling, S.A., Simulated effects of low atmospheric CO_2 on structure and composition of North American vegetation at the last glacial maximum, *Global Ecology and Biogeography*, *8*, 81-93, 1999.

Cowling, S.A., Plant-climate interactions over historical and geological time, Ph.D. thesis, Lund University, Lund, 2000.

Cox, P.M., R.A. Betts, C.D. Jones, S.A. Spall, and I.J. Totterdell, Acceleration of global warming due to carbon-cycle feedbacks in a coupled climate model, *Nature*, 408, 184-187, 2000.

Cramer, W., A. Bondeau, F.I. Woodward, I.C. Prentice, R.A. Betts, V. Brovkin, P.M. Cox, V. Fisher, J.A. Foley, A.D. Friend, C. Kucharik, M.R. Lomas, N. Ramankutty, S. Sitch, B. Smith, A. White, and C. Young-Molling, Global response of terrestrial ecosystem structure and function to CO_2 and climate change: Results from six dynamic global vegetation models, *Global Change Biology*, in press.

Crutzen, P.J., and C. Bruhl, A model study of atmospheric temperatures and the concentrations of ozone, hydroxyl, and some other photochemically active gases during the glacial, the preindustrial Holocene and the present, *Geophysical Research Letters*, *20* (11), 1047-1050, 1993.

Dällenbach, A., T. Blunier, J. Flückiger, B. Stauffer, J. Chappellaz, and D. Raynaud, Changes in the atmospheric CH_4 gradient between Greenland and Antarctica during the Last Glacial and the transition to the Holocene, *Geophysical Research Letters*, *27* (7), 1005-1008, 2000.

Darwin, C., *Journal of Researches into the Natural History and Geology of the Countries visited during the Voyage of H.M.S. Beagle round the World*, John Murray, London, 1845.

de Noblet, N.I., C. Prentice, S. Joussaume, D. Texier, A. Botta, and A. Haxeltine, Possible role of atmosphere-biosphere interactions in triggering the last glaciation, *Geophysical Research Letters*, *23* (22), 3191-3194, 1996.

Donovan, L., and J. Ehleringer, Carbon isotope discrimination, water-use efficiency, growth, and mortality in a natural shrub population, *Oecologia*, *100*, 347-354, 1994.

Edwards, M.E., P.M. Anderson, L.B. Brubaker, T. Ager, A.A. Andreev, N.H. Bigelow, L.C. Cwynar, W.R. Eisner, S.P. Harrison, F.-S. Hu, D. Jolly, A.V. Lozhkin, G.M. McDonald, C.J. Mock, J.C. Ritchie, A.V. Sher, R.W. Spear, J. Williams, and G. Yu, Pollen-based biomes for Beringia 18,000, 6000 and 0 ^{14}C yr B.P., *Journal of Biogeography*, in press.

Ehleringer, J.R., Z.F. Lin, C.B. Field, G.C. Sun, and C.Y. Kuo, Leaf carbon isotope ratios of plants from a subtropical monsoon forest, *Oecologia*, *72*, 109-114, 1987.

FAO, Digital Soil Map of the World and Derived Soil Properties, Food and Agriculture Organization, Rome, 1995.

Farquhar, G., On the nature of carbon isotope discrimination in C_4 species, *Australian Journal of Plant Physiology*, *10*, 205-226, 1983.

Farquhar, G., M. O'Leary, and J.A. Berry, On the relationship between carbon isotope discrimination and the intercellular carbon dioxide concentration in leaves, *Australian Journal of Plant Physiology*, *9*, 121-137, 1982.

Farquhar, G.D., S.V. Caemmerer, and J.A. Berry, A biochemical model of photosynthetic CO_2 assimilation in leaves of C_3 species, *Planta*, *149* (1), 78-90, 1980.

Flanagan, L.B., and A.R. Ehleringer, Ecosystem-atmosphere CO_2 exchange: interpreting signals of change using stable isotope ratios, *Trends in Ecology & Evolution*, *13* (1), 10-14, 1998.

Foley, J.A., Net primary productivity in the terrestrial biosphere: the application of a global model, *Journal of Geophysical Research-Atmospheres*, *99* (D10), 20773-20783, 1994.

Foley, J.A., J.E. Kutzbach, M.T. Coe, and S. Levis, Feedbacks between climate and boreal forests during the Holocene epoch, *Nature*, *371* (6492), 52-54, 1994.

Foley, J.A., I.C. Prentice, N. Ramankutty, S. Levis, D. Pollard, S. Sitch, and A. Haxeltine, An integrated biosphere model of land surface processes, terrestrial carbon balance, and vegetation dynamics, *Global Biogeochemical Cycles*, *10* (4), 603-628, 1996.

Fung, I., C.B. Field, J.A. Berry, M.V. Thompson, J.T. Randerson, C.M. Malmstrom, P.M. Vitousek, G.J. Collatz, P.J. Sellers, D.A. Randall, A.S. Denning, F. Badeck, and J. John, Carbon 13 exchanges between the atmosphere and biosphere, *Global Biogeochemical Cycles*, *11* (4), 507-533, 1997.

Gorham, E., Biogeochemistry: its origins and development, *Biogeochemistry*, *13* (3), 199-239, 1991.

Guehl, J., A. Domenach, M. Bereau, T. Barigah, H. Casabianca, A. Ferhi, and J. Garbaye, Functional diversity in an Amazonian rainforest of French Guyana: a dual isotope approach ($\delta^{15}N$ and $\delta^{13}C$), *Oecologia*, *116*, 316-330, 1998.

Guiot, J., F. Torre, R. Cheddadi, O. Peyron, P. Tarasov, D. Jolly, and J.O. Kaplan, The climate of the Mediterranean basin and of Eurasia of the last glacial maximum as reconstructed by inverse vegetation modelling and pollen data, *Ecologia Mediterranea*, *25* (2), 193-204, 1999.

Hallgren, W.S., and A.J. Pitman, The uncertainty in simulations by a global biome model (BIOME3) to alternative parameter values, *Global Change Biology*, *6* (5), 483-496, 2000.

Hanebuth, T., K. Stattegger, and P.M. Grootes, Rapid flooding of the Sunda Shelf: A late-glacial sea-level record, *Science*, *288*, 1033-1035, 2000.

Hattersley, P.W., The distribution of C_3 and C_4 grasses in Australia in relation to climate, *Oecologia*, *57* (1-2), 113-128, 1983.

Haxeltine, A., and I.C. Prentice, BIOME3: an equilibrium terrestrial biosphere model based on ecophysiological constraints, resource availability, and competition among plant functional types, *Global Biogeochemical Cycles*, *10* (4), 693-709, 1996.

Haywood, A., P. Valdes, B. Sellwood, and J. Kaplan, Antarctica during the middle Pliocene: A modelling perspective, *Palaeogeography, Palaeoclimatology, Palaeoecology*, in press.

Heimann, M., G. Esser, A. Haxeltine, J. Kaduk, D.W. Kicklighter, W. Knorr, G.H. Kohlmaier, A.D. McGuire, J. Melillo, B. Moore, III., R.D. Otto, I.C. Prentice, W. Sauf, A. Schloss, S. Sitch, U. Wittenberg, and G. Würth, Evaluation of terrestrial carbon cycle models through simulations of the cycle of atmospheric CO_2: first results of a model intercomparison study, *Global Biogeochemical Cycles*, *12* (1), 1 - 24, 1998.

Holdridge, L.R., Determination of world formations from simple climatic data, *Science*, *105*, 367-368, 1947.

Houweling, S., F. Dentener, J. Lelieveld, B. Walter, and E. Dlugokencky, The modeling of tropospheric methane: How well can point measurements be reproduced by a global model?, *Journal of Geophysical Research-Atmospheres*, *105* (D7), 8981-9002, 2000.

Hutchin, P.R., M.C. Press, J.A. Lee, and T.W. Ashenden, Elevated concentrations of CO_2 may double methane emissions from mires, *Global Change Biology*, *1* (2), 125-128, 1995.

Jackson, R.B., J. Canadell, J.R. Ehleringer, H.A. Mooney, O.E. Sala, and E.D. Schulze, A global analysis of root distributions for terrestrial biomes, *Oecologia*, *108* (3), 389-411, 1996.

Jolly, D., and A. Haxeltine, Effect of low glacial atmospheric CO_2 on tropical African montane vegetation, *Science*, *276*, 786-788, 1997.

Joussaume, S., Modeling extreme climates of the past 20.000 years with general circulation models, in *Modeling the Earth's Climate and its Variability*, edited by W.R. Holland, S. Joussaume, and F. David, Elsevier, Amsterdam, 1999.

Kaminski, T., R. Giering, and M. Heimann, Sensitivity of the seasonal cycle of CO_2 at remote monitoring stations with respect to seasonal surface exchange fluxes determined with the adjoint of an atmospheric transport model, *Physics and Chemistry of the Earth*, *21* (5-6), 457-462, 1996.

Keeling, C.D., The concentration and isotopic abundances of carbon dioxide in rural and marine air, *Geochimica et Cosmochimica Acta*, *24*, 277-298, 1961.

Kennett, J.P., K.G. Cannariato, I.L. Hendy, and R.J. Behl, Carbon isotopic evidence for methane hydrate instability during quaternary interstadials, *Science*, *288* (5463), 128-133, 2000.

Kicklighter, D.W., M. Bruno, S. Donges, G. Esser, M. Heimann, J. Helfrich, F. Ift, F. Joos, J. Kaduk, G.H. Kohlmaier, A.D. McGuire, J.M. Melillo, R. Meyer, B. Moore, III, A. Nadler, I.C. Prentice, W. Sauf, A.L. Schloss, S. Sitch, U. Wittenberg, and G. Wurth, A first-order analysis of the potential role of CO_2 fertilization to affect the global carbon budget: a comparison of four terrestrial biosphere models, *Tellus Series B-Chemical and Physical Meteorology*, *51* (2), 343-366, 1999.

Kloeppel, B.D., S.T. Gower, I.W. Treichel, and S. Kharuk, Foliar carbon isotope discrimination in *Larix* species and sympatric evergreen conifers: a global comparison, *Oecologia*, *114* (2), 153-159, 1998.

Kohfeld, K.E., and S.P. Harrison, How well can we simulate past climates? Evaluating the models using global palaeoenvironmental datasets, *Quaternary Science Reviews*, *19* (1-5), 321-346, 2000.

Köppen, W., *Das Geographisches System der Klimate*, 44 pp., Gebrüder Borntrager, Berlin, 1936.

Körner, C., G.D. Farquhar, and S.C. Wong, Carbon isotope discrimination by plants follows latitudinal and altitudinal trends, *Oecologia*, *88* (1), 30-40, 1991.

Küchler, A.W., A physiognomic classification of vegetation, *Annals of the Association of American Geographers*, *39*, 201-210, 1949.

Kutzbach, J., R. Gallimore, S. Harrison, P. Behling, R. Selin, and F. Laarif, Climate and biome simulations for the past 21,000 years, *Quaternary Science Reviews*, *17* (6-7), 473-506, 1998.

Larcher, W., *Physiological plant ecology: ecophysiology and stress physiology of functional groups*, Springer-Verlag, New York, Berlin, Heidelberg, 1995.

Leemans, R., and W.P. Cramer, The IIASA Database for Mean Monthly Values of Temperature, Precipitation, and Cloudiness on a Global Terrestrial Grid, pp. 62, International Institute for Applied Systems Analysis, Laxenberg, 1991.

Likens, G.E., F.H. Bormann, R.S. Pierce, J.S. Eaton, and N.M. Johnson, *Biogeochemistry of a Forested Ecosystem*, Springer-Verlag, New York, 1977.

Lloyd, J., and G.D. Farquhar, ^{13}C discrimination during CO_2 assimilation by the terrestrial biosphere, *Oecologia*, *99* (3-4), 201-215, 1994.

Lloyd, J., and J.A. Taylor, On the temperature dependence of soil respiration, *Functional Ecology*, *8* (3), 315-323, 1994.

MacDonald, G.M., A.A. Velichko, C.V. Kremenetski, O.K. Borisova, A.A. Goleva, A.A. Andreev, L.C. Cwynar, R.T. Riding, S.L. Forman, T.W.D. Edwards, R. Aravena, D. Hammarlund, J.M. Szeicz, and V.N. Gattaulin, Holocene treeline history and climate change across northern Eurasia, *Quaternary Research*, *53* (3), 302-311, 2000.

Mahowald, N., K. Kohfeld, M. Hansson, Y. Balkanski, S.P. Harrison, I.C. Prentice, M. Schulz, and H. Rodhe, Dust sources and deposition during the last glacial maximum and current climate: A comparison of model results with paleodata from ice cores and marine sediments, *Journal of Geophysical Research-Atmospheres*, *104* (D13), 15895-15916, 1999.

Martinerie, P., G.P. Brasseur, and C. Granier, The chemical composition of ancient atmospheres: a model study constrained by ice core data, *Journal of Geophysical Research-Atmospheres*, *100* (D7), 14291-14304, 1995.

McGuire, A.D., S. Sitch, J.S. Clein, R. Dargaville, G. Esser, J. Foley, F. Joos, J.O. Kaplan, D.W. Kicklighter, R.A. Meier, J.M. Melillo, B. Moore, III., I.C. Prentice, R. Ramankutty, T. Reichenau, A. Schloss, H. Tian, L.J. Williams, and U. Wittenberg, Carbon balance of the terrestrial biosphere in the twentieth century: Analyses of CO_2, climate and land-use effects with four process-based ecosystem models, *Global Biogeochemical Cycles*, in press.

Michelsen, A., S. Jonasson, D. Sleep, M. Havström, and T.V. Callaghan, Shoot biomass, $\delta^{13}C$, nitrogen and chlorophyll responses of two Arctic dwarf shrubs to in situ shading, nutrient application and warming simulating climatic change, *Oecologia*, *105* (1), 1-12, 1996.

Neilson, R., I. Prentice, B. Smith, T. Kittel, and D. Viner, Simulated changes in vegetation distribution under global warming, in *The Regional Impacts of Climate Change*, edited by R. Watson, M. Zinyowera, R. Moss, and D. Dokken, pp. 439-456, Cambridge University Press, Cambridge, 1998.

Neilson, R.P., A model for predicting continental-scale vegetation distribution and water balance, *Ecological Applications*, *5*, 362-385, 1995.

Nisbet, E.G., The end of the Ice Age, *Canadian Journal of Earth Sciences*, *27* (1), 148-157, 1990.

Oechel, W., S. Hastings, G. Vourlitis, M. Jenkins, G. Riechers, and N. Grulke, Recent change of Arctic tundra ecosystems from a net carbon dioxide sink to a source, *Nature*, *361*, 520-523, 1993.

Osmond, C., H. Ziegler, W. Stichler, and P. Trimborn, Carbon isotope discrimination in alpine succulent plants supposed to be capable of crassulacean acid metabolism (CAM), *Oecologia*, *18*, 209-217, 1975.

Petit-Maire, N., M. Fontugne, and C. Rouland, Atmospheric methane ratio and environmental changes in the Sahara and Sahel during the last 130 kyrs, *Palaeogeography Palaeoclimatology Palaeoecology*, *86* (1-2), 197-204, 1991.

Pinot, S., G. Ramstein, S.P. Harrison, I.C. Prentice, J. Guiot, M. Stute, S. Joussaume, and P.p. groups, Tropical paleoclimates at the Last Glacial Maximum: comparison of Paleoclimate Modeling Intercomparison Project (PMIP) simulations and paleodata, *Climate Dynamics*, *15*, 857-874, 1999.

Pinto, J.P., and M.A.K. Khalil, The stability of tropospheric OH during ice ages, inter-glacial epochs and modern times, *Tellus Series B-Chemical and Physical Meteorology*, *43* (5), 347-352, 1991.

Prentice, I.C., W. Cramer, S.P. Harrison, R. Leemans, R.A. Monserud, and A.M. Solomon, A global biome model based on plant physiology and dominance, soil properties and climate, *Journal of Biogeography*, *19*, 117-134, 1992.

Prentice, I.C., J. Guiot, B. Huntley, D. Jolly, and R. Cheddadi, Reconstructing biomes from palaeoecological data: a general method and its application to European pollen data at 0 and 6 ka, *Climate Dynamics*, *12*, 185-194, 1996.

Prentice, I.C., D. Jolly, and BIOME6000 participants, Mid-Holocene and glacial-maximum vegetation geography of the northern continents, *Journal of Biogeography*, in press.

Prentice, I.C., and T. Webb, III., BIOME 6000: reconstructing global mid-Holocene vegetation patterns from palaeoecological records, *Journal of Biogeography*, *25*, 997-1005, 1998.

Rathgeber, C., A. Nicault, J. Guiot, J.O. Kaplan, and P. Roche, Simulated responses of Pinus halepensis forest productivity to climate change and CO_2 increase using a biogeochemistry model, *Global Change Biology*, submitted.

Ridgwell, A.J., S.J. Marshall, and K. Gregson, Consumption of atmospheric methane by soils: A process-based model, *Global Biogeochemical Cycles*, *13* (1), 59-70, 1999.

Running, S.W., and E.R. Hunt, Generalization of a forest ecosystem process model for other biomes, BIOME-BGC, and an application for global-scale models, in *Scaling Processes Between Leaf and Landscape Levels*, edited by J.R. Ehleringer, and C. Field, pp. 141-158, Academic Press, San Diego, 1993.

Schimel, D., D. Alves, I. Enting, M. Heimann, F. Joos, D. Raynaud, T. Wigley, M. Prather, R. Derwent, D. Ehhalt, P. Fraser, E. Sanhueza, X. Zhou, P. Jonas, R. Charlson, H. Rodhe, S. Sadasivan, K.P. Shine, Y. Fouquart, V. Ramaswamy, S. Solomon, J. Srinivasan, D. Albritton, R. Derwent, I. Isaksen, M. Lal, and D. Wuebbles, Radiative forcing of climate change, in *Climate Change 1995: The Science of Climate Change*, edited by J.T. Houghton, L.G. Meira Filho, B.A. Callander, N. Harris, A. Kattenberg, and K. Maskell, pp. 65-131, Cambridge University Press, Cambridge, 1996.

Schimel, D., J. Melillo, H.Q. Tian, A.D. McGuire, D. Kicklighter, T. Kittel, N. Rosenbloom, S. Running, P. Thornton, D. Ojima, W. Parton, R. Kelly, M. Sykes, R. Neilson, and B. Rizzo, Contribution of increasing CO_2 and climate to carbon storage by ecosystems in the United States, *Science*, *287* (5460), 2004-2006, 2000.

Schimper, A.F.W., *Plant-Geography Upon a Physiological Basis*, Clarendon Press, Oxford, 1903.

Schulze, E.-D., R. Ellis, W. Schulze, and P. Trimborn, Diversity, metabolic types and $\delta^{13}C$ carbon isotope ratios in the grass flora of Namibia in relation to growth form, precipitation and habitat conditions, *Oecologia*, *106* (3), 352-369, 1996.

Schulze, E.-D., R. Williams, G. Farquhar, W. Schulze, J. Langridge, J. Miller, and B. Walker, Carbon and nitrogen isotope discrimination and nitrogen nutrition of trees along a rainfall gradient in northern Australia, *Australian Journal of Plant Physiology*, *25*, 413-425, 1998.

Shafer, S., Potential Vegetation Response to Future Climate Change in Western North America and Its Implications for Biological Conservation and Geographical Conceptualizations of Place, Ph.D. thesis, University of Oregon, Eugene, 2000.

Sitch, S., The Role of Vegetation Dynamics in the Control of Atmospheric CO_2 Content, Ph.D. thesis, Lund University, Lund, 2000.

Six, K., and E. Maier-Reimer, Effects of plankton dynamics on seasonal carbon fluxes in an ocean general circulation model, *Global Biogeochemical Cycles*, *10* (4), 559-583, 1996.

Tarasov, P.E., D. Jolly, and J.O. Kaplan, A continuous Late Glacial and Holocene record of vegetation changes in Kazakhstan, *Palaeogeography, Palaeoclimatology, Palaeoecology*, *136*, 281-292, 1997.

TEMPO members, The potential role of vegetation feedback in the climate sensitivity of high-latitude regions: a case study at 6000 years before present, *Global Biogeochemical Cycles*, *10* (4), 727-736, 1996.

Thompson, A.M., J.A. Chappellaz, I.Y. Fung, and T.L. Kucsera, The atmospheric CH_4 increase since the Last Glacial Maximum (2). Interactions with oxidants, *Tellus Series B-Chemical and Physical Meteorology*, *45* (3), 242-257, 1993.

VEMAP members, Vegetation/ecosystem modeling and analysis project: Comparing biogeography and biogeochemistry models in a continental-scale study of terrestrial ecosystem responses to climate-change and CO_2 doubling, *Global Biogeochemical Cycles*, *9* (4), 407-437, 1995.

von Humboldt, A., *Aspects of Nature, in Different Lands and Different Climates; With Scientific Elucidations*, Lea and Blanchard, Philadelphia, 1850.

Walter, H., *Vegetation of the Earth in Relation to Climate and the Eco-Physiological Conditions*, Springer-Verlag, New York, 1973.

Walter, H., E. Harnickell, and D. Mueller-Dombois, *Climate-diagram Maps*, Springer-Verlag, Berlin, Heidelberg, 1975.

Webb, T., III, P.J. Bartlein, S.P. Harrison, and K.H. Anderson, Vegetation, lake levels and climate in eastern North America for the past 18,000 years, in *Global changes since the last glacial maximum*, edited by H.E. Wright, Jr, J.E. Kutzbach, T. Webb, III, W.F. Ruddiman, F.A. Street-Perrott, and P.J. Bartlein, pp. 415-467, University of Minnesota Press, Minneapolis, 1993.

Whiting, G.J., and J.P. Chanton, Primary production control of methane emission from wetlands, *Nature*, *364*, 794-795, 1993.

Williams, J.W., R.L. Summer, and T. Webb, III, Applying plant functional types to construct biome maps from eastern North American pollen data: comparisons with model results, *Quaternary Science Reviews*, *17*, 607 - 627, 1998.

Woodward, F.I., *Climate and plant distribution*, 174 pp., Cambridge University Press, Cambridge, 1987.

Woodward, F.I., and B.G. Williams, Climate and plant distribution at global and local scales, *Vegetatio*, *69* (1-3), 189-197, 1987.

Worthy, D.E.J., I. Levin, F. Hopper, M.K. Ernst, and N.B.A. Trivett, Evidence for a link between climate and northern wetland methane emissions, *Journal of Geophysical Research-Atmospheres*, *105* (D3), 4031-4038, 2000.

2 Climate change and Arctic ecosystems II
Modeling, paleodata-model comparisons, and future projections

J.O. Kaplan[1,2], N.H. Bigelow[3], P.J. Bartlein[4], T.R. Christensen[5], W. Cramer[6], S.P. Harrison[1,7], N.V. Matveyeva[8], A.D. McGuire[9], D.F. Murray[10], I.C. Prentice[1], V.Y. Razzhivin[8], B. Smith[5], D.A. Walker[11,12], P.M. Anderson[13], A.A. Andreev[14], L.B. Brubaker[15], M.E. Edwards[12,16], A.V. Lozhkin[17], and J.C. Ritchie[18]

[1]Max Planck Institute for Biogeochemistry, Jena, Germany
[2]Plant Ecology, Department of Ecology, Lund University, Lund, Sweden
[3]Alaska Quaternary Center, University of Alaska Fairbanks, Fairbanks, USA
[4]Department of Geography, University of Oregon, Eugene, USA
[5]Climate Impacts Group, Department of Ecology, Lund University, Sweden
[6]Potsdam Institute for Climate Impacts Research, Potsdam, Germany
[7]Dynamic Paleoclimatology, Lund University, Lund, Sweden
[8]Department of Vegetation of the Far North, Komarov Botanical Institute, St. Petersburg, Russia
[9]Department of Biology and Wildlife, University of Alaska Fairbanks, Fairbanks, USA
[10]University of Alaska Museum, Fairbanks, USA
[11]Institute of Arctic and Alpine Research, University of Colorado, Boulder, USA
[12]Institute of Arctic Biology, University of Alaska Fairbanks, Fairbanks, USA
[13]Quaternary Research Center, University of Washington, Seattle, USA
[14]Alfred Wegner Institute for Polar and Marine Research, Potsdam, Germany
[15]College of Forest Resources, University of Washington, Seattle, USA
[16]Department of Geography, NTNU-Trondheim, Dragvoll Campus, Trondheim, Norway
[17]Northeast Interdisciplinary Scientific Research Institute, Russian Academy of Sciences, Far East Branch, Magadan, Russia
[18]Pebbledash Cottage, Corfe, Taunton, Somerset, UK

Abstract. Large variations in the composition and structure of Arctic ecosystems are determined by climatic gradients, especially of growing-season warmth, soil moisture and snow cover. Structural differences influence water, energy and carbon exchange characteristics. A unified circumpolar classification of tundra types was adopted and shown to reflect bioclimatic controls on plant-type dominance and primary production. These controls were incorporated in the biogeochemistry-biogeography model BIOME4. Present-day vegetation patterns (forest types, tundra types, and the location of the forest-tundra boundary) north of 55°N were generally well simulated. Climate model experiments for the last glacial maximum (LGM) and mid-Holocene (6000 yr BP) were used to modify the baseline simulation and thus to simulate past vegetation patterns. Results were compared with paleovegetation data derived from pollen data [*Bigelow et al.*, submitted]. Simulations with prescribed sea-surface temperatures showed a large range of high-latitude cooling on unglaciated land at the LGM. The observed prevalence of dwarf-

shrub and graminoid-forb tundra and the restricted extent of low- and high-shrub tundra were nevertheless reproduced. The simulated graminoid-forb tundra was 1.5 to 2.5 times more productive than its (spatially restricted) modern equivalents, due to lower latitude and reduced cloud cover. Although orbital changes produced a substantial, zonally symmetric increase in summer and annual insolation at 6000 yr BP relative to the present day, results obtained with coupled atmosphere-ocean models for 6000 yr BP correctly show that mid-Holocene treeline extension was modest and zonally asymmetrical, with maximal extension (on the order of 300 km) in central Siberia and little or no change in Alaska. Projection of the effect of a continued exponential increase in atmospheric greenhouse gas concentration based on a transient coupled simulation suggests a potential for larger changes in Arctic ecosystems during the 21st century than have occurred between 6000 yr BP and present. Simulated physiological effects of the CO_2 increase (to > 700 ppm) at high latitudes were slight compared with the effects of the simulated change in climate.

2.1 Introduction

High-latitude ecosystems are an important component of the global energy balance and carbon budget [*Bonan*, 1995; *Chapin et al.*, 1995a; *Chapin et al.*, 2000; *Christensen et al.*, 1999; *Foley et al.*, 1994; *Oechel et al.*, 1993]. Nevertheless, high-latitude vegetation has been simplistically treated in global modeling and global analyses of paleodata which have commonly lumped these ecosystems as a single biome, "tundra". Differentiation among high-latitude vegetation types is important because there are in fact large structural differences among vegetation types and these would be expected to have a strong influence on land-surface properties, including surface albedo, roughness, and conductance to water vapor.

The Pan-Arctic INitiative (PAIN) has taken a comprehensive approach to describing and modeling terrestrial ecosystems of the northern high latitudes. The philosophy of PAIN has been to base models not only on modern understanding and observations, but also to test the models at key times in the past where validation against paleodata is possible. A robust, validated model can be applied with some confidence to make projections about the sensitivity of Arctic vegetation to possible future changes. By performing analyses of past and possible future changes in parallel and using paleodata as a check we aim to make statements about the sensitivity of Arctic ecosystems to climate change that are more strongly scientifically justified than statements based soley on contemporary observations and modeling. The selection of key times for model evaluation with paleodata (mid-Holocene, 6000 yr BP; Last Glacial Maximum, 21 000 yr BP) follows the Paleoclimate Modelling Intercomparison Project (PMIP), because of the major focus on these times both in paleoclimate modeling and data synthesis in PMIP and in other projects [*Harrison*, 2000; *Joussaume and Taylor*, 2000; *Kohfeld and Harrison*, 2000]. A future projection, used as an illustrative example, used one of the same coupled atmo-

sphere-ocean models used in the mid-Holocene simulations, with a greenhouse gas (GHG) forcing assumed to follow a "business as usual" (IS92a) scenario with continuing exponential increase in GHG concentrations up to the end of the 21st century.

We present a new, standardized classification of Arctic vegetation at the biome level which may be identified floristically in the field and in pollen records, and simulated using a global vegetation model. We apply the model to four times: the present-day, the Last Glacial Maximum (LGM), the mid-Holocene, and 100 years into a hypothetical future with unchecked GHG increase and the climate change that this implies. We compare the modeled vegetation result to a map of present day vegetation distribution based on satellite and field observations, and to paleovegetation distributions inferred from pollen spectra. The future scenario then allows us to assess the sensitivity of Arctic vegetation to anthropogenic change in atmospheric CO_2 concentration and climate.

2.2 Methods

2.2.1 Classification of tundra vegetation types

Most previous classifications of tundra vegetation types have been based on species assemblages and tailored to specific regions. Application of these schemes outside the region for which they were designed can be problematic. Furthermore, widely used but loosely-defined terms, such as "high Arctic", "subarctic", and "polar desert" have geographical connotations which cause confusion especially when applied to the radically different environmental conditions of the past. We have therefore adopted a new classification scheme for tundra vegetation types at the biome level [*Walker*, 2000]. Each biome is defined in terms of physical structure and dominant life forms, with the additional requirement that each biome must be floristically distinguishable, both in modern vegetation and in pollen-based reconstructions of paleovegetation. Given that species-level recognition of pollen is not often possible, the requirement that a biome can be reconstructed from pollen data is a strong constraint but it greatly increases the usefulness of the classification system by allowing modern and paleo-observations to be analyzed in a compatible way. Finally, we required that each biome occupy a unique and definable bioclimate space, so that the classification scheme could be translated into a set of limiting environmental factors for implementation in a model.

Our scheme (Table 2.1) distinguishes five tundra biomes: cushion forb, lichen and moss tundra; graminoid and forb tundra; prostrate dwarf-shrub tundra; erect dwarf-shrub tundra; and low- and high-shrub tundra. Although it is possible to distinguish low-shrub and high-shrub tundra on physical grounds, and it might be important to make such a distinction in the context of land-surface interactions

Table 2.1. Circumpolar tundra biome classification

Biome	Definition	Typical taxa
Low- and high-shrub tundra	Continuous shrubland, 50 cm to 2 m tall, deciduous or evergreen, sometimes with tussock-forming graminoids and true mosses, bog mosses and lichens	*Alnus*, *Betula*, *Salix*, *Pinus pumila* (in eastern Siberia), *Eriophorum*, *Sphagnum*
Erect dwarf-shrub tundra	Continuous shrubland 2 to 50 cm tall, deciduous or evergreen, with graminoids, true mosses, and lichens	*Betula*, *Cassiope*, *Empetrum*, *Salix*, *Vaccinium*, Gramineae, Cyperaceae
Prostrate dwarf-shrub tundra	Discontinuous shrubland of prostrate deciduous shrubs 0 to 2 cm tall	*Salix*, *Dryas*, *Pedicularis*, *Asteraceae*, *Caryophyllaceae*, Gramineae, true mosses
Cushion forb, lichen, and moss tundra	Discontinuous cover of rosette plants or cushion forbs with lichens and mosses	*Saxifragaceae*, *Caryophyllaceae*, *Papaver*, *Draba,* lichens, true mosses
Graminoid and forb tundra	Predominantly herbaceous vegetation dominated by forbs, graminoids, true mosses, and lichens	*Artemisia*, *Kobresia*, *Brassicaceae*, *Asteraceae*, *Caryophyllaceae*, Gramineae, true mosses

with the atmosphere, it is not possible to distinguish these two vegetation types floristically and we therefore do not attempt to do so.

Fig. 2.1 was developed initially as a topology, based on field experience; quantitative expressions of the boundaries between biomes were developed empirically through the process of model development. The tundra biomes form a sequence along the gradient of accumulated growing-season temperature (expressed here as the growing degree days above 0°C: GDD_0). The various forms of shrub-tundra are replaced by graminoid and forb tundra in dry habitats, especially areas that are regularly denuded of snow. Graminoid and forb tundra occurs with progressively higher levels of soil moisture as the growing season temperature sum decreases. Figure 2.1 also shows the bioclimatic relationship between the tundra biomes and other high- to mid-latitude biomes: specifically boreal and temperate forests, temperate grasslands, and temperate xerophytic shrublands. The limits of temperate grassland and xerophytic shrubland are expressed in terms of soil moisture and GDD criteria. The boundary between tundra and boreal forests is expressed as a function of net primary productivity (NPP). Under modern climate conditions in the Arctic, forest NPP is highly correlated with GDD [*Gower et al.*, 1997; *Schulze et al.*, 1999]. However, the definition of this limit in terms of NPP is somewhat more mechanistic as it reflects the requirement for a minimum carbon balance to sustain the growth of trees. Furthermore, the use of NPP as a limit on tree growth may provide a more realistic way of simulating treeline in the past under lowered atmo-

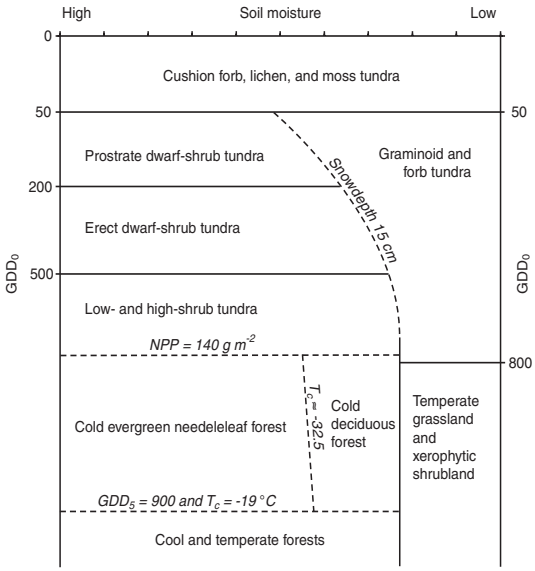

Fig. 2.1. Climate space occupied by the Arctic biomes defined in BIOME4

spheric CO_2 concentrations [*Arno and Hammerly*, 1984; *Cowling*, 1999; *Jolly and Haxeltine*, 1997; *Körner*, 1999; *MacDonald and Gajewski*, 1992; *Street-Perrott et al.*, 1997; *Tranquillini*, 1979; *Walter*, 1973].

2.2.2 The BIOME4 model

BIOME4 is an equilibrium terrestrial biosphere model derived from the BIOME3 model of Haxeltine and Prentice [1996a]. Like its predecessor, BIOME4 is a coupled carbon and water flux model that predicts global vegetation distribution, structure, and biogeochemistry, taking account of interactions among these aspects. The model is driven by long-term averages of monthly mean temperature and cloudiness and monthly total precipitation, and long-term values of absolute minimum temperature. In addition, the model requires information on soil texture and soil depth in order to determine water holding capacity and percolation rates.

The operation of BIOME4 at a global scale is based on 12 Plant Functional Types (PFTs), representing broad, physiologically distinct classes ranging from arctic cushion forbs to tropical rainforest trees [*Kaplan*, 2001]. Each PFT is assigned a limited set of bioclimatic limits which determine whether it is considered to be present in a given grid-cell, and therefore whether its potential net primary productivity (NPP) is calculated; and a set of parameter values which define its carbon and water exchange characteristics. The computational core of the model is a coupled carbon and water flux scheme, which determines the seasonal maximum leaf area

Table 2.2. Distinctive bioclimatic limits and physiological parameters for tundra PFTs. GDD_0, sum of GDD_0 required to grow a full canopy; R_s, presence of sapwood respiration; optratio, maximum attainable c_i/c_a ratio; *kk*, the Beer's law extinction coefficient; T_{pC3}, minimum mean monthly temperature for photosynthesis; T_{curve}, modifier to the curve response of photosynthesis to temperature; *Alloc*, modifier to the minimum allocation

PFT	Cold shrub	Cold graminoid or forb	Cushion forb
Bioclimatic limits			
min GDD_0 (°C)	50	50	
min snowdepth (cm)	15		
Physiological parameters			
Phenology	evergreen	summergreen	evergreen
GDD_0 (°C)		25	
R_s	yes	no	yes
optratio	0.9	0.75	0.8
kk	0.5	0.3	0.6
T_{pC3} (°C)	-7	-7	-12
T_{curve}	0.6	0.6	0.5
Alloc	1	1	1.5

index (LAI) that maximizes NPP for any given PFT, based on a daily time-step simulation of soil water balance and monthly calculations of canopy conductance, photosynthesis, and respiration [*Haxeltine and Prentice*, 1996a].

To choose the biome for a given grid cell, the model ranks the tree and non-tree PFTs that were calculated for that grid cell. The ranking is defined according to a rule-base defined from the computed biogeochemical variables, which include NPP, LAI, and mean annual soil moisture. The resulting ranked combinations of PFTs lead to an assignment to one of 27 biomes.

2.2.3 High-latitude PFTs and biomes in BIOME4

High-latitude biomes are represented in BIOME4 by combinations of a limited set of PFTs. Several of these PFTs have been recognized and used in earlier versions of the BIOME model (e.g. temperate grass, temperate needleleaf evergreen tree) [*Kaplan*, 2001]. Three PFTs (cold shrub, cold graminoid or forb, and cushion forb) used to distinguish the tundra biomes are newly defined here. Each of these tundra PFTs was assigned values of required model parameters (Table 2.2) based on available physiological information [see e.g. *Berry and Björkman*, 1980; *Berry and Downton*, 1982; *Ehleringer and Björkman*, 1977; *Farquhar and von Caemmerer*, 1982; *Kirschbaum and Farquhar*, 1984; *Körner*, 1999; *Larcher*, 1995] with supplementary limits inferred by comparison of species distributions with climate data. These tundra PFTs use the C_3 photosynthetic pathway and are shallow rooting, and suceptible to water stress and fire.

The non-tundra PFTs used by BIOME4 to simulated high latitude vegetation types include cold and temperate broadleaf and needleleaf trees, xerophytic shrubs, and temperate grasses. These PFTs are also defined by a set of bioclimatic limits and physiological parameters [*Kaplan*, 2001]. Where tree PFTs satisfy bioclimatic limits and NPP and soil moisture requirements, they always dominate over grass and shrub PFTs. Temperate xerophytic shrub and temperate grass PFTs may use both the C_3 and C_4 photosynthetic pathways; carbon gain is optimized for the pathway on a seasonal basis for grasses. All tree PFTs use C_3 photosynthesis. Other physiological parameters which vary among the tree PFTs are canopy architecture, root depth distribution, transpiration characteristics, phenology, leaf habit, and the reponse of photosynthesis and respiration to temperature.

Biomes are assigned on the basis of a rule-based scheme using the dominant PFT, in some cases the sub-dominant PFTs, and certain environmental limits (Fig. 2.1). Thus, there is no simple correspondence between the presence/absence of PFTs and the assignment of biomes in the model. This is an important conceptual difference between the modelling approach described here and the approach of reconstructing biomes from pollen using biomisation [e.g. *Bigelow et al.*, submitted], in which the complete set of available floristic information is used to diagnose the biome.

2.2.4 Climate scenarios

2.2.4.1 Baseline climatology

We used a long-term mean climatology for the late 20th century (CLIMATE 2.2) [*W. Cramer pers. comm.* 1998]. CLIMATE 2.2 is an update of Leemans and Cramer [1991]. This climatology was used for the modern vegetation simulation, and as the baseline for the other modeling experiments. Version 2.2 of CLIMATE includes more station data from sparsely populated regions and an improved estimation of elevational gradients of climate variables over several parts of the Earth compared to earlier versions of the dataset (see http://www.pik-potsdam.de/~cramer/climate.htm). The dataset was generated by interpolating long-term mean values for monthly temperatures and percent of potential sunshine hours, and for monthly total precipitation, from station data. The three-dimensional interpolation of the climate variables uses the method of thin-plate smoothing splines, in which elevation is an independent variable and variations of each variable with elevation are estimated internally from the data [*Hutchinson*, 1995; *Hutchinson and Bischof*, 1983]. The method of thin-plate smoothing splines is an appropriate technique for interpolating climate data from a sparse network of stations, and has been shown to minimize errors in areas of complex terrain relative to other methods [*Price et al.*, 2000]. The method yields functions which can be evaluated at any combination of geographic location and elevation. Here, the functions were calculated for each grid

cell of a 0.5° geographic grid at the modal elevation for each grid cell [*GETECH*, 1996]. The grid includes all land grid cells north of 55° N, including "virtual" land grid cells on the continental shelf areas that were exposed at the LGM. The LGM land mask was derived by tracing the contour of LGM sea level (-125 m) [*Fleming et al.*, 1998] on modern topography [*GETECH*, 1996].

An atmospheric CO_2 concentration of 324 ppm was used to force BIOME4 for the present-day baseline simulation. This is the mean [CO_2] during the period of measurement of the station data upon which the climatology is based.

2.2.4.2 Paleoclimate Simulations

We have made BIOME4 simulations for two key times in the past: the last glacial maximum (LGM, ca 21000 calendar yr BP) and the mid-Holocene (ca 6000 yr BP). These two periods have been a major focus for paleoclimate simulations [e.g. *Joussaume and Taylor*, 1995; *Joussaume and Taylor*, 2000; *Kohfeld and Harrison*, 2000] because they represent two extremes in climate forcing. At the LGM, the earth's orbital configuration was fairly similar to today but greenhouse gas concentrations were low [*Raynaud et al.*, 1993], northern-hemisphere ice sheets were expanded [*Denton and Hughes*, 1981] and sea level was therefore lower [*Fairbanks*, 1989]. In addition to the large changes in terrestrial geography, the ocean surface was significantly colder and the distribution of sea ice was expanded [*CLIMAP*, 1981]. The configuration of the earth's orbit was however substantially different from today (and LGM) during the early to mid-Holocene. The phasing of the precession (23 kyr) and obliquity (41 kyr) cycles has been such that the high latitudes of the northern hemisphere received a maximum in insolation (incoming solar radiation), both during boreal summer and annually, at ca. 11000 calendar yr BP. This anomaly decayed gradually towards the present. As a direct result of the changes in orbital forcing, many regions of the Arctic experienced summer temperatures considerably higher than present already during the early Holocene [see e.g. *Bradley*, 2000; *Elias*, 2001; *MacDonald et al.*, 2000; *Ritchie et al.*, 1983]. The Laurentide ice sheet, although substantially reduced from the LGM, was still sufficiently large to have a major downwind cooling effect during the early Holocene [*Harrison et al.*, 1992; *Mitchell et al.*, 1988]. Northern Europe and eastern North America therefore experienced a thermal maximum several thousand years after the insolation maximum [*Wright et al.*, 1993]. For this reason, investigations of the impact of insolation changes on climate have conventionally focused on 6000 yr BP, when the difference in orbital configuration was still large but the impact of the residual Laurentide ice sheet was small and essentially local.

Several atmospheric general circulation models (AGCMs) have performed identically-forced simulations of the LGM within the framework of the Paleoclimate Modelling Intercomparison Project (PMIP) [*Joussaume and Taylor*, 1995; *Joussaume and Taylor*, 2000]. In these simulations, orbital parameters were set to those appropriate for 21000 calendar yr BP [*Berger*, 1978], the extent and height of the ice

sheets was prescribed from Peltier [1994], land-sea distribution, sea-surface temperatures and the seasonally-varying distribution of sea ice were prescribed from CLIMAP [1981] and CO_2 concentrations was set to 200 ppm [*Raynaud et al.*, 1993]. Recent compilations of paleoceanographic data have suggested that the CLIMAP representation of the LGM ocean is incorrect in some respects. Seasonal changes in SSTs and sea-ice extent in the North Atlantic were probably greater than shown by CLIMAP [*de Vernal and Hillaire-Marcel*, 2000; *Sarnthein et al.*, 1995] while the tropical ocean surface was generally cooler than shown by CLIMAP [*Hostetler and Mix*, 1999; *Mix et al.*, 1986]. Several models within PMIP also ran LGM simulations using coupled atmosphere mixed-layer ocean models, instead of prescribing SSTs and sea-ice limits from CLIMAP. Although comparisons of the PMIP simulations and paleoenvironmental data from the tropics suggests that the mixed-layer ocean simulations may be more realistic in some ways than those driven by CLIMAP [*Pinot et al.*, 1999], the mixed-layer ocean simulations differ greatly from one another while none adequately captures the spatial patterning in tropical cooling shown by the data. There has been no systematic analysis of the performance of the mixed-layer ocean models compared to the atmosphere-only simulations in the high latitudes. We have therefore adopted CLIMAP-driven simulations, while recognizing that they may contain certain biases.

We chose four PMIP simulations for the LGM to encompass a range of simulated high-latitude climates (especially simulated summer temperature and precipitation changes). We used simulations performed with two versions of the Laboratoire de Météorologie Dynamique (LMD) model (LMD4, LMDH) [*Le Treut et al.*, 1994; *Masson et al.*, 1998; *Ramstein et al.*, 1998], the Meteorological Research Institute, Japan GCM-IIb model (MRI2) [*Kitoh et al.*, 1995], and the UK Universities' Global Atmospheric Modelling Programme model (UGAMP) [*Dong and Valdes*, 1998].

The mid-Holocene was also a focus for PMIP [*Joussaume*, 1999; *Joussaume and Taylor*, 2000]. However, the PMIP simulations were made using AGCMs in which ocean conditions were prescribed to be the same as in the control simulation. Ocean feedbacks are now known to have a significant impact on mid-Holocene climates, both in the tropics and at high-latitudes [*Kutzbach and Liu*, 1997; *Texier et al.*, 1997] and the use of atmosphere-alone simulations in which no attempt is made to take ocean feedbacks into account is therefore inappropriate. Simulations of the climate of 6000 yr BP have recently been performed by several fully coupled atmosphere-ocean general circulation models (AOGCMs) [*Braconnot et al.*, 2000; *Hewitt and Mitchell*, 1998; *Otto-Bliesner*, 1999]. We used output from two such models: version 2 of the United Kingdom Meteorological Office coupled model (HADCM2) [*Hewitt and Mitchell*, 1998] and the Institut Pierre Simon Laplace coupled model (IPSL-CM1) [*Braconnot et al.*, 2000]. We also used output from HADCM2 for our simulation of the response to possible future climate change (see below). Both of the 6000 yr BP simulations were forced only by changes in orbital configuration. CO_2 concentrations, land-sea geography and land-surface parameters were prescribed to be the same at 6000 yr BP as in the control simulation.

None of the paleoclimate simulations used here take into account the changes in physical land-surface conditions that are known to have occurred at the LGM and during the mid-Holocene. Changes in land-surface parameters such as albedo and surface roughness associated with changes in vegetation have been shown to impact both on monsoonal and high-latitude climates [*Broström et al.*, 1998; *de Noblet-Ducoudré et al.*, 2000; *Foley et al.*, 1994; *Kutzbach et al.*, 1996; *TEMPO*, 1996; *Texier et al.*, 2000; *Texier et al.*, 1997]. Braconnot [1999] investigated the interaction between oceanic and vegetation feedbacks on the mid-Holocene climate using an ocean-atmosphere model coupled asynchronously to a vegetation model (BIOME). Levis [1999] and Doherty [2000] have used an AGCM fully coupled to a dynamic vegetation model (IBIS) to investigate the role of vegetation feedbacks at the LGM and the mid-Holocene respectively. However, none of these models provides a full dynamic linkage between the ocean, atmosphere and vegetation and thus these simulations do not fully capture the synergism between these components. Given this limitation in currently available model results, we have confined our analyses to simulations which adopt standard protocols and thus can be considered comparable to one another.

Paleoclimate scenarios for the LGM and mid-Holocene used for running BIOME4 were derived by an anomaly procedure. The anomaly method consists of was produced by subtracting the control (present-day) simulation of a GCM from the paleo simulation, and adding this anomaly (with suitable interpolation) to the present-day baseline climatology. The anomaly approach compensates for first-order bias in the GCM control simulations. However, we cannot rule out that biases in the GCM also affect the sensitivity of the GCM to boundary condition changes [*de Noblet-Ducoudré et al.*, 2000]. In generating the LGM climatologies, we made a small correction of temperature to account for the topographic difference between the LGM land surface as modeled by Peltier [1994] and the simplified topography used in the GCM, using a standard lapse rate.

The CO_2 concentration prescribed in the GCM simulations for their present-day control simulations was 345 ppm. The CO_2 concentration prescribed for the present-day control simulation of BIOME4 was 324 ppm. To compensate for the difference in baseline [CO_2] between the GCMs and BIOME4 we prescribed [CO_2] in the paleo simulations with BIOME4 such that

$$P_{B4} = C_{B4} - C_{GCM}\left[\frac{P_{GCM}}{C_{GCM}}\right] \tag{2.1}$$

where P_{B4} is the [CO_2] used by BIOME4 in the paleo-simulation, C_{B4} is the BIOME4 control [CO_2], and where P_{GCM} and C_{GCM} are the CO_2 concentrations defined in the GCM paleo- and control-simulations respectively. This resulted in a nominal BIOME4 [CO_2] of 296 ppm for the mid-Holocene simulations and 211 ppm for the LGM simulations. We additionally performed all of the paleoclimate experiments again using BIOME4's unchanged present-day baseline CO_2 concentration (324 ppm), as a sensitivity test to separate the effects of climate and physiological effects of CO_2.

2.2.4.3 Future projection

To assess the sensitivity of Arctic vegetation to possible future climate changes we used results from the HADCM2-SUL model forced by the IS92a greenhouse gas concentration scenario for the 21st century [*Hulme et al.*, 1999]. The "SUL" suffix indicates that this simulation incorporates an estimate of the effects of anthropogenic sulfate aerosols on the climate. We used the mean climate anomalies given from the final ten years of the simulation (i.e. 2090-2100). This same GCM scenario has been applied in other studies on the sensitivity of vegetation to future climate change [*Cramer et al.*, in press; *Malcolm and Markham*, 2000; *Neilson et al.*, 1998]. The scenario does not include the potentially significant feedbacks between land-surface and atmosphere. It is used here simply to illustrate a possible course of the climate change and thus to give an impression of the sensitivity of Arctic ecosystems to the climate changes that might be induced by increasing GHGs if GHG forcing continues to increase at its present rate.

2.2.5 Earth surface properties

As input to BIOME4, we used the land area and derived soil properties defined in the FAO digital soil map of the world [*FAO*, 1995] to create a data set on soil water holding capacity and depth for the present-day and future simulations. For the LGM simulations we used the present-day soils dataset as a baseline and overlaid information on ice sheets [*Denton and Hughes*, 1981; *Dyke and Prest*, 1987; *Svendsen et al.*, 1999], sea level [*Fleming et al.*, 1998], and lakes and inland seas [*Dyke and Prest*, 1987; *Kvasov*, 1975a; *Kvasov*, 1975b]. For the mid-Holocene simulations we used sea level and ice data from Peltier [1994] (ftp://ftp.ngdc.noaa.gov/paleo/ice_topo/).

2.2.6 Validation Data Sets

A provisional map of present-day potential natural vegetation north of 55°N (Fig. 2.2a) was produced by combining information from two sources. Tundra vegetation distributions are based on the preliminary mapping by Walker [2000]. The distribution of other vegetation types was derived from the potential natural vegetation map of Haxeltine and Prentice [1996a], with minor modifications of nomenclature.

Maps of vegetation at the LGM (defined as $18\,000 \pm 1000$ ^{14}C yr BP, approximately equivalent to 21 000 calendar yr BP) and for the mid-Holocene (defined as 6000 ± 500 ^{14}C yr BP) have been produced at individual pollen sites from the region north of 55°N using a standard, objective procedure (biomisation) [*Prentice et al.*, 1996] and the classification scheme for tundra and boreal biomes used in BIOME4

(Fig. 2.1, Table 2.1) [*Bigelow et al.*, submitted]. The sampling locations, age models used for the selection of samples, allocation of pollen taxa to PFTs, and the allocation of PFTs to biomes are described in detail by Bigelow *et al.* [submitted].

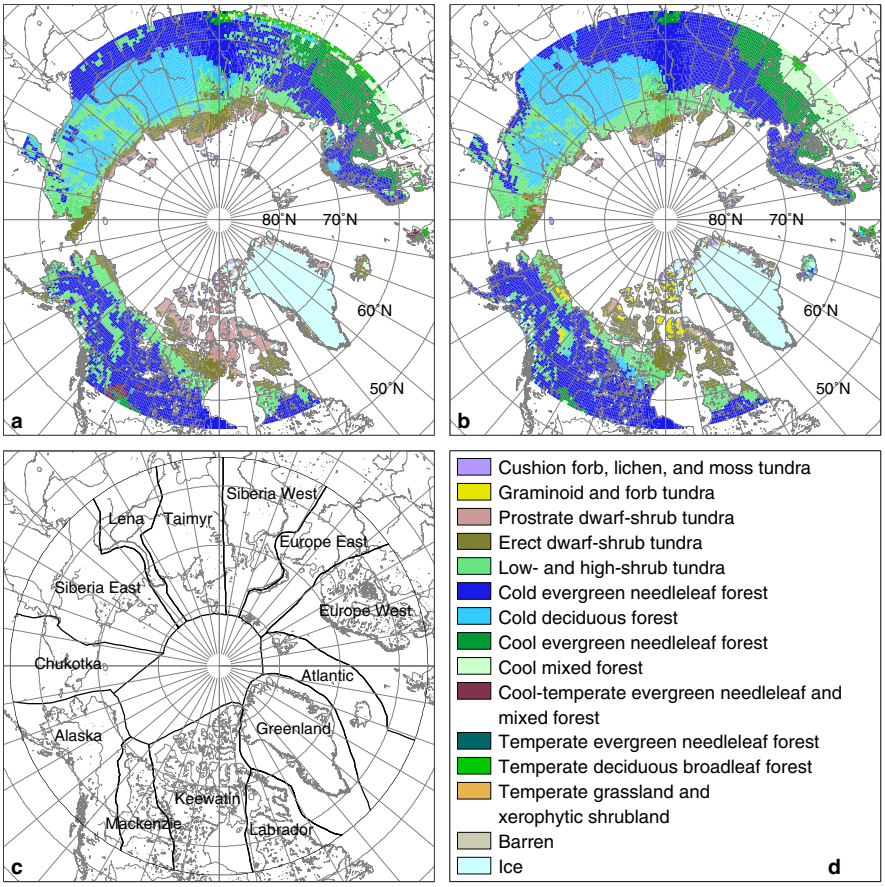

Fig. 2.2. Present-day potential natural vegetation of the Arctic from floristic surveys **a**, and simulated by BIOME4 **b** with 20th century mean climatology. Sectors used in calculating treeline changes **c** and legend **d** for this figure and figures 2.3 and 2.4

2.3 Results

2.3.1 The present-day

BIOME4, driven by the present-day baseline climatology, is generally successful at reproducing the broad-scale patterns of circumpolar vegetation distribution (Figure 2.2). In particular, the model accurately reproduces the placement of the forest-tundra boundary across most regions and successfully predicts whether treeline is formed by evergreen or deciduous species. The broad patterns of decreasing tundra height with latitude are also well produced. A few discrepancies between the simulated vegetation map (Figure 2.2b) and the modern potential vegetation map (Figure 2.2a) are mentioned here.

In maritime tundra regions where BIOME4 simulates forest (e.g. SW Alaska and Iceland), the influence of heavy cloud cover at high latitudes (i.e. low sun angles) on surface solar radiation may be responsible for the disagreement. Additional sensitivity experiments (not shown) demonstrated that a reduction in incoming shortwave radiation by ~25% would produce low- and high-shrub tundra in these regions where BIOME4 normally simulates cold evergreen forest. Such a reduction, compared with the values simulated by the simple empirical cloud-radiation algorithm in BIOME4 [*Linacre*, 1968; *Prescott*, 1940], is plausible based on observations [*Henderson-Sellers*, 1986], suggesting that this aspect of the model could be improved by coupling to a physically based radiation code (e.g., by direct coupling to an atmospheric GCM). Graminoid-forb tundra, while not recorded at the scale of the potential natural vegetation map, nevertheless occurs locally in suitable habitats throughout drier parts of the Arctic [*Edwards and Armbruster*, 1989; *Lloyd et al.*, 1994; *Young*, 1976; *Yurtsev*, 1982]. Shrub vegetation, with buds above ground, requires the insulating effect of snow cover to survive extremely cold winter conditions. BIOME4 simulates more extensive graminoid-forb tundra in some areas of the Arctic where station data are inadequate and that have very low (and likely too low) precipitation figures in the baseline climatology. Global runs of BIOME4 show that graminoid-forb tundra is also predicted in highly oceanic regimes in the southern hemisphere, e.g. at high elevation in New Zealand, islands of the Southern Ocean, and in some tropical montane environments, where no snowpack forms. This prediction is correct, although the floristic composition of such graminoid-forb tundras is very different from that found in cold-winter environments of the Arctic [*Kaplan*, 2001]. Some other discrepancies may be more apparent than real. For example, the boundary between erect and prostrate dwarf-shrub tundra in the Canadian Arctic seems to be misplaced, but it is unlikely that this boundary occurs at different GDD_0 in Canada and Siberia; resolution of this issue may require improved mapping of the vegetation boundaries, especially in the Canadian Arctic [*Walker*, 2000]. More generally, the sparse distribution of climate observations may

be responsible for local artefacts in the simulation, e.g. in Alaska [*Fleming et al.* 2000].

Simulated NPP in the tundra biomes ranged from > 200 g m^{-2} yr^{-1} in high- and low-shrub tundra to < 70 g m^{-2} yr^{-1} for cushion-forbs (Table 2.2). Simulated productivity varied especially widely for graminoid-forb tundra, shown in both very cold, dry climates with low productivity and mild maritime climates with higher productivity. The ranges for simulated productivity are similar to those measured in the field, though particularly favorable micro-site conditions may lead to measurements of higher productivity (> 300 g m^{-2} yr^{-1}) in small areas [*Christensen et al.*, 2000; *Shaver and Chapin*, 1991].

Table 2.3. NPP for tundra biomes in the present-day simulation

Biome	NPP g m^{-2} yr^{-1}	SD
Low- and high-shrub tundra	226	51
Erect dwarf-shrub tundra	163	35
Prostrate dwarf-shrub tundra	101	26
Cushion forbs, lichen, and moss tundra	72	39
Graminoid and forb tundra	168	154

2.3.2 Last Glacial Maximum

BIOME4, driven by climatologies derived from four different AGCMs, simulates major changes in vegetation cover at the LGM compared to present (Fig. 2.3). Tundra vegetation was considerably more extensive than today and forests were confined to the southernmost part of the region. These predictions are generally in good agreement with paleoenvironmental observations (Fig. 2.3e), which show a comparably large expansion of tundra vegetation. Indeed, none of the pollen sites north of 55°N shows forest. Reconstructions of the vegetation cover to the south of our study region in southern Europe [*Elenga et al.*, 2000] and Russia [*Tarasov et al.*, 2000] also indicate non-forest (grassland or tundra) vegetation at the LGM . Thus, even the limited presence of forests in the southern part of the region, as shown in these simulations, may be an overestimate. Evaluations of the PMIP LGM simulations, including the four models presented here, suggest that the models do not produce a sufficiently large cooling in the mid- to high-latitudes compared to paleoenvironmental observations [*Kageyama et al.*, 2001]. Nevertheless, the fact that the BIOME4 simulations reproduce a large part of the change in the extent of tundra vegetation shown by paleoenvironmental observations shows that the vegetation model is capable of responding appropriately to very large changes in climate.

The four climate models used for LGM simulations were deliberately chosen to yield very different high-latitude temperature and precipitation changes. The simu-

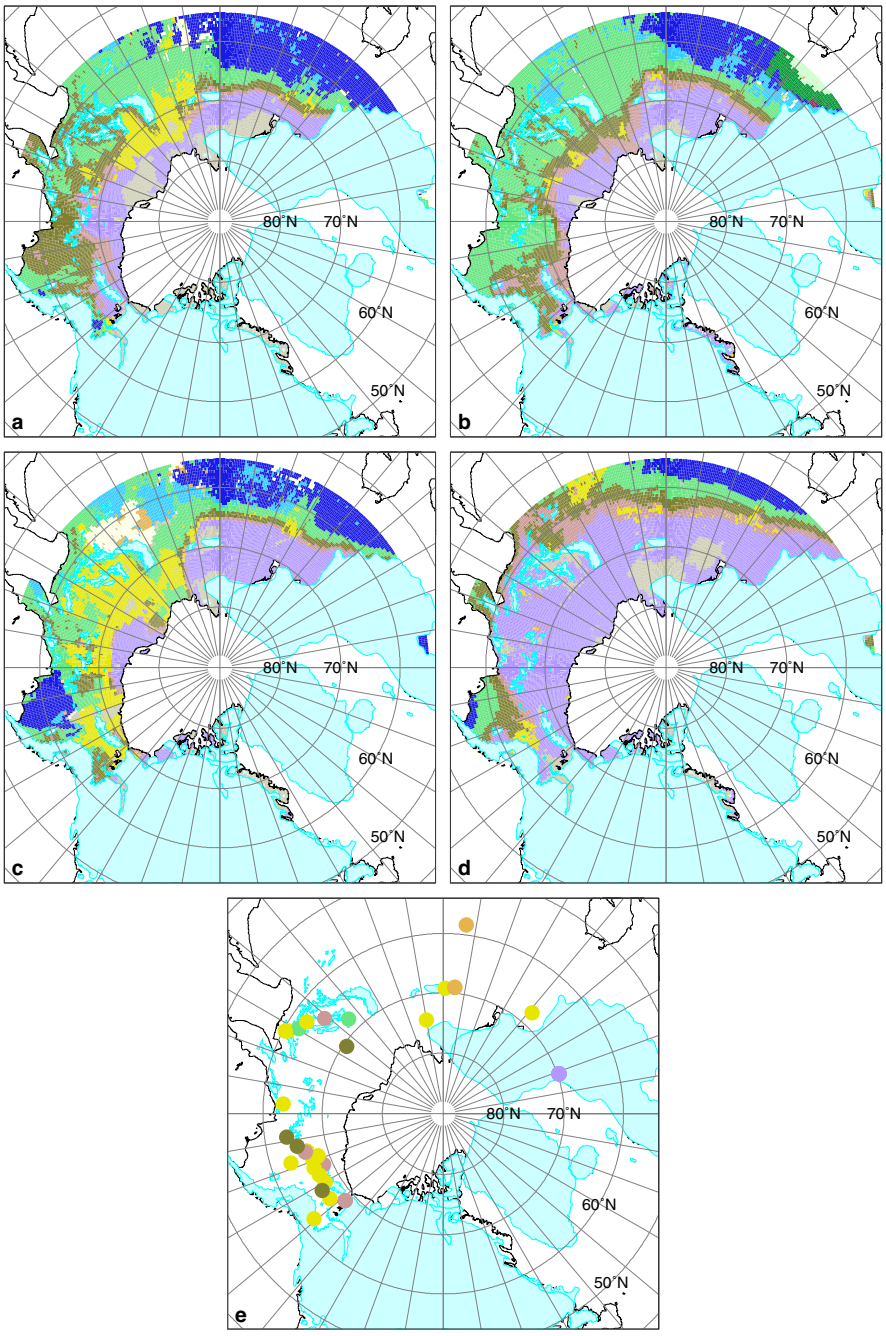

Fig. 2.3. LGM vegetation simulated with 4 AGCMs: **a** MRI2, **b** LMD4, **c** LMDH, and **d** UGAMP. Observed vegetation **e** based on pollen reconstructions from Bigelow et al. (submitted). Pale yellow areas are simulated desert.

lated changes in the extent of different tundra biomes reflect this range of model results. Thus, the LMDH simulation produces more arid conditions (particularly in eastern Siberia) than any of the other models and this is reflected in the greater simulated extent of graminoid and forb tundra, and a small area of desert, in the BIOME4 simulation based on LMDH. The UGAMP simulation produces colder conditions in the far north than the other simulations, and this is reflected by the much greater extent of cushion forb, lichen and moss tundra in the BIOME4 simulation based on UGAMP. Given the large uncertainties in the climate simulations, which are reflected in the differences in the BIOME4 simulations, these simulations can not be expected to perfectly reproduce the paleoenvironmental data. The simulated climate of eastern Siberia may also tend to have a bias towards being less cold and dry than the real LGM climate because the PMIP boundary conditions include an East Siberian ice sheet, which has since been shown to be non-existent at the LGM and which creates an unrealistic circulation pattern [*Felzer*, 2001]. Nevertheless, important features of the observed changes in LGM vegetation distributions can be seen in the BIOME4 results.

Paleoenvironmental data show that low- and high-shrub tundra was greatly reduced in extent at the LGM compared to today, being largely confined to the Beringian land bridge, while graminoid and forb tundra was very much more widespread [*Bigelow et al.*, submitted]. Graminoid and forb tundra occupies only restricted areas today, but is correctly simulated as occupying much larger areas at the LGM. Indeed, the extent of graminoid and forb tundra simulated using the anomaly climatology from LMDH approximates the observed distribution, according to the data in Bigelow et al. [submitted]. The extent of graminoid and forb tundra simulated using the LGM climatology from MRI2 also approximates the observed distribution in western and central Siberia, although low temperatures in eastern Siberia in MRI2 result in the simulation of cushion forb, lichen, and moss tundra over too large an area. The existence and nature of a herbaceous vegetation type with floristic affinities to tundra and yet capable of supporting significant populations of large mammals has been a subject of much debate [*Brubaker et al.*, 1983; *Guthrie*, 1985; *Guthrie and Stoker*, 1990; *Lloyd et al.*, 1994; *Ritchie*, 1985; *Yurtsev*, 2001]. The ability of the BIOME4 model, when forced by a suitable LGM climatology, to simulate an expansion in graminoid and forb tundra enables us to re-examine this problem. According to our simulations, the LGM graminoid and forb tundra in Beringia and Siberia was significantly more productive than this biome is today, despite low temperatures and low [CO_2] (Table 2.4). The increased productivity is explained by greater solar radiation, partly because the biome occurs at lower latitudes than it does today, and partly because these regions (according to the simulations) show significantly reduced cloudiness, allowing more photosynthetically active radiation (PAR) to be absorbed and used in photosynthesis.

The simulated expansion of cushion forb, lichen and moss tundra, which is most pronounced in the BIOME4 simulation using the UGAMP anomaly climatology but is shown in all of the simulations, is one feature of the LGM results which is hard to evaluate from paleo-observations. A single site (Andøya, in Norway) is

Table 2.4. Productivity and cloudiness in graminoid and forb tundra

Simulation	$[CO_2]$ ppm	Mean annual % of full sunshine	Mean summer (JJA) % of full sunshine	Mean NPP g m^{-2} yr^{-1}
Present-day	324	35.8	37.5	17.1
LGM LMD4	211	53.6	46.6	24.9
LGM UGAMP	211	51.4	44.1	39.5
LGM LMDH	211	47.3	45.4	40.7
LGM MRI2	211	46.5	41.3	38.3

characterized as cushion forb, lichen and moss tundra in the LGM paleovegetation reconstruction (Fig. 2.3e) [*Bigelow et al.*, submitted]. However, the core areas of the simulated expansion of cushion forb, lichen and moss tundra (along the northern Siberian coast and along the eastern margin of the European ice sheet) are not represented in the existing pollen data network. The extreme conditions which give rise to cushion forb, lichen and moss tundra are generally unfavorable for the creation of suitable sedimentary sites for the accumulation of pollen. This tundra-type is therefore always likely to be under-represented in paleoenvironmental data sets.

2.3.3 Mid-Holocene

The changes in high-latitude vegetation cover between now and 6000 yr BP as simulated by BIOME4, driven by climatologies derived from the IPSL-CM1 and HADCM2 models, are relatively small (Fig. 2.3, Table 2.5). Treeline is simulated up to 200km north of its modern position in central Siberia (Taimyr sector), and in eastern Canada. There is little or no change in the simulated position of treeline in Alaska, the Mackenzie Delta region, eastern Siberia and Chukotka. The simulated northward shifts in tundra vegetation belts are also most pronounced in central Siberia and in Labrador/Keewatin. Very little change in tundra vegetation is simulated in other Arctic regions. Simulated changes in vegetation south of the treeline are more pronounced. In both simulations, the margin of the cool evergreen needleleaf forest in Scandinavia and eastern Europe is 300-500 km north of its position in the modern simulation. The northern margin of cool mixed forest is also displaced northward, though slightly less than the cool evergreen forest, on the order of 50-200 km (west to east). Large northward displacements of cool and temperate forest zones are also observed in North America, mainly south of the area shown in our maps. In the continental interior of Eurasia, the simulations show a significant area of temperate grasslands and xerophytic shrublands consequent on increased aridity. Expansion of less-moisture-demanding vegetation, including temperate grasslands and xerophytic shrublands, is also simulated in mid-continental North America.

Several key aspects of the 6000 yr BP BIOME4 simulations are supported by the paleoenvironmental data (Fig. 2.4c). Pollen-based reconstructions show major dif-

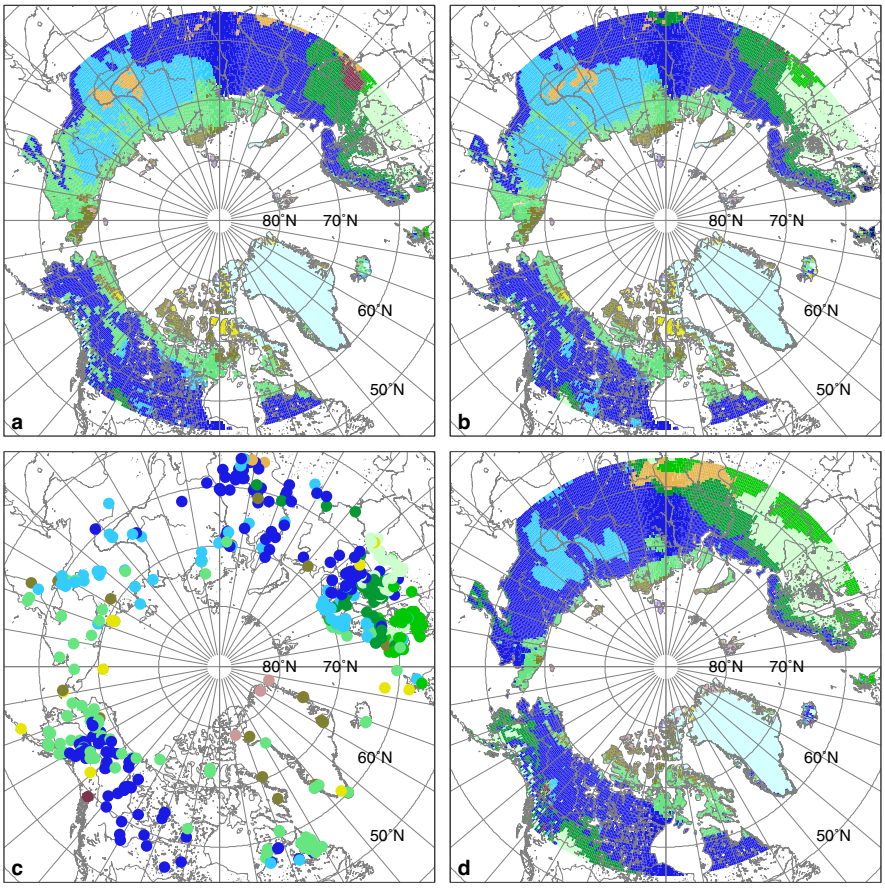

Fig. 2.4. Simulated Arctic vegetation at the mid-Holocene with **a** the IPSL-CM1 AOGCM and with **b** the HADCM2 AOGCM. Observed vegetation at the mid-Holocene **c** from pollen data. Simulated potential vegetation for 2090 to 2100 **d** with the HADCM2-S GCM using the IS92a greenhouse-gas scenario.

ferences in the magnitude of the shift of treeline in different sectors, suggesting a significant circum-polar asymetry in summer warming between 6000 yr BP and present. Indeed, in most sectors, the reconstructed changes (or lack of changes) in treeline are similar to those shown in the simulations (Table 2.5). The change in western and central Siberia was at most 300km, according to both models and data. The data show no change in Alaska and only a slight extension in the Mackenzie Delta region, eastern Siberia and Chukotka. The reconstructions of treeline shifts presented here are consistent with earlier estimates of the changes in these regions summarized by TEMPO [1996] and Prentice et al. [1998] and with independent reconstructions based on megafossil (tree stump) remains in Eurasia [*MacDonald et al.*, 2000]. The most noticeable discrepancy between the reconstructed and simu-

Table 2.5. Changes in the position of Arctic treeline

Sector	6k - present-day			Future - present-day
	HADCM2	IPSL-CM1	Pollen	HADCM2-S IS92a scenario
Alaska	ø	ø	ø	+++
Mackenzie	ø	-	ø	+
Keewatin	+	+	-	++++
Labrador	+	++	------	+++
Greenland	ø	ø	ø	++++++++
Atlantic	----	-	ø	ø
Europe West	ø	ø	+	+
Europe East	ø	ø	ø	++
Siberia West	+	+	++	+++
Taimyr	++	ø	+++	++++
Lena	ø	ø	ø	+
Siberia East	ø	ø	++	+++
Chukotka	ø	ø	ø	+++++

The tree line position in each sector is defined as the maximum latitude band where ≥50% of the gridcells are a forest biome. Each + or - symbol represents a difference of 1° (ca. 110 km), a ø represents no change. The sectors were defined to represent climatically contiguous regions within which local topographic influence (e.g. deep river valleys) and regional circulation effects (e.g. ocean currents and ice sheets) on the location of treeline are minimized.

lated changes in treeline occurs in Québec and Labrador, where the pollen data indicate that treeline was ca 500-700 km *south* of its present position whereas the simulation suggest it lay ca. 300 km north of its present position. The southward displacement of the treeline in Québec and Labrador at that time probably reflects the localized cooling caused by the persistence of small ice sheets in this region until at least 5500 yr BP [*Clark et al.*, 2000; *Richard*, 1995; *Richard et al.*, 1997]. Relicts of the Laurentide ice sheet have not been included in the climate model simulations for the mid-Holocene; this omission probably explains the marked discrepancy between the observations and the model results for eastern Canada at 6000 yr BP.

The paleovegetation maps also confirm the results of the 6000 yr BP simulations in showing that the northward shift of cool and temperate forests was significantly larger than changes in the northern treeline in any sector. Indeed, the pollen data suggest that the simulated northward shifts (e.g. of temperate deciduous broadleaf forest in the European sector) may have been smaller than actually occurred. There are at least two possible explanations for why changes further south appear to be larger than those further north. There is a steep gradient in summer temperature near the Arctic coast, due to the presence of sea ice. As a result, large changes in summer temperature are required to produce a significant poleward shift in the northern vegetation zones, and particularly in northern treeline. Further south, smaller changes in temperature would be required to produce a given geographical change in the northern limits of the cool and temperate forest zones. In addition,

many of the observed changes in temperate forest distribution in the mid-Holocene imply that winters were substantially warmer at 6000 yr BP than today in some temperate mid-latitude regions [*Cheddadi et al.*, 1997; *Prentice et al.*, 2000; *Yu et al.*, 1998]. Thus, there is no reason why the magnitude of the northward shift in cool and temperate forests should be similar to the magnitude of the changes in northern treeline, which are controlled primarily by changes in growing-season temperatures and their effect on NPP and tree growth.

The pollen-based reconstructions of mid-Holocene vegetation (Fig. 2.4c) do not show any expansion of less moisture-demanding vegetation in the continental interior of Eurasia. This result is consistent with earlier reconstructions based on pollen data [e.g. *Tarasov et al.*, 1998], and with independent evidence based on geomorphic and biostratigraphic records of changes in lake status that show little or no change in the regional water balance of central Eurasia in the mid-Holocene [*Harrison et al.*, 1996]. The reason for this discrepancy between the observations and the simulations is not known.

2.3.4 Future sensitivity

In the illustrative simulation of a "greenhouse climate", the potentially forested area of the Arctic increases substantially compared to the present day; tundra is correspondingly reduced (Fig. 2.4). The simulated treeline is farther north than in any of the mid-Holocene simulations, and treeline is shown to advance relative to the present in all sectors of the Arctic. Trees are shown potentially invading coastal Greenland and Chukotka, where only fragments of forest exist today. The area of potential cold deciduous forest is also strongly reduced in Siberia, opposite to the mid-Holocene simulations, because of a simulated strong warming in winter in the greenhouse climate. During the mid-Holocene, low insolation in the boreal winter has little effect at high latitudes (where midwinter insolation is always very low) and acts counter to the summertime forcing further south, producing *colder* than present winters e.g. in Siberia, according to the model results. In the future simulation, in contrast GHG forcing (by trapping outgoing long wave radiation) results in winter temperatures higher than present throughout the region, reaching anomalies as great as +14° C in eastern Siberia (Fig. 2.5).

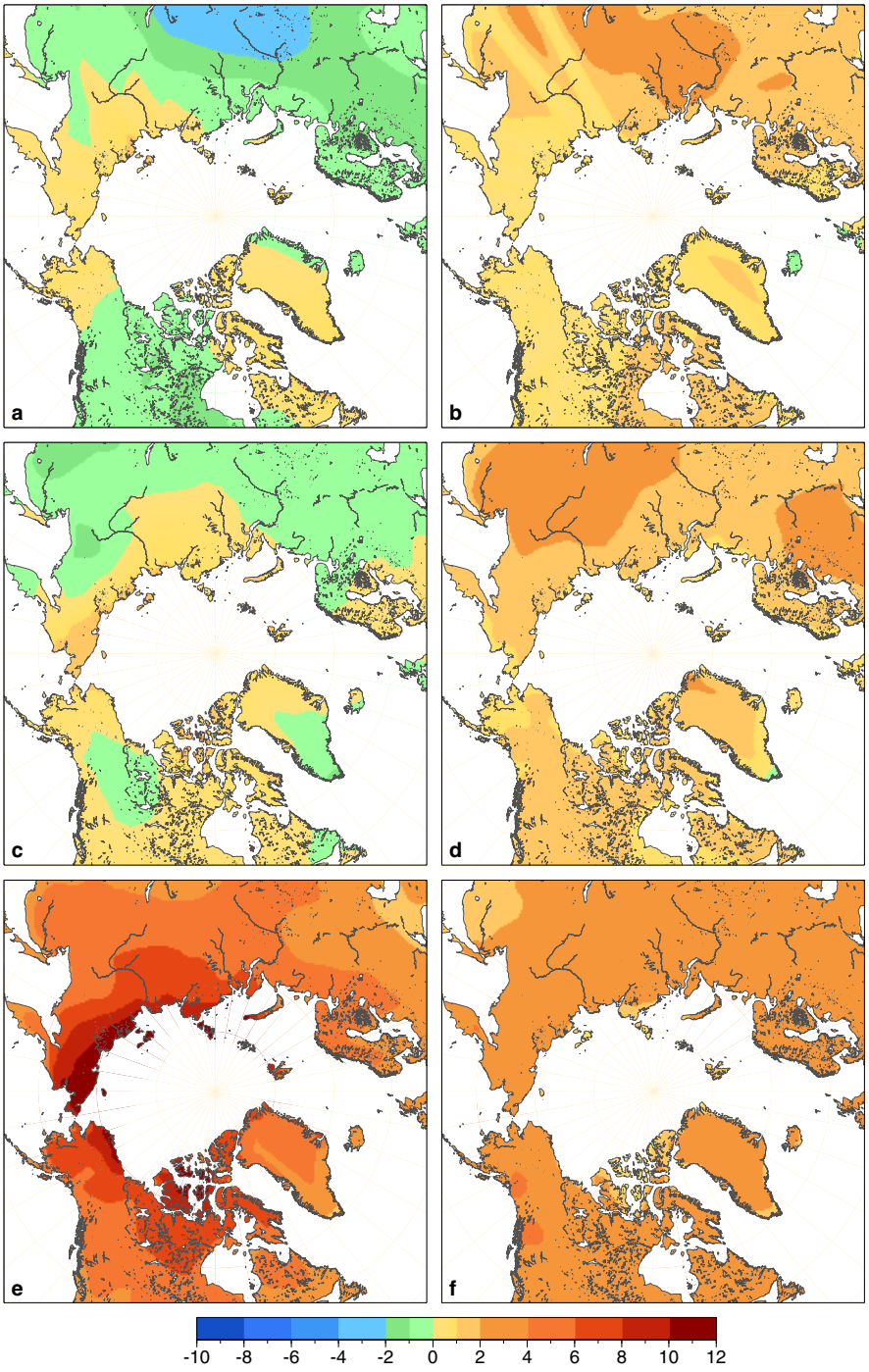

Fig. 2.5. Mean surface air temperature anomaly in winter (DJF, left) and summer (JJA, right). IPSL-CM1 **a**,**b**; HADCM2 (6 kya) **c**,**d**; HADCM2-SUL (2100) **e**,**f**

2.4 Discussion and conclusion

BIOME4 has proved successful in capturing the important features of Arctic vegetation distribution: the position of the northern treeline, and the variety of tundra vegetation types present on the modern landscape. Simulated estimates of tundra productivity are within the range of those measured in the field. In highly oceanic areas where the model fails to reproduce the observed position of the treeline, the main cause is hypothesized to lie in the effects of low sun angle in extremely cloudy climates. All of the BIOME models have used the empirical linear relationship between cloudiness and short-wave irradiance of Ångström, [1924] as modified by Prescott [1940] to predict short-wave irradiance at the earth's surface ϕ_s:

$$\phi_s = \phi_\infty \left(a + b \frac{n}{N} \right) \tag{2.2}$$

where ϕ_∞ is the solar radiation at the top of the atmosphere, n/N is the ratio of actual to potential sunshine hours, and a and b are empirical constants: a relates to the opacity of clouds and $(a + b)$ represents the transmissivity of clear air. The values for a and b are determined through measurements and have typically been assigned global values of about 0.23 and 0.5 respectively [*Haxeltine and Prentice*, 1996a; *Landsberg and Gower*, 1997; *Linacre*, 1968; *Prentice et al.*, 1992; *Roderick*, 1998; *Stigter*, 1980]. Analyses of station data for solar radiation however indicate a considerable range in a, e.g. 0.19 measured on Macquarie Island in the Southern Ocean [*Roderick*, 1998] and values as low as 0.05 in Canada [*Davies and Hay*, 1980; *Henderson-Sellers*, 1986]. Alternative empirical formulations include models that explicitly make a a function of latitude [e.g. *Glover and McCulloch*, 1958], though this formulation was not intended to be applied at latitudes > 60° [*Lin et al.*, 1999]. At lower latitudes the Prescott [1940] formulation with $a = 0.23$ and $b = 0.48$ appears to work best [*Lin et al.*, 1999], but this formulation cannot capture the low values of ϕ_s (< 0.23) measured at high latitudes. Biosphere models should in the future include more explicit physical treatments of radiation; this could be achieved most straightforwardly by direct coupling to an atmospheric model.

We have assessed the performance of BIOME4 in reproducing the vegetation of LGM paleoenvironments drastically different from those of today, including a vegetation type (graminoid and forb tundra) that has no large-scale analog on the modern landscape. Given several caveats about the paleoclimate scenarios, the BIOME4 simulations satisfactorily reproduce many of the major features observed in paleorecords of the LGM. The widespread occurrence of graminoid and forb tundra is a prominent and well-known feature of the LGM. This biome is of interest for several reasons. Herbaceous tundra has markedly different biophysical properties from woody tundra; the implications of this difference for the LGM climate has not yet been explored in global climate models. Furthermore, this biome was the primary habitat and source of nutrition for the large mammoth populations that existed at

that time [*Guthrie*, 2001]. The driest areas may have also been significant sources of aeolian dust [*Mahowald et al.*, 1999]. According to our model results, the LGM graminoid-forb tundra was generally more productive than the graminoid-forb tundra that is found locally in the present-day Arctic, because it grew at lower latitude and under less cloudy conditions than it does at present, resulting in increased absorption of PAR. These factors may also have contributed to the floristic diversity of the graminoid-forb tundra at the LGM [*Vartanyan et al.*, 1993; *Yurtsev*, 1982]. The xerophyte and cryoxerophyte grass, sedge, and forb taxa found in common association in the graminoid-forb tundra are not all found together on the modern landscape. The phenomenon of a plant association with no modern analog is widespread at the LGM and has been explained in various ways. One interpretation points to the interplay between climate and low CO_2 concentrations [*Jackson et al.*, 2000; *Solomon and Shugart*, 1984], but in this case [CO_2] is less of an issue; it is the combination of climate and radiation conditions that is distinctive in our model results. It has also been suggested that the floristic diversity of this vegetation was promoted by continual inputs of calcareous aeolian dust [*Goetcheus and Birks*, 2001; *Walker et al.*, 2001].

Our model results do not invoke vegetation feedbacks, nor any direct influence of large grazing animals on the vegetation [*Zimov et al.*, 1995], to explain the widespread distribution of graminoid and forb tundra at LGM. Nevertheless, it seems likely that more complete understanding of the high-latitude vegetation on climate at the LGM will include vegetation feedbacks [*Levis et al.*, 1999; *Chapin et al.*, 2000] and will take account of major differences in the physical characteristics of tundra biomes.

Climate changes in the early Holocene drastically restricted the geographic range of graminoid-forb tundra. Wrangel Island, off the coast of northeastern Siberia, has retained the largest contiguous community of graminoid-form tundra anywhere in the Arctic [*Yurtsev*, 1982]. While floristically depauperate, the vegetation of Wrangel Island has a higher diversity of herbaceous tundra species than anywhere else in the Arctic and is considered to have survived throughout the Holocene as relic of the Pleistocene graminoid-forb tundra [*Lozhkin et al.*, 2001]. It was on Wrangel Island where mammoth populations survived longest, with dwarf species persisting until at least 3700 years ago, nearly 6000 years longer than on the Eurasian mainland [*Vartanyan et al.*, 1993].

During the early and mid-Holocene the northern high latitudes were subject to greater summertime and total annual insolation than present, allowing warmer than present summer temperatures to develop, particularly in continental areas (Fig. 2.5). Eurasia, because of its greater size, warmed more than North America during summer, and therefore the northern vegetation changes were greater in Eurasia. Simulated treeline was further north than the present in central Siberia, where the summertime warming was maximal according to the models. Thus a simple explanation for the circumpolar asymmetry of the treeline shift, as seen both in the data and the simulations, invokes the differential heating of the continents. However other factors may be involved, including a shift of the sea ice limit specifically

in the European sector [*Vavrus*, 1999], assisted by increased northward penetration of warm water from the North Atlantic, contrasting with persistent, perennial sea ice in the other regions of the Arctic [*C. Hewitt, pers. comm.,* 2001].

Feedback between the land-surface and atmosphere related to forest extent at the mid-Holocene may have been overestimated in earlier work [*Foley et al.*, 1994] in light of the new data on vegetation distribution [*Bigelow et al.*, submitted; *MacDonald et al.*, 2000] which indicate a more modest treeline extension than was assumed previously. However, vegetation-atmosphere feedbacks may be more important in the future. For example, Levis [2000] showed that vegetation feedbacks under a doubled CO_2 climate could produce an additional 3° C warming during spring (April-May) in the region north of 60° N. Such findings suggest that our estimate of Arctic treeline sensitivity to possible future climate changes represents a minimum estimate, as it is based on a model without vegetation feedback.

Comparison of the mid-Holocene simulations and the future projection suggests that the vulnerability of Arctic ecosystems to climate change depends on the seasonality of the climatic forcing and, possibly, the resulting response of sea-ice distribution. Mid-Holocene climate was influenced by a positive radiative forcing with maximum effect in summer and at high latitudes essentially no effect in winter; lower latitudes experienced negative radiative forcing in winter. Forcing from increased GHGs may have a larger effect because it is positive everywhere, and effective year-round even in high latitudes. The simulated direct physiological effect of CO_2 on these cold-climate vegetation types is small compared to the climate effect. The response of leaf-level photosynthesis to CO_2 concentrations is strongly dependent on temperature, with significant competition between CO_2 and O_2 for beginning only at ambient temperatures over ~15° C [*Farquhar et al.*, 1980]. Therefore, these results are not contrary to modeling studies on tropical vegetation which show a much greater sensitivity to low CO_2 concentration [*Cowling*, 2000] or to paleodata suggesting a response of tropical treeline to low [CO_2] at LGM [*Street-Perrott et al.*, 1997].

Recent studies have proposed that high-latitude vegetation will gain in productivity due to increased nutrient availability as a result of warming in the Arctic [*Chapin et al.*, 1995b; *Melillo et al.*, 1993; *Oechel et al.*, 1994; *Oechel et al.*, 2000]. In our simulations with BIOME4 we assume that the ecosystem optimizes its nutrient demand relative to supply [*Haxeltine and Prentice*, 1996b]. Therefore, possible short-term gains in productivity that may be observed in field experiments cannot be discounted by our analysis.

Several studies [e.g. *Cavalieri et al.*, 1997; *Chapman and Walsh*, 1993; *Johannessen et al.*, 1995; *Johannessen et al.*, 1999; *Maslanik et al.*, 1996; *Parkinson et al.*, 1999; *Vinnikov et al.*, 1999] have shown a significant decrease in the extent of northern-hemisphere sea ice during recent decades. The most recent analysis suggests that summer sea ice extent has declined monotonically 4 to 6% during the last four decades [*Deser*, 2000] due to changes in late spring temperatures, amplified by the ice-albedo feedback. In our GHG scenario, as in other simulations of the impact of potential changes in future climate, the area of perennial sea ice is dramatically

reduced as is the extent of seasonal sea ice, and simulated temperatures are increased year-round.

In conclusion, the vegetation and ecosystems of the high latitudes of the northern hemisphere appear to be especially sensitive to increased radiative forcing of climate due to increases in GHG concentrations. In a modeling study with the same future scenario as we used here, Malcom and Markham [2000] projected that global ecosystem habitat loss would be greatest in Canada, Russia, and the Nordic countries. Local species loss under doubled CO_2 climates could be as much as 20% in the cold forests and tundra areas of the circumpolar Arctic [*Malcolm and Markham*, 2000]. The time scale of our future scenario is such that we would not expect the changes to be fully realized during the century; tree line expansion depends on the establishment and growth of trees, which is expected to take several centuries [*Cramer et al.*, in press], as has been shown in a simulation using the LPJ dynamic global vegetation model [*Kittel et al.*, 2000]. These results illustrate what could happen if GHG concentrations continue to increase at the present rate for the next 100 years. The simulations indicate that the mid-Holocene situation, with modest Arctic treeline extension, is in no sense an analog for the effect of GHGs; however, the data-model comparisons give us confidence in the ability of the modeling procedure to simulate the potential consequences of GHG forcing for climate and vegetation in the Arctic.

Acknowledgments. The Pan-Arctic Initiative has been supported by PALE (NSF), FATE (IASC/IGBP), IGBP-GAIM, IGBP-DIS, PIK, and MPI-BGC. Climate model results were provided by P. Braconnot and G. Ramstein (LMD4 and LMDH), P. Valdes and B. Dong (UGAMP), A. Kitoh and H. Koide (MRI2), P. Braconnot (IPSL-CM1), C. Hewitt (HADCM2, 6ka), and D. Viner (HADCM2-SUL, future).

References

Ångström, A., Solar and terrestrial radiation, *Quarterly Journal of the Royal Meteorological Society*, *50*, 121, 1924.

Arno, S.F., and R.P. Hammerly, *Timberline: Mountain and Arctic Forest Frontiers*, 304 pp., The Mountaineers, Seattle, 1984.

Berger, A.L., Long-term variations of daily insolation and Quaternary climatic changes, *Journal of the Atmospheric Sciences*, *35* (12), 2362-2367, 1978.

Berry, J., and O. Björkman, Photosynthetic response and adaptation to temperature in higher plants, *Annual Review of Plant Physiology and Plant Molecular Biology*, *31*, 491-543, 1980.

Berry, J.A., and W.J.S. Downton, Environmental regulation of photosynthesis, in *Photosynthesis: Development, Carbon Metabolism, and Plant Productivity*, edited by Govindjee, pp. 263-343, Academic Press, 1982.

Bigelow, N.H., L.B. Brubaker, M.E. Edwards, S.P. Harrison, I.C. Prentice, P.M. Anderson, A.A. Andreev, P.J. Bartlein, T.R. Christensen, W. Cramer, J.O. Kaplan, A.V. Lozhkin, N.V. Matveyeva, D.F. Murray, A.D. McGuire, V.Y. Razzhivin, J.C. Ritchie, B. Smith, D.A. Walker, S.L. Clayden, T. Ebel, K. Gajewski, J. Hahne, B.H. Holmqvist, Y. Igarashi, J.W. Jordan, K.V. Kremenetskii, M. Melles, W.W. Oswald, A. Paus, M.F.J. Pisaric, G.N. Shilova, C. Siegert, V.S. Volkova, and V.G. Wolf, Climate change and Arctic ecosystems I: Biome reconstruction of tundra vegetation types at 0, 6, and 18 radiocarbon kyr in the Arctic, *Climate Dynamics*, submitted.

Bonan, G.B., Land atmosphere CO_2 exchange simulated by a land surface process model coupled to an atmospheric general circulation model, *Journal of Geophysical Research-Atmospheres*, *100* (D2), 2817-2831, 1995.

Braconnot, P., S. Joussaume, O. Marti, and N. de Noblet, Synergistic feedbacks from ocean and vegetation on the African monsoon response to mid-Holocene insolation, *Geophysical Research Letters*, *26* (16), 2481-2484, 1999.

Braconnot, P., O. Marti, S. Joussaume, and Y. Leclainche, Ocean feedback in response to 6 kyr BP insolation, *Journal of Climate*, *13* (9), 1537-1553, 2000.

Bradley, R.S., Past global changes and their significance for the future, *Quaternary Science Reviews*, *19* (1-5), 391-402, 2000.

Broström, A., M. Coe, S.P. Harrison, R. Gallimore, J.E. Kutzbach, J. Foley, I.C. Prentice, and P. Behling, Land surface feedbacks and palaeomonsoons in northern Africa, *Geophysical Research Letters*, *25* (19), 3615-3618, 1998.

Brubaker, L.B., H.L. Garfinkel, and M.E. Edwards, A late Wisconsin and Holocene vegetation history from the central Brooks Range: implications for Alaskan paleoecology, *Quaternary Research*, *20*, 194-214, 1983.

Cavalieri, D.J., P. Gloersen, C.L. Parkinson, J.C. Comiso, and H.J. Zwally, Observed hemispheric asymmetry in global sea ice changes, *Science*, *278* (5340), 1104-1106, 1997.

Chapin, F.S.III, M.S. Bret-Harte, S.E. Hobbie, and H.L. Zhong, Plant functional types as predictors of transient responses of Arctic vegetation to global change, *Journal of Vegetation Science*, *7* (3), 347-358, 1995a.

Chapin, F.S.III, G.R. Shaver, A.E. Giblin, K.J. Nadelhoffer, and J.A. Laundre, Responses of Arctic tundra to experimental and observed changes in climate, *Ecology*, *76* (3), 694-711, 1995b.

Chapin, F.S.III, A.D. McGuire, J. Randerson, R. Pielke, D. Baldocchi, S.E. Hobbie, N. Roulet, W. Eugster, E. Kasischke, E.B. Rastetter, S.A. Zimov, and S.W. Running, Arctic and boreal ecosystems of western North America as components of the climate system, *Global Change Biology*, *6* (*s1*), 211-223, 2000.

Chapman, W.L., and J.E. Walsh, Recent variations of sea ice and air-temperature in high-latitudes, *Bulletin of the American Meteorological Society*, *74* (1), 33-47, 1993.

Cheddadi, R., G. Yu, J. Guiot, S.P. Harrison, and I.C. Prentice, The climate of Europe 6000 years ago, *Climate Dynmaics*, *13*, 1-9, 1997.

Christensen, T.R., T. Friborg, M. Sommerkorn, J. Kaplan, L. Illeris, H. Soegaard, C. Nordstroem, and S. Jonasson, Trace gas exchange in a high-arctic valley 1. Variations in CO_2 and CH_4 flux between tundra vegetation types, *Global Biogeochemical Cycles*, *14* (3), 701-713, 2000.

Christensen, T.R., S. Jonasson, T.V. Callaghan, and M. Havstrom, On the potential CO_2 release from tundra soils in a changing climate, *Applied Soil Ecology*, *11* (2-3), 127-134, 1999.

Clark, C.D., J.K. Knight, and J.T. Gray, Geomorphological reconstruction of the Labrador Sector of the Laurentide Ice Sheet, *Quaternary Science Reviews*, *19* (13), 1343-1366, 2000.

CLIMAP, Seasonal reconstructions of the Earth's surface as the Glacial Maximum, Geological Society of America, Boulder, 1981.

Cowling, S.A., Simulated effects of low atmospheric CO_2 on structure and composition of North American vegetation at the last glacial maximum, *Global Ecology and Biogeography*, *8*, 81-93, 1999.

Cowling, S.A., Plant-climate interactions over historical and geological time, Ph.D. thesis, Lund University, Lund, 2000.

Cramer, W., A. Bondeau, F.I. Woodward, I.C. Prentice, R.A. Betts, V. Brovkin, P.M. Cox, V. Fisher, J.A. Foley, A.D. Friend, C. Kucharik, M.R. Lomas, N. Ramankutty, S. Sitch, B. Smith, A. White, and C. Young-Molling, Global response of terrestrial ecosystem structure and function to CO_2 and climate change: Results from six dynamic global vegetation models, *Global Change Biology*, in press.

Davies, J.A., and J.E. Hay, Calculation of the solar radiation incident on a horizontal surface, in *Proceedings of the 1st Canadian Solar Radiation Data Workshop*, edited by J.E. Hay, and T.K. Won, pp. 32-58, Ministry of Supply and Services, Ottawa, Ontario, Canada, 1980.

de Noblet-Ducoudré, N., M. Claussen, and I.C. Prentice, Mid-Holocene greening of the Sahara: first results of the GAIM 6000 yr BP experiment with two asychronously coupled atmosphere/biosphere models, *Climate Dynamics*, *16*, 643-659, 2000.

de Vernal, A., and C. Hillaire-Marcel, Sea-ice cover, sea-surface salinity and halo-/thermocline structure of the northwest North Atlantic: modern versus full glacial conditions, *Quaternary Science Reviews*, *19* (1-5), 65-86, 2000.

Denton, G.H., and T.J. Hughes, The Last Great Ice Sheets, John Wiley and Sons, New York, 1981.

Deser, C., On the teleconnectivity of the "Arctic Oscillation", *Geophysical Research Letters*, *27* (6), 779-782, 2000.

Doherty, R., J. Kutzbach, J. Foley, and D. Pollard, Fully coupled climate/dynamical vegetation model simulations over Northern Africa during the mid-Holocene, *Climate Dynamics*, *16* (8), 561-573, 2000.

Dong, B.W., and P.J. Valdes, Simulations of the Last Glacial Maximum climates using a general circulation model: Prescribed versus computed sea surface temperatures, *Climate Dynamics*, *14*, 571-591, 1998.

Dyke, A.S., and V.K. Prest, The Late Wisconsin and Holocene History of the Laurentide Ice Sheet, *Géographie Physique et Quaternaire*, *41* (2), 237-263, 1987.

Edwards, M.E., and W.S. Armbruster, A tundra-steppe transition on Kathul Mountain, Alaska, USA, *Arctic and Alpine Research*, *21* (3), 296-304, 1989.

Ehleringer, J.R., and O. Björkman, Quantum yields for CO_2 uptake in C_3 and C_4 plants: Dependence on temperature CO_2 and O_2 concentration, *Plant Physiology*, *59*, 86-90, 1977.

Elenga, H., O. Peyron, R. Bonnefille, D. Jolly, R. Cheddadi, J. Guiot, V. Andrieu, S. Bottema, G. Buchet, J.-L.D. Beaulieu, A.C. Hamilton, J. Maley, R. Marchant, R. Perez-Obiol, M. Reille, G. Riollet, L. Scott, H. Straka, D. Taylor, E.V. Campo, A. Vincens, F. Laarif, and H. Jonson, Pollen-based biome reconstruction for southern Europe and Africa 18,000 yr BP, *Journal of Biogeography*, *27* (3), 621-634, 2000.

Elias, S.A., Mutual climatic range reconstructions of seasonal temperatures based on Late Pleistocene fossil beetle assemblages in Eastern Beringia, *Quaternary Science Reviews*, *20* (*1-3*), 77-91, 2001.

Fairbanks, R.G., A 17,000-year glacio-eustatic sea level record: influence of glacial melting rates on the younger dryas event and deep-ocean circulation, *Nature*, *342*, 637-642, 1989.

FAO, Digital Soil Map of the World and Derived Soil Properties, Food and Agriculture Organization, Rome, 1995.

Farquhar, G.D., S.V. Caemmerer, and J.A. Berry, A biochemical model of photosynthetic CO_2 assimilation in leaves of C_3 species, *Planta*, *149* (1), 78-90, 1980.

Farquhar, G.D., and S. von Caemmerer, Modelling of photosynthesis response to environmental conditions, in *Physiological Plant Ecology II: Water Relations & Carbon Assimilation*, edited by O.L. Lange, P.S. Nobel, C.B. Osmond, and H. Ziegler, pp. 549-587, Springer-Verlag, Berlin, 1982.

Felzer, B., Climate impacts of an ice sheet in East Siberia during the Last Glacial Maximum, *Quaternary Science Reviews*, *20* (*1-3*), 437-447, 2001.

Fleming, K., P. Johnston, D. Zwartz, Y. Yokoyama, K. Lambeck, and J. Chappell, Refining the eustatic sea-level curve since the Last Glacial Maximum using far- and intermediate-field sites, *Earth and Planetary Science Letters*, *163* (1-4), 327-342, 1998.

Fleming, M.D., F.S. Chapin III, W. Cramer, G.L. Hufford, and M.C. Serreze, Geographic patterns and dynamics of Alaskan climate interpolated from a sparse station record, *Global Change Biology*, *6* (*s1*), 49-58, 2000.

Foley, J.A., J.E. Kutzbach, M.T. Coe, and S. Levis, Feedbacks between climate and boreal forests during the Holocene epoch, *Nature*, *371* (6492), 52-54, 1994.

GETECH, Global DTM5, Geophysical Exploration Technology, Leeds, 1996.

Glover, J., and J.S.G. McCulloch, The empirical relation between solar radiation and hours of sunshine, *Quarterly Journal of the Royal Meteorological Society*, *84*, 172-175, 1958.

Goetcheus, V.G., and H.H. Birks, Full-glacial upland tundra vegetaion preserved under tephra in the Beringia National Park, Seward Peninsula, Alaska, *Quaternary Science Reviews*, *20* (*1-3*), 135-147, 2001.

Gower, S.T., J.G. Vogel, J.M. Norman, C.J. Kucharik, S.J. Steele, and T.K. Stow, Carbon distribution and aboveground net primary production in aspen, jack pine, and black spruce stands in Saskatchewan and Manitoba, Canada, *Journal of Geophysical Research-Atmospheres*, *102* (D24), 29029-29041, 1997.

Guthrie, R.D., Wooly arguments against the Mammoth Steppe: A new look at the palynological data, *Quarterly Review of Archaeology*, *6*, 9-16, 1985.

Guthrie, R.D., and S. Stoker, Paleoecological significance of mummified remains of Pleistocene horses from the north slope of the Brooks Range, Alaska, *Arctic*, *43*, 267-274, 1990.

Guthrie, R.D., Origin and causes of the mammoth steppe: a story of cloud cover, woolly mammal tooth pits, buckles, and inside-out Beringia, *Quaternary Science Reviews*, *20* (*1-3*), 549-574, 2001.

Harrison, S.P., Paleoenvironmental data sets and model evaluation in PMIP, in *Paleoclimate Modeling Intercomparison Project (PMIP)*, edited by P. Braconnot, pp. 25-42, WMO/WCRP, La Huardiére, Canada, 2000.

Harrison, S.P., I.C. Prentice, and P.J. Bartlein, Influence of insolation and glaciation on atmospheric circulation in the North-Atlantic sector - implications of general-circulation model experiments for the Late Quaternary climatology of Europe, *Quaternary Science Reviews*, *11* (3), 283-299, 1992.

Harrison, S.P., G. Yu, and P.E. Tarasov, Late Quaternary lake-level record from Northern Eurasia, *Quaternary Research*, *45*, 138-159, 1996.

Haxeltine, A., and I.C. Prentice, BIOME3: an equilibrium terrestrial biosphere model based on ecophysiological constraints, resource availability, and competition among plant functional types, *Global Biogeochemical Cycles*, *10* (4), 693-709, 1996a.

Haxeltine, A., and I.C. Prentice, A general model for the light-use efficiency of primary production, *Functional Ecology*, *10*, 551-561, 1996b.

Henderson-Sellers, B., Calculating the surface energy balance for lake and reservoir modeling: a review, *Reviews of Geophysics*, *24* (3), 625-649, 1986.

Hewitt, C.D., and J.F.B. Mitchell, A fully coupled GCM simulation of the climate of the mid-Holocene, *Geophysical Research Letters*, *25* (3), 361-364, 1998.

Hostetler, S.W., and A.C. Mix, Reassessment of ice-age cooling on the tropical oceans and atmosphere, *Nature*, *399*, 673-676, 1999.

Hulme, M., J. Mitchell, W. Ingram, J. Lowe, T. Johns, M. New, and D. Viner, Climate change scenarios for global impacts studies, *Global Environmental Change-Human and Policy Dimensions*, *9*, S3-S19, 1999.

Hutchinson, M.F., Interpolating mean rainfall using thin plate smoothing splines, *International Journal of GIS*, *9*, 385-403, 1995.

Hutchinson, M.F., and R.J. Bischof, A new method of estimating mean seasonal and annual rainfall for the Hunter Valley, New South Wales, *Australian Meteorological Magazine*, *31*, 179-184, 1983.

Jackson, S.T., R.S. Webb, K.H. Anderson, J.T. Overpeck, T.I. Webb, J.W. Williams, and B.C.S. Hansen, Vegetation and environment in Eastern North America during the Last Glacial Maximum, *Quaternary Science Reviews*, *19* (6), 489-508, 2000.

Johannessen, O.M., M. Miles, and E. Bjorgo, The Arctic's shrinking sea ice, *Nature*, *376*, 126-127, 1995.

Johannessen, O.M., E.V. Shalina, and M.W. Miles, Satellite evidence for an Arctic sea ice cover in transformation, *Science*, *286* (5446), 1937-1939, 1999.

Jolly, D., and A. Haxeltine, Effect of low glacial atmospheric CO_2 on tropical African montane vegetation, *Science*, *276*, 786-788, 1997.

Joussaume, S., Modeling extreme climates of the past 20.000 years with general circulation models, in *Modeling the Earth's Climate and its Variability*, edited by W.R. Holland, S. Joussaume, and F. David, Elsevier, Amsterdam, 1999.

Joussaume, S., and K.E. Taylor, Status of the Paleoclimate Modeling Intercomparison Project (PMIP), in *Proceedings of the First International AMIP Scientific Conference, 15-19 May 1995*, edited by W.L. Gates, pp. 532 pp, Monterey, CA, 1995.

Joussaume, S., and K.E. Taylor, The Paleoclimate Modeling Intercomparison Project, in *Paleoclimate Modeling Intercomparison Project (PMIP)*, edited by P. Braconnot, pp. 9-24, WMO/WCRP, La Huardiére, Canada, 2000.

Kageyama, M., O. Peyron, S. Pinot, P. Tarasov, J. Guiot, S. Joussaume, and G. Ramstein, The Last Glacial Maximum climate over Europe and western Siberia: a PMIP comparison between models and data, *Climate Dynamics*, *17* (1), 23-43, 2001.

Kaplan, J.O., Geophysical Applications of Vegetation Modeling, Lund University, Lund, 2001.

Kirschbaum, M.U.F., and G.D. Farquhar, Temperature dependance of whole-leaf photosynthesis in *Eucalyptus pauciflora* Sieb. ex Spreng., *Australian Journal of Plant Physiology*, *11*, 519-538, 1984.

Kitoh, A., A. Noda, Y. Nikaidou, T. Ose, and T. Tokioka, AMIP simulations of the MRI GCM, *Papers in meteorology and geophysics*, *45*, 121-148, 1995.

Kittel, T.G., W.L. Steffen, and F.S. Chapin III, Global and regional modelling of Arctic-boreal vegetation distribution and its sensitivity to altered forcing, *Global Change Biology*, *6* (*s1*), 1-18, 2000.

Kohfeld, K.E., and S.P. Harrison, How well can we simulate past climates? Evaluating the models using global palaeoenvironmental datasets, *Quaternary Science Reviews*, *19* (1-5), 321-346, 2000.

Körner, C., *Alpine Plant Life: Functional Plant Ecology of High Mountain Ecosystems*, 338 pp., Springer-Verlag, Berlin, 1999.

Kutzbach, J., G. Bonan, J. Foley, and S.P. Harrison, Vegetation and soil feedbacks on the response of the African monsoon to orbital forcing in the early to middle Holocene, *Nature*, *384* (6610), 623-626, 1996.

Kutzbach, J.E., and Z. Liu, Response of the African monsoon to orbital forcing and ocean feedbacks in the middle Holocene, *Science*, *278* (5337), 440-443, 1997.

Kvasov, D.D., *The Late Quaternary History of Large Lakes and Inland Seas of Eastern Europe*, 71 pp., Suomalainen Tiedeakatemia, Helsinki, 1975a.

Kvasov, D.D., *Late Quaternary History of Large Lakes and Inland Seas of Eastern Europe [in Russian]*, 248 pp., Leningrad, 1975b.

Landsberg, J.J., and S.T. Gower, *Applications of physiological ecology to forest management*, 354 pp., Academic Press, San Diego, 1997.

Larcher, W., *Physiological plant ecology: ecophysiology and stress physiology of functional groups*, Springer-Verlag, New York, Berlin, Heidelberg, 1995.

Le Treut, H., Z.X. Li, and M. Forichon, Sensitivity of the LMD general circulation model to greenhouse forcing associated with two different cloud water parameterizations, *Journal of Climate*, *7*, 1827-1841, 1994.

Leemans, R., and W.P. Cramer, The IIASA Database for Mean Monthly Values of Temperature, Precipitation, and Cloudiness on a Global Terrestrial Grid, pp. 62, International Institute for Applied Systems Analysis, Laxenberg, 1991.

Levis, S., J.A. Foley, and D. Pollard, CO2, climate, and vegetation feedbacks at the Last Glacial Maximum, *Journal of Geophysical Research-Atmospheres*, *104* (D24), 31191-31198, 1999.

Levis, S., J.A. Foley, and D. Pollard, Large-scale vegetation feedbacks on a doubled CO_2 climate, *Journal of Climate*, *13* (7), 1313-1325, 2000.

Lin, W.X., W.F. Gao, S.X. Pu, and E.R. Lu, Ranking the overall performance of eight sunshine-based global solar radiation models with a nonparametric statistical procedure, *Energy Conversion and Management*, *40* (3), 233-241, 1999.

Linacre, E.T., Estimating the net-radiation flux, *Agricultural Meteorology*, *5*, 49-63, 1968.

Lloyd, A.H., W.S. Armbruster, and M.E. Edwards, Ecology of a steppe-tundra gradient in interior Alaska, *Journal of Vegetation Science*, *5*, 897-912, 1994.

Lozhkin, A.V., P.M. Anderson, S.L. Vartanyan, T.A. Brown, B.V. Belaya, and A.N. Kotov, Late Quaternary paleoenvironments and modern pollen data from Wrangel Island (Northern Chukotka), *Quaternary Science Reviews*, *20* (*1-3*), 217-233, 2001.

MacDonald, G.M., and K. Gajewski, The northern treeline of Canada, in *Geographical Snapshots of North America. Commerating the 27th Congress of the International Geographical Union and Assembly*, edited by D.G. Janelle, pp. 34-37, The Guilford Press, New York, London, 1992.

MacDonald, G.M., A.A. Velichko, C.V. Kremenetski, O.K. Borisova, A.A. Goleva, A.A. Andreev, L.C. Cwynar, R.T. Riding, S.L. Forman, T.W.D. Edwards, R. Aravena, D. Hammarlund, J.M. Szeicz, and V.N. Gattaulin, Holocene treeline history and climate change across northern Eurasia, *Quaternary Research*, *53* (3), 302-311, 2000.

Mahowald, N., K.E. Kohfeld, M. Hansson, Y. Balkanski, S.P. Harrison, I.C. Prentice, M. Schulz, and H. Rodhe, Dust sources and deposition during the last glacial maximum and current climate: A comparison of model results with paleodata from ice cores and marine sediments, *Journal of Geophysical Research-Atmospheres*, *104* (D13), 15895-15916, 1999.

Malcolm, J.R., and A. Markham, Global Warming and Terrestrial Biodiversity Decline, pp. 23, World Wildlife Fund for Nature, Gland, Switzerland, 2000.

Maslanik, J.A., M.C. Serreze, and R.G. Barry, Recent decreases in Arctic summer ice cover and linkages to atmospheric circulation anomalies, *Geophysical Research Letters*, *23* (13), 1677-1680, 1996.

Masson, V., S. Joussaume, S. Pinot, and G. Ramstein, Impact of parameterizations on simulated winter mid-Holocene and Last Glacial Maximum climatic changes in the northern hemisphere, *Journal of Geophysical Research-Atmospheres*, *103* (D8), 8935-8946, 1998.

Melillo, J.M., A.D. McGuire, D.W. Kicklighter, B. Moore, C.J. Vorosmarty, and A.L. Schloss, Global climate change and terrestrial net primary production, *Nature*, *363* (6426), 234-240, 1993.

Mitchell, J.F.B., N.S. Grahame, and K.J. Needham, Climate simulations for 9000 years before present: seasonal variations and effect of the Laurentide ice sheet, *Journal of Geophysical Research-Atmospheres*, *93* (D7), 8283-8303, 1988.

Mix, A.C., W.F. Ruddiman, and A. McIntyre, Late Quaternary paleoceanography of the tropical Atlantic, 1: spatial variability of annual mean sea-surface temperatures, 0-20,000 years B.P., *Paleoceanography*, *1* (1), 43-66, 1986.

Neilson, R., I. Prentice, B. Smith, T. Kittel, and D. Viner, Simulated changes in vegetation distribution under global warming, in *The Regional Impacts of Climate Change*, edited by R. Watson, M. Zinyowera, R. Moss, and D. Dokken, pp. 439-456, Cambridge University Press, Cambridge, 1998.

Oechel, W., S. Hastings, G. Vourlitis, M. Jenkins, G. Riechers, and N. Grulke, Recent change of Arctic tundra ecosystems from a net carbon dioxide sink to a source, *Nature*, *361*, 520-523, 1993.

Oechel, W.C., S. Cowles, N. Grulke, S.J. Hastings, B. Lawrence, T. Prudhomme, G. Riechers, B. Strain, D. Tissue, and G. Vourlitis, Transient nature of CO_2 fertilization in Arctic tundra, *Nature*, *371* (6497), 500-503, 1994.

Oechel, W.C., G.L. Vourlitis, S.J. Hastings, R.C. Zulueta, L. Hinzman, and D. Kane, Acclimation of ecosystem CO_2 exchange in the Alaskan Arctic in repsonse to decadal climate warming, *Nature*, *406*, 978-981, 2000.

Otto-Bliesner, B.L., El Nino La Nina and Sahel precipitation during the middle Holocene, *Geophysical Research Letters*, *26* (1), 87-90, 1999.

Parkinson, C.L., D.J. Cavalieri, P. Gloersen, H.J. Zwally, and J.C. Comiso, Arctic sea ice extents, areas, and trends, 1978-1996, *Journal of Geophysical Research-Oceans*, *104* (C9), 20837-20856, 1999.

Peltier, W.R., Ice Age paleotopography, *Science*, *265* (5169), 195-201, 1994.

Pinot, S., G. Ramstein, S.P. Harrison, I.C. Prentice, J. Guiot, M. Stute, S. Joussaume, and P.p. groups, Tropical paleoclimates at the Last Glacial Maximum: comparison of Paleoclimate Modeling Intercomparison Project (PMIP) simulations and paleodata, *Climate Dynamics*, *15*, 857-874, 1999.

Prentice, I.C., W. Cramer, S.P. Harrison, R. Leemans, R.A. Monserud, and A.M. Solomon, A global biome model based on plant physiology and dominance, soil properties and climate, *Journal of Biogeography*, *19*, 117-134, 1992.

Prentice, I.C., J. Guiot, B. Huntley, D. Jolly, and R. Cheddadi, Reconstructing biomes from palaeoecological data: a general method and its application to European pollen data at 0 and 6 ka, *Climate Dynamics*, *12*, 185-194, 1996.

Prentice, I.C., S.P. Harrison, D. Jolly, and J. Guiot, The climate and biomes of Europe at 6000 yr BP: Comparison of model simulations and pollen-based reconstructions, *Quaternary Science Reviews*, *17* (6-7), 659-668, 1998.

Prentice, I.C., D. Jolly, and BIOME6000 Participants, Mid-Holocene and glacial-maximum vegetation geography of the northern continents, *Journal of Biogeography*, *27 (3)*, 507-519, 2000.

Prescott, J.A., Evaporation from a water surface in relation to solar radiation, *Transactions of the Royal Society of Australia*, *64*, 114-118, 1940.

Price, D.T., D.W. McKenney, I.A. Nalder, M.F. Hutchinson, and J.L. Kesteven, A comparison of two statistical methods for spatial interpolation of Canadian monthly mean climate data, *Agricultural and Forest Meteorology*, *101* (2-3), 81-94, 2000.

Ramstein, G., Y.S.-L. Treut, H.L. Treut, M. Forichon, and S. Joussaume, Cloud processes associated with past and future climate changes, *Climate Dynamics*, *14*, 233 - 247, 1998.

Raynaud, D., J. Jouzel, J.M. Barnola, J. Chappellaz, R.J. Delmas, and C. Lorius, The ice record of greenhouse gases, *Science*, *259*, 926-934, 1993.

Richard, P.J.H., The vegetational cover of Québec-Labrador at 6000 years BP: an essay, *Géographie physique et Quaternaire*, *49* (1), 117-140, 1995.

Richard, P.J.H., J.J. Veillette, A.C. Larouche, B. Hetu, J.T. Gray, and P. Gangloff, Chronology of ice retreat over Gaspesie: new evidence and implications, *Géographie physique et Quaternaire*, *51* (2), 163-184, 1997.

Ritchie, J.C., Late Quaternary climatic and vegetational change in the lower Mackenzie Basin, northwest Canada, *Ecology*, *66* (2), 612-621, 1985.

Ritchie, J.C., L.C. Cwynar, and R.W. Spear, Evidence from northwest Canada for an early Holocene Milankovitch thermal maximum, *Nature*, *305* (5930), 126-128, 1983.

Roderick, M.L., Estimating the diffuse component from daily and monthly measurements of global radiation, *Agricultural and Forest Meteorology*, *95* (3), 169-185, 1998.

Sarnthein, M., E. Jansen, M. Weinelt, M. Arnold, J.C. Duplessy, H. Erlenkeuser, A. Flat¿y, G. Johannessen, T. Johannessen, S. Jung, N. Koc, L. Labeyrie, M. Maslin, U. Pflaumann, and H. Schulz, Variations in Atlantic surface ocean paleoceanography, 50°-80°N: a time-slice record of the last 30,000 years, *Paleoceanography*, *10* (6), 1063-1094, 1995.

Schulze, E.D., J. Lloyd, F.M. Kelliher, C. Wirth, C. Rebmann, B. Luhker, M. Mund, A. Knohl, I.M. Milyukova, W. Schulze, W. Ziegler, A.B. Varlagin, A.F. Sogachev, R. Valentini, S. Dore, S. Grigoriev, O. Kolle, M.I. Panfyorov, N. Tchebakova, and N.N. Vygodskaya, Productivity of forests in the Eurosiberian boreal region and their potential to act as a carbon sink - a synthesis, *Global Change Biology*, *5* (6), 703-722, 1999.

Shaver, G.R., and F.S. Chapin III, Production: biomass relationships and element cycling in contrasting Arctic vegetation types, *Ecological Monographs*, *61* (1), 1-31, 1991.

Solomon, A.M., and H.H. Shugart, Integrating forest-stand simulations with paleoecological records to examine long-term forest dynamics, in *State and Change of Forest Ecosystems - Indicators in Current Research*, edited by G.I. Âgren, pp. 333-356, Swedish University of Agricultural Science, Department of Ecology and Environmental Research, Uppsala, 1984.

Stigter, C.J., Solar radiation as statistically related to sunshine duration: A comment using low-latitude data, *Agricultural Meteorology*, *21*, 173-178, 1980.

Street-Perrott, F.A., Y. Huang, R.A. Perrott, G. Eglington, P. Barker, L.B. Khelifa, D.D. Harkness, and D.O. Olago, Impact of lower atmospheric carbon dioxide on tropical mountain ecosystems, *Science*, *278*, 1422-1426, 1997.

Svendsen, J.I., V.I. Astakhov, D.Y. Bolshiyanov, I. Demidov, J.A. Dowdeswell, V. Gataullin, C. Hjort, H.W. Hubberten, E. Larsen, J. Mangerud, M. Melles, P. Möller, M. Saarnisto, and M.J. Siegert, Maximum extent of the Eurasian ice sheets in the Barents and Kara Sea region during the Weichselian, *Boreas*, *28*, 234-242, 1999.

Tarasov, P.E., T.W. III, A.A. Andreev, N.B. Afanas'eva, N.A. Berezina, L.G. Bezusko, T.A. Blyakharchuk, N.S. Bolikhovskaya, R. Cheddadi, M.M. Chernavskaya, G.M. Chernova, N.I. Dorofeyuk, V.G. Dirksen, G.A. Elina, L.V. Filimonova, F.Z. Glebov, J. Guiot, V.S. Gunova, S.P. Harrison, D. Jolly, V.I. Khomutova, E.V. Kvavadze, I.M. Osipova, N.K. Panova, I.C. Prentice, L. Saarse, D.V. Sevastyonov, V.S. Vokova, and V.P. Zernitskaya, Present-day and mid-Holocene biomes reconstructed from pollen and plant macrofossil data from the former Soviet Union and Mongolia, *Journal of Biogeography*, *25*, 1029-1053, 1998.

Tarasov, P.E., V.S. Volkova, T.W. III, J. Guiot, A.A. Andreev, L.G. Bezusko, T.V. Bezusko, G.V. Bykova, N.I. Dorofeyuk, E.V. Kvavadze, I.M. Osipova, N.K. Panova, and D.V. Sevastyanov, Last glacial maximum biomes reconstructed from pollen and plant macrofossil data from northern Eurasia, *Journal of Biogeography*, *27* (3), 609-620, 2000.

TEMPO, M., The potential role of vegetation feedback in the climate sensitivity of high-latitude regions: a case study at 6000 years before present, *Global Biogeochemical Cycles*, *10* (4), 727-736, 1996.

Texier, D., N. de Noblet, and P. Braconnot, Sensitivity of the African and Asian monsoons to mid-Holocene insolation and data-inferred surface changes, *Journal of Climate*, *13* (1), 164-181, 2000.

Texier, D., N. de Noblet, S.P. Harrison, A. Haxeltine, D. Jolly, S. Joussaume, F. Laarif, I.C. Prentice, and P. Tarasov, Quantifying the role of biosphere-atmosphere feedbacks in climate change: coupled model simulations for 6000 years BP and comparison with palaeodata for northern Eurasia and northern Africa, *Climate Dynamics*, *13* (12), 865-882, 1997.

Tranquillini, W., *Physiological Ecology of the Alpine Timberline*, 137 pp., Springer-Verlag, Berlin, 1979.

Vartanyan, S.L., V.E. Garutt, and A.V. Sher, Holocene dwarf mammoths from Wrangel Island in the Siberian Arctic, *Nature*, *362*, 337-340, 1993.

Vavrus, S.J., The response of the coupled arctic sea ice-atmosphere system to orbital forcing and ice motion at 6 kyr and 115 kyr BP, *Journal of Climate*, *12* (3), 873-896, 1999.

Vinnikov, K.Y., A. Robock, R.J. Stouffer, J.E. Walsh, C.L. Parkinson, D.J. Cavalieri, J.F.B. Mitchell, D. Garrett, and V.F. Zakharov, Global warming and Northern Hemisphere sea ice extent, *Science*, *286* (5446), 1934-1937, 1999.

Walker, D.A., Hierarchical subdivision of Arctic tundra based on vegetation response to climate, parent material and topography, *Global Change Biology*, *6 (s1)*, 19-34, 2000

Walker, D.A., J.G. Bockheim, F.S. Chapin, W. Eugster, F.E. Nelson, and C.L. Ping, Calcium-rich tundra, wildlife, and the "Mammoth Steppe", *Quaternary Science Reviews*, *20* (*1-3*), 149-163, 2001.

Walter, H., *Vegetation of the Earth in Relation to Climate and the Eco-Physiological Conditions*, Springer-Verlag, New York, 1973.

Wright, H.E., Jr., J.E. Kutzbach, T. Webb, III, W.F. Ruddiman, F.A. Street-Perrott, and P.J. Bartlein, Global Climates since the Last Glacial Maximum, pp. 569, University of Minnesota Press, Minneapolis, 1993.

Young, S.B., Is steppe-tundra alive and well in Alaska?, in *Abstracts of the Fourth Biennial Meeting of the American Quaternary Association*, pp. 84-88, Arizona State University, Tempe, AZ, 1976.

Yu, G., X.J. Sun, B.Q. Qin, C.Q. Song, H.Y. Li, I.C. Prentice, and S.P. Harrison, Pollen-based reconstruction of vegetation patterns of China in mid-Holocene, *Science in China Series D-Earth Sciences*, *41* (2), 130-136, 1998.

Yurtsev, B.A., Relics of the xerophyte vegetation of Beringia in northeastern Asia, in *Paleoecology of Beringia*, edited by D.M. Hopkins, J.V. Matthews, C.E. Schweger, and S.B. Young, pp. 157-177, Academic Press, New York, 1982.

Yurtsev, B.A., The Pleistocene "Tundra-Steppe" and the productivity paradox: the landscape approach, *Quaternary Science Reviews*, *20* (*1-3*), 165-174, 2001.

Zimov, S.A., V.I. Chuprynin, A.P. Oreshko, F.S. Chapin III, J.F. Reynolds, and M.C. Chapin, Steppe-tundra transition: a herbivore driven biome shift at the end of the Pleistocene, *American Naturalist*, *146* (5), 765-794, 1995.

3 Wetlands at the Last Glacial Maximum
Distribution and methane emissions

Jed O. Kaplan
Max Planck Institute for Biogeochemistry, Jena, Germany

Abstract. The global distribution of potential wetlands and their methane (CH_4) emissions at the present-day and the Last Glacial Maximum (LGM) are estimated using a bottom-up modeling approach. LGM climate was derived from the coupled atmosphere-vegetation simulation of Levis [1999]. The biological model combines the climate and soils driven global vegetation model BIOME4 with simple but effective algorithms for determining wetland area based on topography and soil moisture, and CH_4 emission based on ecosystem carbon turnover in seasonally or perennially wet soils. The global CH_4 sink is also estimated, following Ridgwell [1999]. Simulated LGM wetland area was 15% larger than present, but simulated global CH_4 emissions were 24% less. Extensive wetlands were simulated on the continental shelves. Simulated emissions of 140 Tg per year at the present and 107 Tg at the LGM are within the range of previous estimates. The soil sink for CH_4 was simulated as 14 Tg at present but < 0.5 Tg at the LGM due to substrate limitation. The simulated increase in natural CH_4 emissions since the LGM is largely due to the increase in substrate availability caused by increased wetland productivity. While rapid climate changes may have had an immediate effect on CH_4 emissions from wetlands, other physical changes at the Earth's surface may have modulated the long-term wetland CH_4 source. The 100% increase in atmospheric CH_4 concentration measured in ice cores between the LGM and the pre-industrial period may have been caused in part by changes in the atmospheric OH sink due to altered emissions of other reactive trace gases.

3.1 Introduction

Natural sources of methane (CH_4) may have contributed to the increase in atmospheric CH_4 since pre-industrial time. CH_4 is an important greenhouse gas, accounting for about 17% of total trace-gas induced atmospheric radiative forcing [*Schimel et al.*, 1996]. During the last 250 years atmospheric CH_4 concentrations have increased on average nearly 2.5% per year [*Aselmann and Crutzen*, 1989]. However, the increase has not been continuous. In particular, the atmospheric rate of increase in CH_4 decreased from the 1970's through the 1990's; the effect of climate variability on wetland area and productivity has been proposed as one of the causes [*Bartlett and Harriss*, 1993; *Schimel et al.*, 1996].

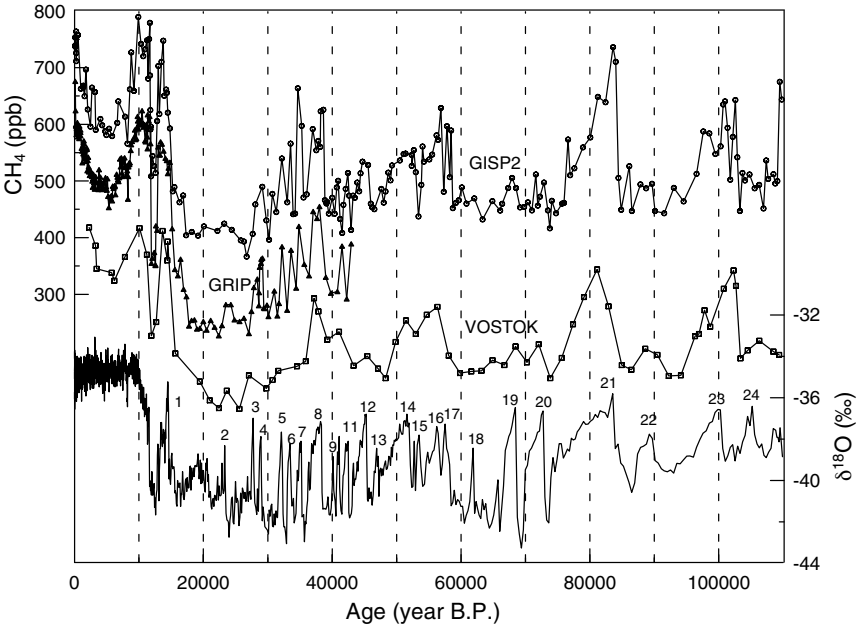

Fig. 3.1. Polar temperature and atmospheric CH_4 concentrations during the last 110 000 years from the GISP2 [*Brook et al.* 1996], GRIP [*Chappellaz et al.* 1993] and Vostok [*Chappellaz et al.* 1990] ice cores. The time scale for all three CH_4 profiles is from Brook et al. [1996] and Chappellaz et al. [2000] The GRIP and Vostok profiles are reduced by 120 and 250 ppb, for clarity. The GISP2 isotopic profile, which represents polar temperature, is shown for comparison [*Grootes et al.* 1993]. Numbers 1 to 24 indicate the Dansgaard-Oeschger events. Adapted with permission from Chappellaz et al. [2000].

Atmospheric CH_4 concentrations fluctuated between approximately 350 and 700 ppb over the last 400 000 years [*Petit et al.*, 1999]. Between the Last Glacial Maximum (LGM, 18 000 yr BP) and pre-industrial Holocene (to ~1850), CH_4 concentrations in the atmosphere increased nearly 100% and more closely parallel the higher-frequency component of polar temperature records than any other measured trace gas (Fig. 3.1) [*Chappellaz et al.*, 1990; *Chappellaz et al.*, 1993a; *Raynaud et al.*, 1988].

Recent studies agree that CH_4 emissions from wetlands are the driving component to prehistoric changes in ice-core CH_4, but conflict as to the location of the wetlands and the primary environmental factors controlling CH_4 emission [*Chappellaz et al.*, 1993*b*; *Dällenbach et al.*, 2000; *Worthy et al.*, 2000]. In addition, given the potency of CH_4 as a greenhouse gas (20.6 times more effective than CO_2), it seems likely that there are strong feedbacks between temperature and wetland CH_4 emissions [*Schimel et al.*, 1996]. I present here a new estimate of wetland area and CH_4 emissions for the present-day and the LGM, using a "bottom-up" ecosystem modeling technique.

Several estimates of present-day wetland area and corresponding CH_4 emission have been presented in the past decade [*Aselmann and Crutzen*, 1989; *Bartlett and Harriss*, 1993; *Chappellaz et al.*, 1993*b*; *Matthews and Fung*, 1987]. Recently, modeling studies have attempted to assimilate new information on methanogenesis and oxidation (methanotrophy) to give more process-based estimates of global and regional CH_4 production [*Cao et al.*, 1996; *Christensen et al.*, 1996; *Walter*, 1998]. Inverse modeling has been used to build a global budget of CH_4 using atmospheric flask measurements for the present-day [*Dlugokencky et al.*, 1994; *Hein et al.*, 1997; *Houweling*, 1999; *Houweling et al.*, 2000]. However, these models have not also been used to predict wetland area, and were therefore limited in their ability to estimate CH_4 production for time periods other than the present. Continental hydrology models exist that can simulate horizontal flow of water across landscapes, river flow, and lake and wetland area, but because of their complexity and requirement for detailed information on topography and soil physical properties, their use has so far been limited to regional studies [*Coe*, 1995; *Coe*, 1998].

Because of the geographically sparse nature of ice-core data, the inverse problem of determining sources and sinks of CH_4 through time is highly unconstrained [*McElroy*, 1989]. Nevertheless, several recent studies used the interhemispheric difference in CH_4 concentrations measured in Greenland and Antarctic ice-cores to determine CH_4 sources from the tropics and northern and southern hemisphere extra-tropics [*Brook et al.*, 2000; *Chappellaz et al.*, 1997; *Dällenbach et al.*, 2000].

Chappellaz *et al.* [1993*b*] have made the only other process-based estimate on global wetland area and CH_4 emissions at the LGM to date. Their methods combined information on topography and paleo-vegetation to determine wetland area and the CH_4 source. This study also used a photochemical model to establish the atmosphere OH sink for CH_4, which, because of the closely linked CH_4-OH feedback, was assumed to vary in phase with CH_4 concentrations [*Lu and Khalil*, 1991; *Pinto and Khalil*, 1991; *Thompson et al.*, 1993; *Valentin*, 1990]. Chappellaz *et al.* [1993*b*] estimated the wetland CH_4 source at 180 Tg for the pre-industrial Holocene and 120 Tg at LGM. Since then, inverse modeling studies based on widespread flask sampling and isotopic data have made estimates of the wetland CH_4 source from 135 to 232 Tg per year for the present-day (Table 3.2).

Chappellaz *et al.* [1993*b*] made several key simplifications. First, they used a LGM vegetation map based on a subjective analysis of paleo-data [*Adams et al.*, 1990]. The reliability of the Adams *et al.* [1990] vegetation map has since been challenged [e.g. *Prentice et al.*, 1993]. Second, the digital terrain model used to constrain wetlands to appropriate slopes was aggregated to a 1 degree (nearly 100 km) grid. Recent studies have shown that small-scale topography and hydrology can have a strong relationship to CH_4 emission [*Christensen et al.*, 1995; *Christensen et al.*, 1999]. Widespread wetlands less than 10 km in size may contribute significantly to the global CH_4 source. Third, estimates of wetland area were not constrained by climate or plant physiology. However several studies have indicated that low atmospheric CO_2 concentration may have increased plant sensitivity to drought [eg. *Cowling and Sykes*, 1999; *Jolly and Haxeltine*, 1997]. Therefore, vegetation type data

alone may not be a reliable proxy for moisture conditions at the LGM. Finally, Chappellaz *et al.* [1993*b*] did not take into account changes in substrate availability due to changes in climate and CO_2 concentration; these factors have a major effect on CH_4 production [*Christensen et al.*, 1996; *Walter*, 1998; *Whiting and Chanton*, 1993].

In this study I used a high-resolution digital elevation model to determine suitable low-relief areas for extensive wetland formation. I ran the global biogeography and biogeochemistry model BIOME4, forced only by climate and atmospheric CO_2 concentration, to determine the wetland area (soil moisture), substrate availability (NPP), and potential CH_4 production rate as a fraction of heterotrophic respiration. I combined the topographic and biogeochemical information to simulate the CH_4 emissions. Here I present simulated wetland area and CH_4 emissions for both the pre-industrial period, forced by modern observed climate, and the LGM, driven by a fully-coupled atmosphere-vegetation-general circulation model (AVGCM) climatology [*Levis et al.*, 1999].

3.2 Methods

3.2.1 General methodology

Model simulation of wetland areas and their corresponding CH_4 emissions had four parts. First a driver climatology and soils dataset were developed for the pre-industrial and LGM. I used these data to drive the BIOME4 global vegetation model in order to define biomes and to generate spatially and temporally explicit fields of soil moisture, NPP and heterotrophic respiration. I estimated wetland area and extent based on these outputs plus topographic information. Finally I combined the vegetation model output with the information on wetland area to simulate CH_4 emission.

I used a long-term mean climatology for the late 20^{th} century (CLIMATE v2.2) [*W. Cramer, pers. comm.* 1998] as the baseline for the experiments. The climatology includes more station data from sparsely populated regions and an improved estimation of lapse rate over several parts of the Earth compared to the earlier versions of the dataset [*Leemans and Cramer*, 1991] (http://www.pik-potsdam.de/~cramer/climate.htm). The climatology was also extrapolated over continental shelf areas that were exposed at the LGM to provide a baseline for the LGM climatology. I used the derived soil properties from the FAO digital soil map of the world [*FAO*, 1995] for information on soil texture and depth.

I used the BIOME4 global biosphere model to simulate monthly soil wetness, NPP, and potential CH_4 production. A 5-minute global digital terrain model [*GETECH*, 1996] was used to identify areas flat enough to support wetlands. Potential CH_4 emissions were calculated where wetland areas were identified.

The BIOME4 global biosphere model is a coupled biogeography and biogeochemistry model developed from the BIOME3 model [*Haxeltine and Prentice*, 1996]. The model uses a plant-functional-type approach to simulate the distribution and behavior of global vegetation. Major differences between BIOME3 and BIOME4 include the addition of three new PFTs to better represent tundra vegetation [*Kaplan et al.*, this volume], PFT-specific parameterization of the physiological information used by the model, and an improved competition scheme which uses biogeochemical outputs more directly to determine the dominant PFT and biome. Inputs to the model are monthly fields of mean temperature and percent sunshine, monthly total precipitation, and two vertical layers of soil physical parameters related to the water holding capacity and percolation rate of water in the soil column. BIOME3 has been used in to simulate LGM vegetation and soil moisture conditions in a variety of simulations [*Harrison et al.*, in prep. *Jolly and Haxeltine*, 1997; *Mahowald et al.*, 1999].

3.2.2 Climate and CO_2 scenarios

For the potential natural present-day simulation I ran BIOME4 with the baseline climatology described above and a CO_2 concentration of 324 ppm (the mean ambient atmospheric [CO_2] during the period on which the climatology is based). For the LGM experiment I used a climatology derived from the GENESIS/IBIS atmosphere-vegetation general circulation model (AVGCM) and a atmospheric CO_2 concentrations of both 211 ppm (glacial minimum) and 324 ppm (control).

I used the GENESIS/IBIS AVGCM output to drive the BIOME4 model for the LGM climate scenario described by Levis [1999]. This simulation is unique because it represents the only available dynamically-linked 3D atmosphere-vegetation simulation of LGM climate conditions. Sensitivity tests with GENESIS/IBIS demonstrated the importance of feedbacks between atmosphere and vegetation, and the effect of low [CO_2] on vegetation, in reaching an equilibrium climate at the LGM [*Levis et al.*, 1999]. Vegetation-atmosphere feedbacks are particularly important in controlling the moisture balance of the continental interiors and therefore are key to controlling wetland and CH_4 formation.

The boundary conditions used in the GENESIS/IBIS simulations were prescribed sea surface temperatures (SST) in both control and LGM simulations, calculated orbital forcing, individual greenhouse gas forcing, and a simple parameterization of tropospheric aerosols. SSTs for the present were prescribed according to Shea *et al.* [1992] for the present and CLIMAP [1981] for the LGM. GENESIS/IBIS ran at a R15 spectral resolution (about 4.5° latitude by 7.5° longitude).

I used the GENESIS/IBIS LGM-RPV model simulation, which included the full dynamic vegetation-atmosphere coupling and the direct effect of low CO_2 on the vegetation. To generate a climatology for BIOME4, I subtracted the LGM-RPV simulation results from the present-day control simulation to generate anomalies for

mean monthly temperature, mean percent sunshine, and total precipitation. These climate anomalies were interpolated from the native GCM resolution to a 0.5-degree resolution grid and added to the baseline modern climatology, with corrections for differences between real paleotopography and the GCM's representation of the Earth's surface.

3.2.3 Locating wetland areas

BIOME4 simulates global vegetation distribution in the form of 28 biomes, plus monthly fields of NPP, soil moisture, heterotrophic respiration, and other biogeochemical variables. I combined these data with topographical information to determine the extent of wetlands. The algorithm selects gridcells which are sufficiently flat and with a high enough soil moisture, calculated on a monthly basis. On low-relief terrain under wet conditions, water will not flow horizontally across the landscape sufficiently to prevent the soil from becoming waterlogged. If water inputs are great enough wetlands will form on moderately flat terrain. To determine if a gridcell was flat enough to be a candidate for wetland formation I calculated the slope of every gridcell in a global five-minute digital terrain model [*GETECH*, 1996]. I ran BIOME4 for modern climate conditions and simulated wetland areas by combining monthly soil moisture with the global slope dataset. By comparing the slope-wetness result to maps of well-known wetland areas, I defined threshold values for slope (0.3%) and mean soil moisture (65% of field capacity).

3.2.4 Methane emission model

CH_4 is produced by methanogens during the anaerobic decomposition of organic matter. The primary controls on CH_4 production in wetlands are: position of the water table, soil temperature, and availability of substrate [*Walter*, 1998]. CH_4 is released to the atmosphere through diffusion, plant-mediated transport, and ebullition. Methanotrophs living in aerated conditions in the soil and on plants consume a significant amount of total CH_4 production before it reaches the free troposphere [*Ridgwell et al.*, 1999; *Walter*, 1998].

Several modeling studies have attempted to simulate CH_4 emissions on a regional or global scale. The modeling approaches differ in their complexity and specific focus on ecosystem processes. Cao *et al.* [1996], Christensen *et al.* [1996], and Potter [1997] used relatively simple parameterizations of the main factors influencing CH_4 production and transport. Walter [1998] developed a more explicit process-based model for CH_4. No previous modeling study has attempted to simulate wetland area concurrently with CH_4 emission.

To simulate CH_4 emissions I used an approach based on Christensen *et al.* [1996] where total CH_4 emission in wetlands is a fraction of simulated total heterotrophic respiration, which in turn at equilibrium is a function of NPP, soil tem-

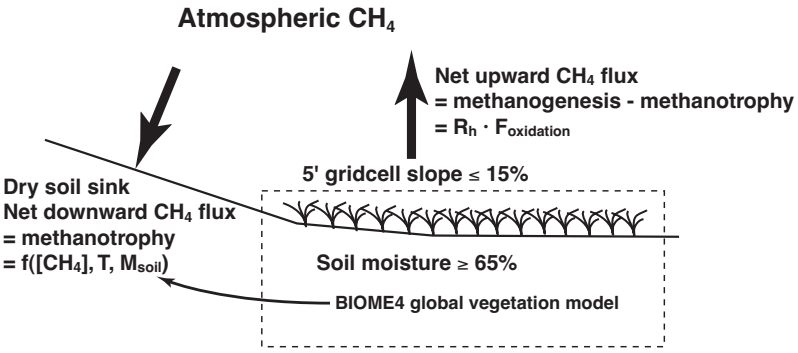

Fig. 3.2. Schematic diagram of the wetland and methane model

perature, and vegetation type (Fig. 3.2). I considered water table depth implicitly in simulating soil moisture on a monthly time step. I further extended the Christensen *et al.* [1996] method by explicitly considering vegetation type and structure to account for differences in the CH_4 oxidizing capacity of ecosystems. Wetland ecosystems dominated by grasses and other herbaceous plants were considered to have a lower oxidizing capacity and a greater propensity for direct transport of CH_4. In mixed forest and grass ecosystems which were classified as wetlands, I varied the CH_4 oxidizing capacity as a function of the ratio of grasses to trees. Forested wetlands had the highest CH_4 oxidation potential. I also adopted the model of Ridgwell [1999] to estimate the sink for CH_4 in non-wetland soils. The model uses information on soil texture, moisture, and atmospheric CH_4 concentration to determine the potential soil sink. Soil texture was derived from the soil texture information used to drive BIOME4 and the soil moisture fields were provided from BIOME4.

3.3 Results

3.3.1 Present-day wetlands

Table 3.1. Wetland areas for present-day, Pre-industrial Holocene (PIH), and LGM in 10^6 km^2

Study	Present-day	PIH	LGM
This study (potential natural)	11.0		12.9
Chappellaz et al. 1993	5.2	6.3	2.6
Aselmann and Crutzen 1989	5.7	7.0	
Cogley 1994	4.6		
Darras et al. 1999	9.5		
Mathews and Fung 1987	5.3		

Global potential natural wetland area was simulated as 11 10^6 km^2, which is considerably larger than previous estimates, but plausible based on comparison to observed wetland datasets and reduction in wetland area by anthropogenic activity. Present-day wetland area estimates from maps, satellite remote sensing, field observation, or a combination of these range from 4.6 to 9.5 10^6 km^2 (Table 3.1). However, comparison among these wetland datasets shows a great deal of disagreement as to the location of wetland areas [*Darras et al.*, 1999; *Hagemann and Dümenil*, 1997]. In a comparison of four wetland distribution datasets, Darras et al. [1999] found that only 28 1° grid cells classified as wetland were common to all datasets. Seasonal wetland area may be underestimated even in the highest total estimates [*Darras et al.*, 1999]. About half of the total global wetland area simulated by BIOME4 exists only seasonally (Fig. 3.3). Additionally, wetland area is generally considered to have decreased during the last 4000 years, and especially in the last 200, as a result of anthopogenic activities [*Aselmann and Crutzen*, 1989; *Chappellaz et al.*, 1993b]. Wetland area may have been 1-2 x 10^6 km^2 greater in the preindustrial compared to the present. Thus, a global estimate of 11.0 x 10^6 km^2 is reasonable, however, it is difficult to assess the performance of the model precisely. Future developments in remotely sensing wetland area using passive microwave techniques (SMMR and SMM/I) [*Hamilton et al.*, 1996; *Sippel et al.*, 1998] and synthetic aperture radar (SAR) [*Kasischke and BourgeauChavez*, 1997; *Kushwaha et al.*, 2000] may provide a robust dataset to validate the wetland model. However, no global compilation of wetland area based on these techniques is available at the present [*Matthews*, 2000].

The major, permanent boreal wetlands of the Western Siberian Lowlands and Hudson Bay Lowlands are easily identifiable. In addition, smaller boreal wetlands are simulated, including the wetlands of southwest Alaska, European Arctic Russia,

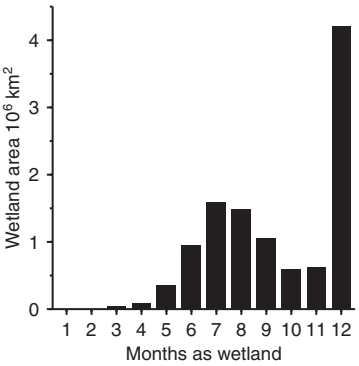

Fig. 3.3. Simulated duration of potential natural wetlands for the present-day

Finland, the Amur River lowland, and the Red Lake wetland complex of northern Minnesota. Among temperate wetlands large, potential wetlands in the Waddenzee-Maas-Waal estuaries of The Netherlands, the Pripet Marshes of Belarus and Poland, and the Yellow River plain in central China are simulated. The subtropical wetlands of the Florida Everglades and many small natural wetlands of South China are also simulated realistically.

In the tropics and Southern Hemisphere, major, permanent wetlands appear in the Amazon and Congo basins, along the lowlands of Sumatra, Borneo, and New Guinea, and in the delta of the Niger River. Only seasonal wetlands are found at the Mouths of the Ganges, presumably because of the extreme seasonality of precipitation related to the Monsoon. Extensive wetlands appear in the lowlands along the Rio Plata in middle South America, and in the Argentine and Uruguayan Pampas. Short-lived seasonal wetlands that have been described in semi-arid eastern Australia and on the Ganges plain were also simulated [*Boon and Lee*, 1997; *Boon and Sorrell*, 1995; *Muller et al.*, 1994].

3.3.2 LGM wetlands

At the LGM, global wetland area increased nearly 15% compared to the potential natural present-day simulation (Table 3.1). In addition there are large shifts in the geographic distribution of wetlands. The low relief of the continental shelves promote wetland formation, especially in the tropics and in Beringia. While the wetlands of Europe, northern Siberia, and Hudson Bay are covered by ice sheets, large wetland areas appear in Beringia, on the Sunda and New Guinea Shelves, and the Atlantic coastal shelves of North and South America. The wetlands of the Yellow-Yangtze River delta expand out to the China Sea shelf and greatly increase in extent compared to the present potential simulation. Wetlands in the Amazon and Congo basins remain roughly the same size. Our prediction of wetland areas are supported by evidence from shallow marine cores shows that extensive river and wetland sys-

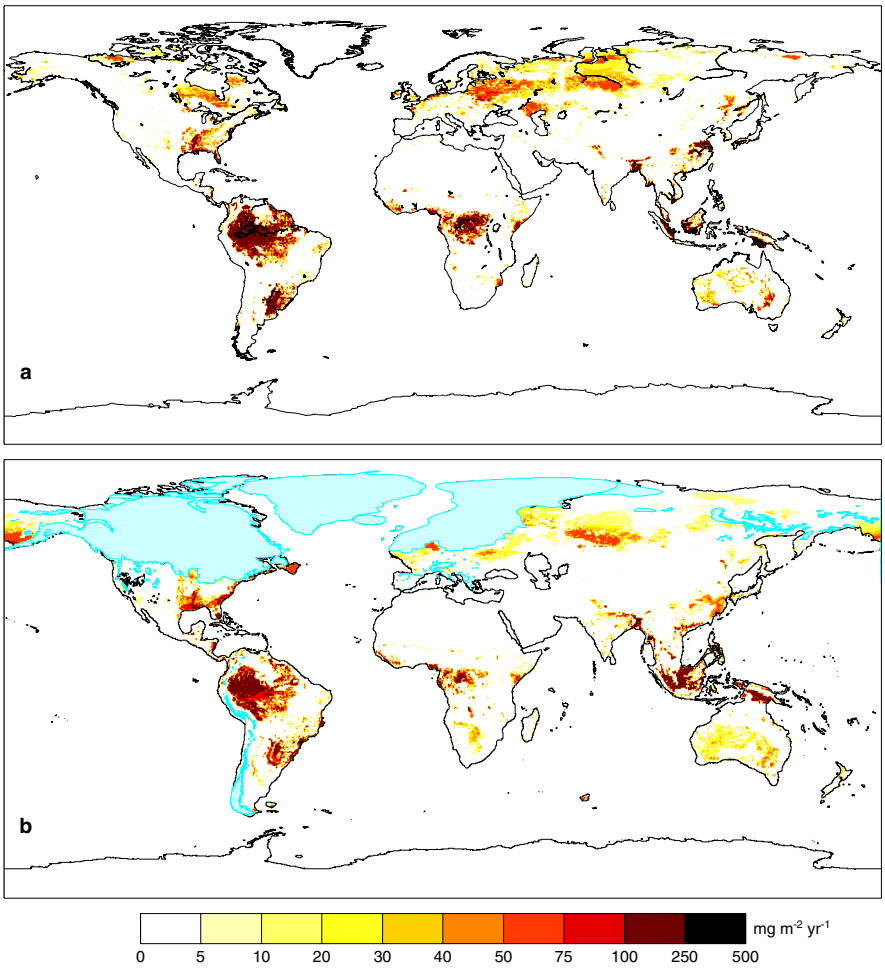

Fig. 3.4. Potential natural wetlands and CH_4 emission simulated for **a** the present-day and **b** the LGM

tems existed on the Sunda shelf at the LGM [*Hanebuth et al.*, 2000]. Pollen and other paleovegetation data indicate the existence of wetland vegetation on Beringia and southeastern North America [*Edwards et al.*, in press; *Webb et al.*, 1993].

3.3.3 CH_4 emissions

Simulated CH_4 emissions for the present-day are 140 Tg per year, which is within the range of several other studies, despite the wide discrepancy in wetland area (Table 3.2) [*Matthews*, 2000]. The greater wetland area simulated by BIOME4 com-

Table 3.2. Estimated global natural CH_4 source in Tg per year, net of the soil CH_4 sink. Bottom-up methods refer to process-based estimates of the CH_4 source, top-down studies use measured tropospheric or ice-core CH_4 concentrations, and may also use isotopic composition, to infer source strengths.

Study	Present-day	PIH	LGM
wetland CH_4 source simulated using bottom-up methods			
This study	140		107
Aselman and Crutzen 1989	80		
Bartlett and Harris 1993	109		
Cao et al. 1996	92		
Chappellaz et al. 1993	115	136	76
Matthews and Fung 1987	110		
Walter 1998	263		
wetland CH_4 source inferred using top-down methods			
Hein et al. 1997	227		
Houweling 1999	131	163	
total CH_4 source inferred using top-down methods			
Brook et al. 2000		159	111
Crutzen and Brühl 1993	570	225	95
Dällenbach et al. 2000			106
Martinerie et al . 1995	496	187	115
McElroy 1989			180
Pinto and Khalil 1991		170	95
Valentin and Crutzen 1990		252	175

pared to other studies may be largely comprised of low productivity or short-lived wetlands which do not have a strong effect on the global CH_4 source. The soil sink for CH_4 is calculated as 14 Tg, similar to other results [*Chappellaz et al.*, 1993b; *Fung et al.*, 1991; *Ridgwell et al.*, 1999].

The majority of global CH_4 emissions come from tropical wetlands in the Amazon basin and Indonesia, where in many areas net flux is simulated over 250 mg CH_4 m^{-2} yr^{-1} (Fig. 3.4). Temperate wetlands have lower annual emissions ranging between 50 and 100 mg m^{-2} yr^{-1}. Boreal and tundra wetlands have annual emissions between 5 and 75 mg m^{-2} yr^{-1}. These values for net CH_4 emissions are comparable to measurements that integrate over wide areas, though higher peak emissions may be measured at point locations [for a review see *Matthews*, 2000]. Sharp contrasts in CH_4 emission rates, and even source/sink transitions, are common over short distances within wetland complexes due to strong vegetation and topographic control [*Christensen et al.*, 2000]. Integration over larger scales tends to reduce average net emissions per unit area, which has been observed in comparison of concurrent chamber and eddy-flux measurements [*Christensen et al.*, 2000; *Friborg et al.*, 2000]. Thus, the very high net CH_4 fluxes (>10000 mg m^{-2} yr^{-1}) which have been

reported in tropical wetlands [*Smith et al.*, 2000], are unlikely to appear when integrated over the 5' (~85 km^2 in the tropics) grid cell used by the model.

At the LGM CH_4 emission rates were typically lower than emissions in the present-day simulation, with tropical wetlands reaching peak emissions of only 250 mg m^{-2} yr^{-1} (Fig. 3.4). Temperate emissions ranged between 10 and 75 mg m^{-2} yr^{-1}. The global simulated net flux of CH_4 was 107 Tg yr^{-1}. Though total wetland area was 15% greater than present, the global CH_4 emissions of were 25% lower compared to the present-day potential. Mean CH_4 emissions per unit area were also lower compared to the present due to lower temperatures and substrate limitation due to low atmospheric CO_2 content. The soil sink for CH_4 is estimated at 0.6 Tg per year because the low ambient atmospheric CH_4 concentration limits the availability of CH_4 for methanotrophs.

3.4 Discussion

The distribution of global wetlands has changed significantly since the LGM. Sea level rise since the end of the glacial period has caused major shifts in global wetland area. Wetlands that once covered large parts of the continental shelves were flooded while new wetlands developed in the wake of retreating ice sheets, especially in boreal Europe and North America. However, the 15% reduction in wetland area was concurrent with a 25% increase in CH_4 production.

Low atmospheric CO_2 concentrations at the LGM limited wetland vegetation productivity that in turn caused a substrate limitation to the formation of CH_4. In a sensitivity test, I used the vegetation-wetland-CH_4 emissions model with the simulated LGM climate scenario but mid-20^{th} century CO_2 concentrations. The result produced a global wetland CH_4 source of 140 Tg per year, identical to the preindustrial simulated source.

The LGM CH_4 source and wetland area may be slightly overestimated because of the GCM climatology. Recent data suggest that the tropical CLIMAP SSTs used by the GCM were too warm [*Farrera et al.*, 1999] and may therefore produce an overestimate of precipitation in the LGM tropics, leading to excess simulated wetland area and CH_4 emissions.

The terrestrial sink for CH_4 increased twentyfold from less than one Tg CH_4 per year at the LGM to nearly 15 Tg CH_4 per year in the present-day, largely due to the increase in atmospheric CH_4 concentrations. At the low CH_4 concentrations of the LGM, the model suggests that methanotrophs were unable to metabolize CH_4 from the atmosphere, limiting the potential sink. Changes in the atmospheric OH sink may therefore be needed to explain the increase in atmospheric CH_4 since the LGM. This result is in contrast to earlier studies which suggested that the long-term increases in atmospheric CH_4 concentration were the effect of changing temperature and precipitation patterns on wetlands (Table 3.2) [*Chappellaz et al.*, 1993*b*; *Crutzen and Bruhl*, 1993; *Martinerie et al.*, 1995; *Petit-Maire et al.*, 1991; *Pinto and*

Khalil, 1991; *Thompson et al.*, 1993]. Atmospheric OH concentrations are strongly regulated by the concentration of other biogenic trace gases (chiefly CO and NO_x). It is expected that source strength and emission patterns of these gases were very different at the LGM due to major alterations in vegetation distribution, climate, and fire regimes. To better constrain LGM OH concentrations requires further research towards building a comprehensive model of trace gas sources to the atmosphere.

3.5 Conclusions

While the location of wetlands since the Last Glacial Maximum has changed greatly, neither the global total wetland area nor consequent CH_4 emissions changed in proportion with the observed changes in atmospheric CH_4 recorded in ice cores. CH_4 emissions are strongly controlled by substrate availability, which at the LGM was strongly limited by low atmospheric CO_2 concentrations. These results place the close co-variance of the ice-core derived polar temperatures and atmospheric CH_4 concentration into a new light, as it appears that the mechanisms controlling the global CH_4 source over glacial-interglacial time scales are less sensitive to climate change than previously thought. On shorter timescales, CH_4 from boreal wetlands may respond rapidly to climate change, as recent work has suggested [*Worthy et al.*, 2000].

CH_4 concentrations increased simultaneously with polar temperature at the end of the LGM [*Blunier et al.*, 1995; *Brook et al.*, 2000]. It has been proposed that sudden releases of methane hydrates from unstable continental shelves could be the cause of the change in ice core CH_4 and a trigger for increased polar temperatures [*Nisbet*, 1990; *Nisbet*, 1992]. However, subsequent, high-resolution ice-core analyses have failed to find the extreme CH_4 "spike" that would be expected under this hypothesis [*Brook et al.*, 2000; *Chappellaz et al.*, 2000; *Dällenbach et al.*, 2000].

Other abiotic factors may have triggered the increase of atmospheric CH_4. This study shows that the large wetland areas in western Siberia and Beringia were relatively small CH_4 sources at the LGM. The wetlands of present-day northern Siberia were not glaciated at the LGM; CH_4 emissions there were limited at the LGM by low temperatures. Recent field studies have emphasized the importance of frozen peat as a potential CO_2 and CH_4 source [*Christensen*, 1999]. Short-term warming events in the high northern latitudes may have led to formation of CH_4 from wetlands in the thawing tundra. Ice-core analyses have suggested that the rapid increase in CH_4 seen at the beginning of the Bølling-Allerod interstadial, were due in large part to northern hemisphere extra-tropical wetlands [*Brook et al.*, 2000; *Dällenbach et al.*, 2000].

Later as sea level rose, tropical wetlands were inundated, reducing total wetland area, which may have counteracted the short-term effect of increased northern CH_4 production. Tropical wetlands have CH_4 emission rates typically five times greater

per unit area than boreal wetlands; even a small decrease in tropical wetland area could have a large impact on the total global CH_4 source.

These hypotheses rest largely on our knowledge of the processes controlling CH_4 formation on land and destruction in the atmosphere. While much good data exist on CH_4 production from Boreal and Arctic wetlands, better process-based understanding of CH_4 emission in tropical wetlands is critical. Tropical wetlands account for more than half of present-day wetland CH_4 emissions. Some data exist for paddy rice and subtropical wet-grasslands but the wide range of oxidation potential and net CH_4 emission measured in temperate and boreal ecosystems leads us to expect the same wide range in tropical systems. Furthermore, while there is a good understanding of their chemistry, the natural sources of other reactive trace gases at the Earth's surface are even less well quantified. Better unified models of biogenic trace gas sources and chemistry, are needed to properly assess the natural role of CH_4 and its feedbacks on the global climate system.

Acknowledgements. I thank S. Levis for providing the GCM simulation output and W. Cramer for the 20th century climatology. I.C. Prentice, S. Shafer, P.J. Bartlein, J.W. Williams and several others contributed to the development of the BIOME4 model. I.C. Prentice and S. Houweling made valuable comments on the manuscript.

References

Adams, J.M., H. Faure, L. Faure-Denard, J.M. McGlade, and F.I. Woodward, Increases in terrestrial carbon storage from the last glacial maximum to the present, *Nature*, *348*, 711-714, 1990.

Aselmann, I., and P.J. Crutzen, Global distribution of natural freshwater wetlands and rice paddies, their net primary productivity, seasonality and possible methane emissions, *Journal of Atmospheric Chemistry*, *8* (4), 307-358, 1989.

Bartlett, K.B., and R.C. Harriss, Review and assessment of methane emissions from wetlands, *Chemosphere*, *26* (1-4), 261-320, 1993.

Blunier, T., J. Chappellaz, J. Schwander, B. Stauffer, and D. Raynaud, Variations in atmospheric methane concentration during the Holocene epoch, *Nature*, *374* (6517), 46-49, 1995.

Boon, P.I., and K. Lee, Methane oxidation in sediments of a floodplain wetland in south-eastern Australia, *Letters in Applied Microbiology*, *25* (2), 138-142, 1997.

Boon, P.I., and B.K. Sorrell, Methane fluxes from an Australian floodplain wetland: The importance of emergent macrophytes, *Journal of the North American Benthological Society*, *14* (4), 582-598, 1995.

Brook, E.J., S. Harder, J. Severinghaus, E.J. Steig, and C.M. Sucher, On the origin and timing of rapid changes in atmospheric methane during the last glacial period, *Global Biogeochemical Cycles*, *14* (2), 559-572, 2000.

Cao, M., S. Marshall, and K. Gregson, Global carbon exchange and methane emission from natural wetlands: Application of a process-based model, *Journal of Geophysical Research*, *101* (D9), 14399-14414, 1996.

Chappellaz, J., J.M. Barnola, D. Raynaud, Y.S. Korotkevich, and C. Lorius, Ice-core record of atmospheric methane over the past 160,000 years, *Nature*, *345*, 127-131, 1990.

Chappellaz, J., T. Blunier, S. Kints, A. Dällenbach, J.-M. Barnola, J. Schwander, D. Raynaud, and B. Stauffer, Changes in the atmospheric CH_4 gradient between Greenland and Antarctica during the Holocene, *Journal of Geophysical Research*, *102* (D13), 15,987 - 15,997, 1997.

Chappellaz, J., T. Blunier, D. Raynaud, J.M. Barnola, J. Schwander, and B. Stauffer, Synchronous Changes in Atmospheric CH_4 and Greenland Climate Between 40-Kyr and 8-Kyr Bp, *Nature*, *366* (6454), 443-445, 1993a.

Chappellaz, J.A., I.Y. Fung, and A.M. Thompson, The atmospheric CH_4 increase since the Last Glacial Maximum (1). Source estimates, *Tellus Series B-Chemical and Physical Meteorology*, *45* (3), 228-241, 1993b.

Christensen, T.R., Potential and actual trace gas fluxes in Arctic terrestrial ecosystems, *Polar Research*, *18* (2), 199-206, 1999.

Christensen, T.R., and P. Cox, Response of methane emission from Arctic tundra to climatic change: results from a model simulation, *Tellus Series B-Chemical and Physical Meteorology*, *47* (3), 301-309, 1995.

Christensen, T.R., T. Friborg, M. Sommerkorn, J. Kaplan, L. Illeris, H. Soegaard, C. Nordstroem, and S. Jonasson, Trace gas exchange in a high-arctic valley 1. Variations in CO_2 and CH_4 flux between tundra vegetation types, *Global Biogeochemical Cycles*, *14* (3), 701-713, 2000.

Christensen, T.R., S. Jonasson, T.V. Callaghan, M. Havstrom, and F.R. Livens, Carbon cycling and methane exchange in Eurasian tundra ecosystems, *Ambio*, *28* (3), 239-244, 1999.

Christensen, T.R., I.C. Prentice, J. Kaplan, A. Haxeltine, and S. Sitch, Methane flux from northern wetlands and tundra - An ecosystem source modelling approach, *Tellus Series B-Chemical and*

Physical Meteorology, *48* (5), 652-661, 1996.
CLIMAP, Seasonal reconstructions of the Earth's surface as the Glacial Maximum, Geological Society of America, Boulder, 1981.
Coe, M.T., The hydrologic cycle of major continental drainage and ocean basins: a simulation of the modern and mid-Holocene conditions and a comparison with observations, *Journal of Climate*, *8* (3), 535-543, 1995.
Coe, M.T., A linked global model of terrestrial hydrologic processes: simulation of modern rivers, lakes, and wetlands, *Journal of Geophysical Research-Atmospheres*, *103* (D8), 8885-8899, 1998.
Cowling, S.A., and M.T. Sykes, Physiological significance of low atmospheric CO_2 for plant-climate interactions, *Quaternary Resear ch*, *52*, 237-242, 1999.
Crutzen, P.J., and C. Bruhl, A model study of atmospheric temperatures and the concentrations of ozone, hydroxyl, and some other photochemically active gases during the glacial, the preindustrial Holocene and the present, *Geophysical Research Letters*, *20* (11), 1047-1050, 1993.
Dällenbach, A., T. Blunier, J. Flückiger, B. Stauffer, J. Chappellaz, and D. Raynaud, Changes in the atmospheric CH_4 gradient between Greenland and Antarctica during the Last Glacial and the transition to the Holocene, *Geophysical Research Letters*, *27* (7), 1005-1008, 2000.
Darras, S., M. Michou, and C. Sarrat, IGBP-DIS Wetland Data Initiative: A first step towards identifying a global delination of wetlands, IGBP-DIS, Tolouse, 1999.
Dlugokencky, E.J., L.P. Steele, P.M. Lang, and K.A. Masarie, The Growth-Rate and Distribution of Atmospheric Methane, *Journal of Geophysical Research-Atmospheres*, *99* (D8), 17021-17043, 1994.
Edwards, M.E., P.M. Anderson, L.B. Brubaker, T. Ager, A.A. Andreev, N.H. Bigelow, L.C. Cwynar, W.R. Eisner, S.P. Harrison, F.-S. Hu, D. Jolly, A.V. Lozhkin, G.M. McDonald, C.J. Mock, J.C. Ritchie, A.V. Sher, R.W. Spear, J. Williams, and G. Yu, Pollen-based biomes for Beringia 18,000, 6000 and 0 ^{14}C yr B.P., *Journal of Biogeography*, 2000.
FAO, Digital Soil Map of the World and Derived Soil Properties, Food and Agriculture Organization, Rome, 1995.
Farrera, I., S.P. Harrison, I.C. Prentice, G. Ramstein, J. Guiot, P.J. Bartlein, R. Bonnefille, M. Bush, W. Cramer, U. von Grafenstein, K. Holmgren, H. Hooghiemstra, G. Hope, D. Jolly, S.-E. Lauritzen, Y. Ono, S. Pinot, M. Stute, and G. Yu, Tropical climates at the last glacial maximum: a new synthesis of terrestrial palaeoclimatic data. I. Vegetation, lake-levels and geochemistry, *Climate Dynamics*, *15*, 823-856, 1999.
Friborg, T., T.R. Christensen, B.U. Hansen, C. Nordstroem, and H. Soegaard, Trace gas exchange in a high-arctic valley 2. Landscape CH4 fluxes measured and modeled using eddy correlation data, *Global Biogeochemical Cycles*, *14* (3), 715-723, 2000.
Fung, I., J. John, J. Lerner, E. Matthews, M. Prather, L.P. Steele, and P.J. Fraser, 3-dimensional model synthesis of the global methane cycle, *Journal of Geophysical Research-Atmospheres*, *96* (D7), 13033-13065, 1991.
GETECH, Global DTM5, Geophysical Exploration Technology, Leeds, 1996.
Hagemann, S., and L. Dümenil, Comparison of two global wetlands datasets, in *Earth Surface Remote Sensing*, edited by G. Cecchi, E.T. Engman, and E. Zilioli, pp. 193-201, 1997.
Hamilton, S.K., S.J. Sippel, and J.M. Melack, Inundation patterns in the Pantanal wetland of South America determined from passive microwave remote sensing, *Archiv Fur Hydrobiologie*, *137* (1), 1-23, 1996.
Hanebuth, T., K. Stattegger, and P.M. Grootes, Rapid flooding of the Sunda Shelf: A late-glacial sea-level record, *Science*, *288*, 1033-1035, 2000.
Haxeltine, A., and I.C. Prentice, BIOME3: an equilibrium terrestrial biosphere model based on ecophysiological constraints, resource availability, and competition among plant functional types, *Global Biogeochemical Cycles*, *10* (4), 693-709, 1996.
Hein, R., P.J. Crutzen, and M. Heimann, An inverse modeling approach to investigate the global atmospheric methane cycle, *Global Biogeochemical Cycles*, *11* (1), 43-76, 1997.
Hostetler, S.W., and A.C. Mix, Reassessment of ice-age cooling on the tropical oceans and atmosphere, *Nature*, *399*, 673-676, 1999.

Houweling, S., Global Modeling of Atmospheric Methane Sources and Sinks, University of Utrecht, Utrecht, 1999.

Houweling, S., F. Dentener, J. Lelieveld, B. Walter, and E. Dlugokencky, The modeling of tropospheric methane: How well can point measurements be reproduced by a global model?, *Journal of Geophysical Research-Atmospheres*, *105* (D7), 8981-9002, 2000.

Jolly, D., and A. Haxeltine, Effect of low glacial atmospheric CO_2 on tropical African montane vegetation, *Science*, *276*, 786-788, 1997.

Kasischke, E.S., and L.L. BourgeauChavez, Monitoring South Florida wetlands using ERS-1 SAR imagery, *Photogrammetric Engineering and Remote Sensing*, *63* (3), 281-291, 1997.

Kushwaha, S.P.S., R.S. Dwivedi, and B.R.M. Rao, Evaluation of various digital image processing techniques for detection of coastal wetlands using ERS-1 SAR data, *International Journal of Remote Sensing*, *21* (3), 565-579, 2000.

Leemans, R., and W.P. Cramer, The IIASA Database for Mean Monthly Values of Temperature, Precipitation, and Cloudiness on a Global Terrestrial Grid, pp. 62, International Institute for Applied Systems Analysis, Laxenberg, 1991.

Levis, S., J.A. Foley, and D. Pollard, CO2, climate, and vegetation feedbacks at the Last Glacial Maximum, *Journal of Geophysical Research-Atmospheres*, *104* (D24), 31191-31198, 1999.

Lu, Y., and M.A.K. Khalil, Tropospheric OH: Model calculations of spatial, temporal and secular variations, *Chemosphere*, *23*, 397-444, 1991.

Mahowald, N., K.E. Kohfeld, M. Hansson, Y. Balkanski, S.P. Harrison, I.C. Prentice, M. Schulz, and H. Rodhe, Dust sources and deposition during the last glacial maximum and current climate: A comparison of model results with paleodata from ice cores and marine sediments, *Journal of Geophysical Research-Atmospheres*, *104* (D13), 15895-15916, 1999.

Martinerie, P., G.P. Brasseur, and C. Granier, The chemical composition of ancient atmospheres: a model study constrained by ice core data, *Journal of Geophysical Research-Atmospheres*, *100* (D7), 14291-14304, 1995.

Matthews, E., Wetlands, in *Atmospheric Methane*, edited by M.A.K. Khalil, Springer-Verlag, Berlin, 2000.

Matthews, E., and I. Fung, Methane emission from natural wetlands: Global distribution, area, and environmental characteristics of sources, *Global Biogeochemical Cycles*, *1* (1), 61-86, 1987.

McElroy, M.B., Studies of Polar Ice: Insights for atmospheric chemistry, in *The Environmental Record in Glaciers and Ice Sheets*, edited by H. Oeschger, and C.C. Langway, pp. 363-377, John Wiley and Sons, New York, 1989.

Muller, K.L., G.G. Ganf, and P.I. Boon, Methane Flux From Beds of Baumea-Arthrophylla (Nees) Boeckeler and Triglochin-Procerum R-Br At Bool Lagoon, South Australia, *Australian Journal of Marine and Freshwater Research*, *45* (8), 1543-1553, 1994.

Nisbet, E.G., The end of the Ice Age, *Canadian Journal of Earth Sciences*, *27* (1), 148-157, 1990.

Nisbet, E.G., Sources of atmospheric CH_4 in early postglacial time, *Journal of Geophysical Research*, *97* (N.O. D12), 12,859-12,867, 1992.

Petit, J.R., J. Jouzel, D. Raynaud, N.I. Barkov, J.M. Barnola, I. Basile, M. Bender, J. Chappellaz, M. Davis, G. Delaygue, M. Delmotte, V.M. Kotlyakov, M. Legrand, V.Y. Lipenkov, C. Lorius, L. Pepin, C. Ritz, E. Saltzman, and M. Stievenard, Climate and atmospheric history of the past 420,000 years from the Vostok ice core, Antarctica, *Nature*, *399* (6735), 429-436, 1999.

Petit-Maire, N., M. Fontugne, and C. Rouland, Atmospheric methane ratio and environmental changes in the Sahara and Sahel during the last 130 kyrs, *Palaeogeography Palaeoclimatology Palaeoecology*, *86* (1-2), 197-204, 1991.

Pinto, J.P., and M.A.K. Khalil, The stability of tropospheric OH during ice ages, inter-glacial epochs and modern times, *Tellus Series B-Chemical and Physical Meteorology*, *43* (5), 347-352, 1991.

Potter, C.S., An ecosystem simulation model for methane production and emission from wetlands, *Global Biogeochemical Cycles*, *11* (4), 495-506, 1997.

Prentice, I.C., M.T. Sykes, M. Lautenschlager, S.P. Harrison, O. Denissenko, and P.J. Bartlein, Modelling global vegetation patterns and terrestrial carbon storage at the last glacial maxi-

mum, *Global Ecology and Biogeography Letters*, *3*, 67-76, 1993.

Raynaud, D., J. Chappellaz, J.M. Barnola, Y.S. Korotkevich, and C. Lorius, Climatic and CH_4 Cycle Implications of Glacial Interglacial Ch4 Change in the Vostok Ice Core, *Nature*, *333* (6174), 655-657, 1988.

Ridgwell, A.J., S.J. Marshall, and K. Gregson, Consumption of atmospheric methane by soils: A process-based model, *Global Biogeochemical Cycles*, *13* (1), 59-70, 1999.

Schimel, D., D. Alves, I. Enting, M. Heimann, F. Joos, D. Raynaud, T. Wigley, M. Prather, R. Derwent, D. Ehhalt, P. Fraser, E. Sanhueza, X. Zhou, P. Jonas, R. Charlson, H. Rodhe, S. Sadasivan, K.P. Shine, Y. Fouquart, V. Ramaswamy, S. Solomon, J. Srinivasan, D. Albritton, R. Derwent, I. Isaksen, M. Lal, and D. Wuebbles, Radiative forcing of climate change, in *Climate Change 1995: The Science of Climate Change*, edited by J.T. Houghton, L.G. Meira Filho, B.A. Callander, N. Harris, A. Kattenberg, and K. Maskell, pp. 65-131, Cambridge University Press, Cambridge, 1996.

Shea, D.J., K.E. Trenberth, and R.W. Reynolds, A global monthly sea surface temperature climatology, *Journal of Climate*, *5*, 987-1001, 1992.

Sippel, S.J., S.K. Hamilton, J.M. Melack, and E.M.M. Novo, Passive microwave observations of inundation area and the area/stage relation in the Amazon River floodplain, *International Journal of Remote Sensing*, *19* (16), 3055-3074, 1998.

Smith, L.K., W.M.J. Lewis, J.P. Chanton, G. Cronin, and S.K. Hamilton, Methane emissions from the Orinoco River floodplain, Venezuela, *Biogeochemistry*, *51* (2), 113-140, 2000.

Thompson, A.M., J.A. Chappellaz, I.Y. Fung, and T.L. Kucsera, The atmospheric CH_4 increase since the Last Glacial Maximum (2). Interactions with oxidants, *Tellus Series B-Chemical and Physical Meteorology*, *45* (3), 242-257, 1993.

Valentin, K.M., Numerical modeling of the climatological and anthropogenic influences on the chemical composition of the troposphere since the Last Glacial Maximum, Johannes-Gutenberg-University, Mainz, 1990.

Walter, B., Development of a Process-Based Model to Derive Methane Emissions from Natural Wetlands for Climate Studies, Universität Hamburg, Hamburg, 1998.

Webb, T., III, P.J. Bartlein, S.P. Harrison, and K.H. Anderson, Vegetation, lake levels and climate in eastern North America for the past 18,000 years, in *Global changes since the last glacial maximum*, edited by H.E. Wright, Jr, J.E. Kutzbach, T. Webb, III, W.F. Ruddiman, F.A. Street-Perrott, and P.J. Bartlein, pp. 415-467, University of Minnesota Press, Minneapolis, 1993.

Whiting, G.J., and J.P. Chanton, Primary production control of methane emission from wetlands, *Nature*, *364*, 794-795, 1993.

Worthy, D.E.J., I. Levin, F. Hopper, M.K. Ernst, and N.B.A. Trivett, Evidence for a link between climate and northern wetland methane emissions, *Journal of Geophysical Research-Atmospheres*, *105* (D3), 4031-4038, 2000.

4 The stable carbon isotope composition of the terrestrial biosphere

Modeling at scales from the leaf to the globe

Jed O. Kaplan[1,2], I. Colin Prentice[1,2], and Nina Buchmann[2]
[1]Plant Ecology, Department of Ecology, Lund University, Sweden
[2]Max Planck Institute for Biogeochemistry, Jena, Germany

Abstract. Global datasets of the stable carbon isotope composition of plant leaves, of CO_2 in canopy air, and of CO_2 in the free troposphere were compiled and compared to results of a global vegetation model (BIOME4) that simulated, at these three scales, the magnitude, direction, and timing of fluxes of CO_2 and ^{13}C between the biosphere and the atmosphere. Carbon isotope data on leaves were classified into 12 Plant Functional Types (PFTs), and measurements from canopy flasks were assigned to 16 biomes, for direct comparison to model results. BIOME4 simulated the observed leaf $\delta^{13}C$ values to within one standard deviation of the measured mean for most PFTs. Modeled $\delta^{13}C$ for C_3 grasses, tundra shrubs, and herbaceous plants of cold climates deviated only slightly more from measurements, perhaps as a result of the wide geographic range and a limited set of measurements of these PFTs. Modeled ecosystem isotopic discrimination against ^{13}C (Δ_e) averaged 18.6‰ globally when simulating potential natural vegetation and 18.1‰ when an agricultural crop mask was superimposed. The difference was mainly due to the influence of C_4 agriculture in areas that are naturally dominated by C_3 vegetation. Model results show a gradient in Δ_e among C_3-dominated biomes as a result of stomatal responses to aridity; this model result is supported by canopy air measurements. At the troposphere scale, BIOME4 was coupled to an adjoint atmospheric tracer transport matrix to simulate seasonally varying concentrations of CO_2 and ^{13}C at remote northern-hemisphere measuring stations. Ocean CO_2 and ^{13}C flux fields were included, using the HAMOCC3 ocean biogeochemistry model [*Six and Maier-Reimer*, 1996]. Model results and observations show similar seasonal cycles, and the model reproduces the inferred latitudinal trend towards smaller isotopic discrimination by the biosphere at lower latitudes. These results indicate that biologically mediated variations in ^{13}C discrimination by terrestrial ecosystems may be significant for atmospheric inverse modeling of carbon sources and sinks, and that such variations can be simulated using a process-based model.

4.1 Introduction

Sources and sinks of carbon (C) in the terrestrial biosphere and the ocean can in principle be separated using measurements of the concentration and stable isotope

composition of atmospheric CO_2 [*Francey et al.*, 1995; *Keeling et al.*, 1979; *Tans*, 1980; *Tans et al.*, 1993]. Because the terrestrial biosphere discriminates strongly against ^{13}C during photosynthesis, the $^{13}C/^{12}C$ ratio of CO_2 in the atmosphere ($\delta^{13}C$) has been used to partition the sources and sinks of atmospheric CO_2 between oceanic and terrestrial components [*Bakwin et al.*, 1998; *Battle et al.*, 2000; *Bousquet et al.*, 1999; *Ciais et al.*, 1995a; *Ciais et al.*, 1995b; *Fung et al.*, 1997; *Trolier et al.*, 1996]. However, the partitioning calculation is sensitive to various quantitative assumptions. A 10% inaccuracy in the assumed carbon isotopic composition of the terrestrial biosphere (1-2‰) will produce a change in the inferred terrestrial C sink equal to the entire magnitude of the sink[*Fung et al.*, 1997]. Furthermore, the carbon isotope signature of the terrestrial biosphere may change from year to year as vegetation composition and carbon-exchange characteristics respond to interannual climatic variability [*McGuire et al.*, in press; *Sitch*, 2000]. Optimal use of atmospheric CO_2 observations for studying the global carbon cycle therefore requires both extensive, precise observations of $\delta^{13}C$ of CO_2 in the atmosphere, and the development of models that can reliably simulate spatial and temporal variability in terrestrial C isotope discrimination.

Here, a global terrestrial vegetation model (BIOME4) is used to simulate the isotopic signature of the terrestrial biosphere. The model results are compared to measurements at three scales: leaf, canopy, and free atmosphere. The simulated Δ_{leaf}, or leaf-level discrimination, is compared to estimates of Δ_{leaf} based on leaf $\delta^{13}C$ measurements. Simulated total ecosystem discrimination Δ_e is compared to canopy-level measurements. The seasonal cycle of tropospheric CO_2 and ^{13}C is simulated by combining BIOME4 with an ocean biogeochemistry model and coupling the resultant flux field to an atmospheric tracer transport matrix. The simulated CO_2 concentrations and $\delta^{13}C$ of atmospheric CO_2 are compared to measurements of free tropospheric air at several stations in the NOAA/CMDL global sampling network.

4.2 Methods

4.2.1 $\delta^{13}C$ of plant leaves

We compiled a global dataset of over 1000 measurements of $\delta^{13}C$ in plant leaves from a wide range of terrestrial ecosystems. Each plant measurement was classified into one of 12 plant functional types (PFTs) [*Buchmann and Kaplan*, in press; *Kaplan*, 2001]. The PFTs represent the major bioclimatic types and growth forms of terrestrial plants and were defined so as to be directly comparable to those used by the vegetation model. Each PFT was represented by at least 50 samples from different individuals. $\delta^{13}C$ measurements on agricultural crops were not included in the

dataset. When Δ_{leaf} was not directly reported, it was calculated from $\delta^{13}C$ measurements using

$$\Delta_{leaf} = \frac{\delta_{atm} - \delta_{leaf}}{1 + \delta_{leaf}} \tag{4.1}$$

where δ_{atm} was assigned the late 20th century mean atmospheric background value of -8‰ [*Ehleringer et al.*, 1987; *Körner et al.*, 1988; *Körner et al.*, 1991].

4.2.2 Ecosystem $\delta^{13}C$

We compiled a global dataset of Δ_e at the ecosystem level from air flask samples taken at 46 field sites spanning 42° S to 63° N latitude. For a detailed description of the flask sampling strategy and Δ_e calculation see Buchmann and Kaplan [in press]. The $\delta^{13}C$ of respired CO_2 during ecosystem respiration ($\delta^{13}C_{ER}$) represents a weighted average of all respiration processes within the ecosystem. The "Keeling plot" method was used to infer Δ_e [*Buchmann et al.*, 1998; *Keeling*, 1958; *Keeling*, 1961]. This method has several advantages over scaling results from small-scale enclosure studies (i.e. on foliage, stem and soil respiration) to an ecosystem level to estimate ecosystem respiration [*Lavigne et al.*, 1997]. The Keeling plot method integrates spatially over all autotrophic and heterotrophic respiration fluxes within the ecosystem. Furthermore, it results in a flux-weighted estimate of $\delta^{13}C_{ER}$ that includes both plant respiration as well as fast and slowly decomposing carbon pools and their carbon isotope signatures.

The Keeling plot [*Keeling*, 1958; *Keeling*, 1961] is based on the principle that the measured, time-varying atmospheric concentration of a tracer can be expressed as a combination of a background amount already present in the atmosphere and an amount that is added or removed by sources or sinks:

$$C_{ER} = C_{atm} + C_{source} \tag{4.2}$$

where C_{ER}, C_{atm} and C_{source} are the concentrations of the tracer in the respired air, the free atmosphere, and in the contributing source respectively. The isotope ratios of these components conform to the mass balance equation:

$$C_{ER}\delta_{ER} = C_{atm}\delta_{atm} + C_{source}\delta_{source} \tag{4.3}$$

where δ_{ER}, δ_{atm} and δ_{source} represent the isotopic composition of the tracer in the respired air, in the atmosphere and the source, respectively.

Combining Eqs. 4.2 and 4.3 and rearranging results in:

$$\delta_{ER} = \left[C_{atm}(\delta_{atm} - \delta_{source})\left(\frac{1}{C_{ER}}\right) + \delta_{source} \right]. \quad (4.4)$$

Thus, when δ_{ER} is plotted versus $1/C_{ER}$, the slope of a line fit through the data estimates C_{atm} (δ_{atm} - δ_{source}) and the intercept of the line estimates δ_{source}.

The isotopic composition of respired CO_2 is used to determine ecosystem discrimination (Δ_e) using:

$$\Delta_e = \frac{\delta_{trop} - \delta_{resp}}{1 + \delta_{resp}} \quad (4.5)$$

where δ_{trop} and δ_{resp} represent the $\delta^{13}C$ values of tropospheric and respired CO_2 [*Buchmann et al.*, 1998; *Buchmann and Kaplan*, in press].

The Keeling plot is subject to error from the extrapolated intercept of the linear regression. Because the intercept is many units away from the actual measurements, small errors in measuring either the isotope ratios or concentration of the tracer can lead to large errors in the extrapolation. Recycling of respired CO_2 may also contribute to errors in estimating the δ values of respired CO_2 [*Buchmann et al.*, 1998; *Sternberg*, 1989]. Nevertheless, the Keeling plot is generally considered a reliable method for estimating ecosystem discrimination and is widely used in studies at scales from canopy measurements integrating 10-100 m^2 to aircraft measurements covering hundreds of km^2 [*Buchmann et al.*, 1998; *Lloyd et al.*, in press].

Results for 46 sites in natural ecosystems were used in this analysis [*Buchmann and Kaplan*, in press] (original data are available as part of the BASIN initiative: http://gcte-focus1.org/basin.html). When more than one estimate of the ^{13}C signature of ecosystem respiration was published, we calculated a growing-season mean [*Buchmann et al.*, 1998].

4.2.3 Tropospheric $\delta^{13}C$

Changes in CO_2 concentration and $\delta^{13}C$ over the seasonal cycle can be used to estimate the ^{13}C signature of the CO_2 source, also using the Keeling plot method. We calculated the isotopic signature of the CO_2 source at six Northern Hemisphere measuring stations in the NOAA/CMDL Cooperative Flask Sampling Network (Table 4.1) [*Conway et al.*, 1994]. Within this network, tropospheric air samples are collected in remote areas and analyzed for [CO_2] and $\delta^{13}C$ at regular intervals; we used the monthly mean concentrations and isotope ratios in our source calculations [*Trolier et al.*, 1996] (see also http://www.cmdl.noaa.gov/ccgg/index.html). We chose stations with a wide distribution in latitude, elevation, and position relative to the continents. The measuring stations are located on oceanic islands (Cape Kumakahi, Mauna Loa, Ragged Point), continental margins (Barrow, Alert) and in a high-elevation, mid-continental location (Niwot Ridge). Stations with less than

two years of record available in the public domain were not considered. Monthly mean data were normalized to remove the long-term trend, then averaged for each month over the number of years in the record [*Bakwin et al.* 1998]. Only months of data where both CO_2 and $\delta^{13}C$ were simultaneously available were used in computing the monthly values.

Table 4.1. Troposphere measuring stations used in calculations

Station name	abbreviation	location	longitude	latitude	elevation m.a.s.l.
Alert	ALT	Ellesmere Island, Canada	62° 31' W	82° 27' N	210
Point Barrow	BRW	Alaska, USA	156° 36' W	71° 19' N	11
Niwot Ridge	NWR	Colorado, USA	105° 35' W	40° 03' N	3475
Mauna Loa	MLO	Hawaii, USA	155° 35' W	19° 32' N	3397
Cape Kumukahi	KUM	Hawaii, USA	154° 49' W	19° 31' N	3
Ragged Point	RPB	Barbados	59° 26' W	13° 10' N	3

4.2.4 The BIOME4 vegetation model

BIOME4 is an equilibrium terrestrial biosphere model based on the BIOME3 model of [*Haxeltine and Prentice*, 1996]. BIOME4's differences from its predecessor include the addition of a module to calculate isotopic discrimination during photosynthesis (Δ_{leaf}), re-parameterization of the original PFTs with the aim of reproducing vegetation distribution and biogeochemistry more realistically, and the addition of several new PFTs to reflect poorly represented vegetation types in cold environments and the arid subtropics. Like BIOME3, BIOME4 is a coupled carbon and water flux model that predicts global vegetation distribution, structure, and biogeochemistry taking into account interactions between these aspects. The model requires as input: latitude; long-term mean monthly values of temperature, precipitation, and relative cloudiness; absolute minimum temperature (T_{min}); ambient CO_2 concentration; and soil water holding capacity and percolation rate (usually based on soil textural data).

In BIOME4, 12 PFTs represent broad physiologically distinct classes of vegetation ranging from cushion forbs, characteristic of extremely cold environments, to desert shrubs and tropical rainforest trees. Each PFT is assigned absolute bioclimatic tolerance limits that determine whether or not its net primary productivity (NPP) is calculated. Such limits are only defined in those cases where a known mechanism exists that restricts the possible range of the PFT (e.g. frost tolerance) [Kaplan, this volume][*Buchmann and Kaplan*, in press]. The core of the model is a coupled carbon and water flux scheme, which determines the value of leaf area index (LAI) that maximizes NPP for each allowable PFT. Given a certain soil water

Table 4.2. Biomes simulated by BIOME4

Number	Biome
1	Tropical evergreen broadleaf forest
2	Tropical semi-evergreen forest
3	Tropical deciduous broadleaf forest and woodland
4	Temperate deciduous broadleaf forest
5	Temperate evergreen needleleaf forest
6	Warm-temperate evergreen broadleaf and mixed forest
7	Cool mixed forest
8	Cool evergreen needlelaf forest
9	Cool-temperate evergreen needleleaf and mixed forest
10	Cold evergreen forest
11	Cold deciduous forest
12	Tropical savanna
13	Tropical xerophytic shrubland
14	Temperate xerophytic shrubland
15	Temperate sclerophyll woodland and shrubland
16	Temperate deciduous broadleaf savanna
17	Temperate evergreen needeleleaf open woodland
18	Cold parkland
19	Tropical grassland
20	Temperate grassland
21	Desert
22	Graminoid and forb tundra
23	Low- and high-shrub tundra
24	Erect dwarf-shrub tundra
25	Prostrate dwarf-shrub tundra
26	Cushion-forb, lichen, and moss tundra

balance, calculated on a daily timestep for numerical stability (interpolated from the monthly input data), the model iteratively calculates the LAI that yields the maximum gross photosynthetic uptake and canopy conductance [*Haxeltine et al.*, 1996]. NPP is then calculated as the difference between gross photosynthetic uptake and growth and maintenance respiration. Environmental factors, including seasonal patterns in precipitation as well as the ambient concentration of atmospheric CO_2, affect transpiration and carbon gain. PFT-specific parameters determine the sensitivity of each PFT to environmental variations. Photosynthetic pathway is PFT-specific: woody plants are generally C_3, while C_4 types represent tropical and subtropical grasses and C_4 desert shrubs (such as some *Atriplex* and *Euphorbia* species). The C_4 subtypes, NADP-ME, NAD-ME and PCK, are not separated. CAM photosynthesis is not considered.

Monthly mean NPP is summed on an annual basis for each PFT. The woody PFT with maximum NPP is considered the dominant PFT, except in special cases where grass or mixtures of grass and trees would be expected to dominate because of an

implied disturbance regime or soil moisture constraints. The combination of dominant and sub-dominant PFTs are classified into 26 biomes representing the major types of terrestrial vegetation (Table 4.2). Biogeochemical output from the model represents the dominant PFT for a grid-cell, as there is no explicit accommodation for mixed-PFT grid-cells. However, in the case of tropical savannas and other mixed tree-grass biomes, the output variables (including Δ_{leaf}) are given as an NPP-weighted average of the grass and tree types.

BIOME4 simulates isotopic discrimination against $^{13}CO_2$ during photosynthesis at the leaf level (Δ_{leaf}) and total ecosystem discrimination (Δ_e) (Fig. 4.1) [*Buchmann et al.*, 1998; *Flanagan and Ehleringer*, 1998]. The discrimination model for Δ_{leaf} is similar in principle to that of Lloyd and Farquhar [1994]. The main difference is that BIOME4 explicitly simulates the concentration of CO_2 inside the leaf using a process-based representation of canopy conductance. The maximum potential intercellular-to-atmospheric CO_2 concentration (c_i/c_a) ratio is prescribed for each PFT, but the actual c_i/c_a is subsequently modeled as the water-limited c_i/c_a, less than or equal to the defined maximum, which can yield a reduced evapotranspiration rate consistent with water limitation. Maximum c_i/c_a ratios were compiled from a literature survey on laboratory studies and from minimum $\delta^{13}C$ values measured for leaf material of all PFTs.

Monthly Δ_e values are estimated as the flux-weighted difference in discrimination against ^{13}C from NPP and heterotrophic respiration (R_h). Photosynthate, with a specific ^{13}C content determined by the Δ_{leaf} value, is incorporated into the plant on a seasonally integrated flux-weighted basis. A simple model for R_h determines the monthly flux of respired CO_2 and $^{13}CO_2$ to the atmosphere [*Foley*, 1995; *Lloyd and Taylor*, 1994]. The source of respired CO_2 is the aggregated annual NPP for the dominant vegetation type in a grid-cell. This carbon stock is divided into three pools which represent different turnover times [*Foley*, 1995; *Sitch*, 2000]. Each pool is subjected to a small isotopic fractionation (Δ_{decomp}) during respiration based upon the assumed decay rate of the pool (0.1-1‰). Because the processes underlying carbon isotope fractionation during respiration are poorly understood, fractionation in each pool is assigned a constant value which increases with pool age [*Buchmann et al.*, 1998; *Buchmann and Kaplan*, in press; *Ehleringer et al.*, 2000].

We ran BIOME4 at a global spatial resolution of 0.5° x 0.5°, driven by the CLIMATE 2.2 global gridded climatology [W. Cramer, *pers. comm.* 1998] (http://www.pik-potsdam.de/~cramer/climate.htm), which is an updated version of [*Leemans and Cramer*, 1991]. Ambient CO_2 concentration was set at the mean pCO_2 during the period on which the climatology is based. Soil physical parameters were derived from a global soils dataset using the IGBP/FAO soil properties scheme, which associates soil name, texture and phase, and drainage classes with water holding capacity and percolation rate [*FAO*, 1995]. Global T_{min} data were provided by P.J. Bartlein [*pers. comm.* 1998].

We generated an agricultural land-use mask for the BIOME4 simulations. The base mask represents the fractional area of agricultural crop land use in a 0.5° grid cell identified in satellite imagery for the early 1990's [*Ramankutty and Foley*, 1999].

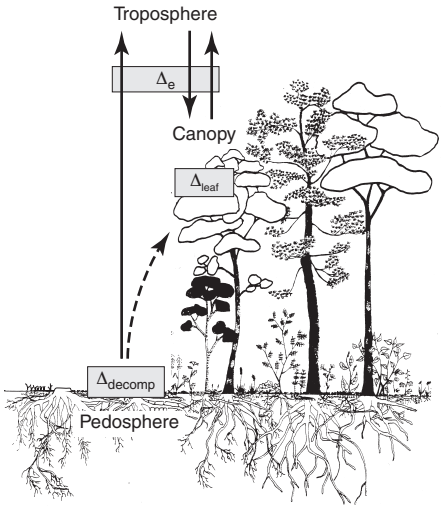

Fig. 4.1. Conceptual diagram of ecosystem discrimination in a forest. Important CO_2 fluxes are represented as arrows; carbon isotope discrimination Δ is represented in the boxes.

We identified areas traditionally dominated by C_4 crops using an economic atlas [*Jones*, 1972]. All agricultural grid cells were simulated with the C_3 and C_4 grass PFTs to obtain alternative C fluxes and $\delta^{13}C$ values. The resulting output was merged with the standard potential natural vegetation simulation of BIOME4. Outside of the climatological limits of C_4 crops, agricultural fluxes were considered to be 100% C_3. Elsewhere, agricultural fluxes were considered 80% C_3 and 20% C_4, except in certain defined places with a concentration of C_4 agriculture (e.g. North American corn belt, sugar cane areas of the Carribbean and Australia) where fluxes were assumed to be 80% C_4 and 20% C_3.

To simulate $\delta^{13}C$ and $[CO_2]$ at the troposphere level, a global flux field of CO_2 and ^{13}C was generated by combining BIOME4 with output from the HAMOCC3 ocean biogeochemistry model [*Six and Maier-Reimer*, 1996]. The seasonal cycle of CO_2 and ^{13}C at specific free-troposphere measuring stations were then simulated with the flux field as input to an adjoint tracer transport matrix derived from the TM2 atmospheric tracer transport model [*Kaminski et al.*, 1996].

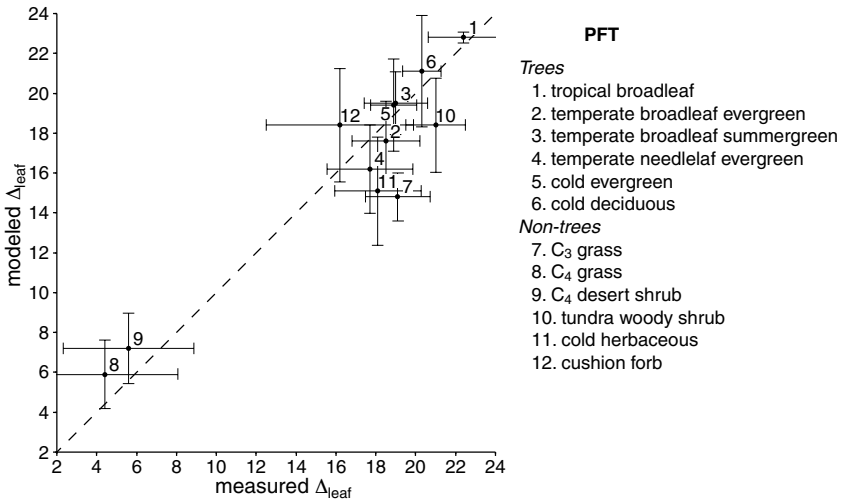

Fig. 4.2. Modeled and measured leaf carbon isotope discrimination Δ_{leaf}. Error bars represent 1 standard deviation around the mean.

4.3 Results and discussion

4.3.1 ^{13}C at the leaf scale

Modeled and measured Δ_{leaf} varied from < 6‰ in C_4 grasses to > 23‰ in tropical broadleaf trees (Fig. 4.2). At the PFT level, the strong bi-modal distribution of Δ_{leaf} between C_3 and C_4 photosynthesis is apparent. Agreement between measured and simulated Δ_{leaf} is good: values correspond within < 2‰ for most PFTs; well within 1 standard deviation around the measured mean (~4‰ for most PFTs). Among C_3 PFTs Δ_{leaf} varies ~4‰ in the simulation and slightly less in measurements. This variability among C_3 PFTs demonstrates the sensitivity of Δ_{leaf} to increasingly arid eco-climates, caused by the stomatal response to decreasing soil moisture and increasing vapor pressure defecit. It is a feature visible in the data and successfully simulated by the model. The model also captures the difference in Δ_{leaf} between C_4 grasses and C_4 desert shrubs. These results show that the model can simulate the diversity in carbon isotope discrimination measured among plants with different ranges and adaptations to climate.

Among C_3 plants, tropical broadleaf trees (1 in Fig. 4.2) have both the greatest measured and modeled Δ_{leaf}. High ratios of carbon assimilation to stomatal conductance found in tropical trees result in high c_i/c_a ratios, and therefore in low leaf carbon isotope discrimination [*Farquhar et al.*, 1989]. Minimum Δ_{leaf} for C_3 plants is measured in cushion forbs (12) but simulated in C_3 grasses (7). Simulated Δ_{leaf}

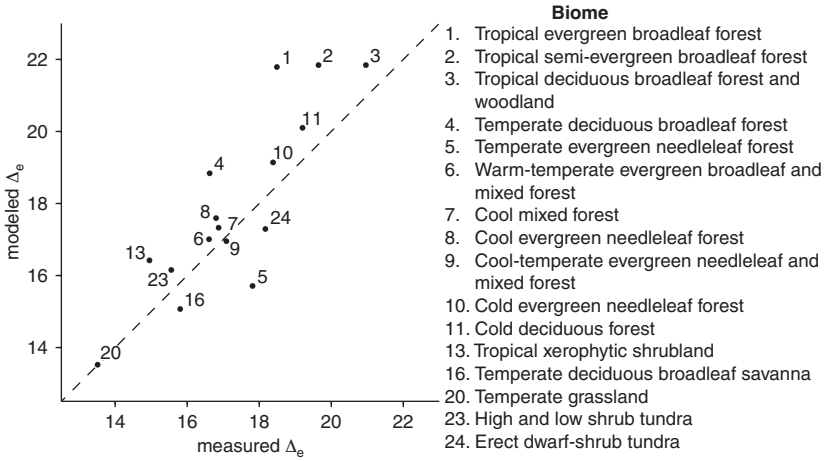

Fig. 4.3. Measured and modeled Δ_e. Flask samples of canopy and neighboring troposphere air were used to measure Δ_e. Modeled values are simulated by BIOME4 using 20th century climatology.

values for the C_3 grass (7) and cold herbaceous (11) PFTs are lower than their measured values. Measured values of Δ_{leaf} in these PFTs may be biased towards samples from mesic habitats, while the simulated Δ_{leaf} represents mainly the arid environments where the PFTs dominate. However, arid grasslands and dry tundra do not contribute greatly to global terrestrial carbon exchange; inaccuracy in model prediction is unlikely to influence the global terrestrial carbon isotope signature. Cold deciduous trees (6) (e.g. *Larix*, *Betula*, *Sorbus*) have higher Δ_{leaf} values than cold evergreen trees (5) with which they sometimes co-exist, presumably because of their physiological ability to transpire more water and hence achieve a higher c_i/c_a ratio. These model results are corroborated by field studies on leaf $\delta^{13}C$ ratios [*Kloeppel et al.*, 1998; *Lloyd and Farquhar*, 1994]. C_4 grasses (8) have lower Δ_{leaf} compared to C_4 shrubs (9) because of differences in both leaf anatomy and photosynthetic pathway (i.e. the NAD, NADP, and PCK subtypes). These differences observed in the data are implicit in the model parameterizations and captured successfully by the simulation.

4.3.2
^{13}C at the ecosystem scale

Biome-averaged measured Δ_e varied globally between 13.5‰ and 21.0‰. Temperate grassland, comprised of a mix of C_3 and C_4 vegetation, had the lowest Δ_e; tropical broadleaf forests had the highest Δ_e (Fig. 4.3, Table 4.3). Physiological constraints on C_3 photosynthesis, as well as the expression of the C_4 photosynthetic pathway, are responsible for this large global variability in Δ_e.

Model results for Δ_e display several features reflecting global trends in vegetation composition and water status. Generally, ecosystems in superhumid environments

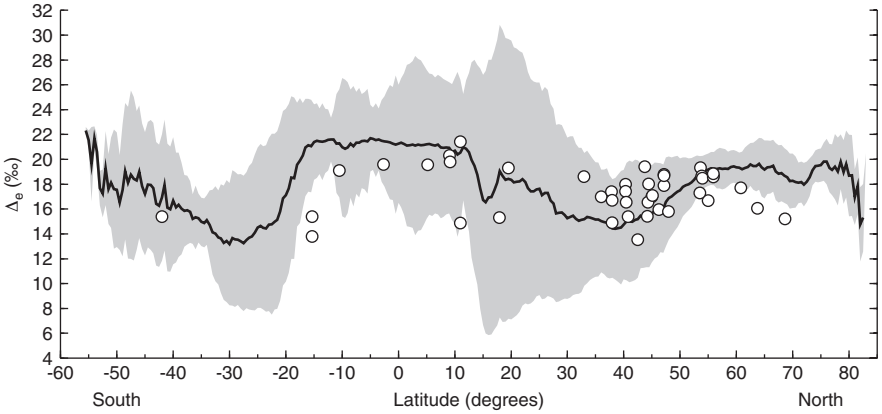

Fig. 4.4. Simulated flux-weighted latitudinal distribution of ecosystem discrimination **solid line** and measured ecosystem discrimination **open circles**. The shaded area represents 1 standard deviation around the simulated mean.

show the highest simulated Δ_e values (21-22‰), whereas C_4 dominated tropical grasslands have the lowest Δ_e values (< 5‰). Measured and modeled mean Δ_e agree within 1‰ for most biomes (Fig. 4.3), which is considerably less than the measured or modeled variability within biomes (Table 4.3). Within the area of C_3 dominated vegetation, there is a wide range of Δ_e values, representing changing water status of the vegetation and plant adaptations to more or less arid environments (Fig. 4). Deserts have characteristically low Δ_e values due to the common occurrence of C_4 species and restricted transpiration by C_3 plants. Latitudinal averages of flux-weighted Δ_e estimates display a tri-modal distribution, with maximum Δ_e values in the boreal zones of both hemispheres and in the humid tropics (Fig. 4.4). Tropical rain forests (between 10° N and S) mask the signal from C_4-dominated equatorial grasslands, such as those in East Africa. In the boreal zone (between 55° and 80° N), Δ_e is generally high because of low ratios of assimilation to stomatal conductance in boreal plants. In addition, waterlogged soils due to permafrost and low evaporative demand in cool-climate regions tend to increase Δ_e. Mean values for modeled Δ_e estimates are lowest in subtropical C_4 dominated grasslands, especially in Africa and Australia. In the temperate prairies of central North America and Eurasia, C_4 grasslands are only seasonally dominant and share latitude bands with both forests and deserts. In these regions, Δ_e values are intermediate.

Discrepancies between measured and modeled Δ_e may be due to both model and measurements. Limitations to the modeled values may come from generalization inherent in the model and inadequate parameterization of the PFTs. However, the main sources of disagreement between model and measurements stem from the limited number of measurements of Δ_e available for a particular biome (one to five point measurements) compared to the wide bioclimatic space integrated by the model, even for a single biome (10^3-10^5 km^2). Two other sources of error should be

Table 4.3. Measured and modeled mean ecosystem discrimination for 16 biomes where canopy flask measurements were available. Where no standard deviation is given, the measurement consisted of only one sample.

Biome	measured Δ_e	SD	modeled Δ_e	SD
Tropical evergreen broadleaf forest	18.5	2.34	21.8	0.22
Tropical semi-evergreen broadleaf forest	19.6	1.60	21.8	0.23
Tropical deciduous broadleaf forest and woodland	21.0	1.50	21.8	0.34
Temperate deciduous forest	16.6	0.71	18.8	1.61
Temperate evergree needleleaf forest	17.8	0.93	15.7	2.23
Warm-temperate evergreen broadleaf and mixed forest	16.6	1.13	17.0	1.60
Cool mixed forest	16.9	4.14	17.3	2.55
Cool evergreen needleleaf forest	16.8	1.00	17.6	2.56
Cool-temperate evergreen needleleaf and mixed forest	17.1	1.26	16.9	3.23
Cold evergreen needleleaf forest	18.4	1.02	19.1	1.39
Cold deciduous forest	19.2	0.67	20.1	2.18
Tropical xerophytic shrubland	14.9	1.13	16.4	8.40
Temperate deciduous broadleaf savanna	15.8		15.1	0.73
Temperate grassland	13.5	0.54	13.5	0.97
High and low shrub tundra	18.2		17.3	2.28
Erect dwarf-shrub tundra	15.6		16.1	2.01

considered for the Δ_e estimates obtained from field measurements, errors associated with the $\delta^{13}C$ of the background free-troposphere CO_2 used to compute Δ_e and the $\delta^{13}C$ of respired CO_2 collected in the canopy. The precision of the tropospheric background data is < 0.5 ppm for $[CO_2]$, and ± 0.03‰ for $\delta^{13}C$ [*Conway et al.*, 1994; *Trolier et al.*, 1996]. The larger error is associated with the estimates of $\delta^{13}C_{ER}$ extrapolating to the y-intercept. Summarizing 49 Keeling plot analyses, the standard error for $\delta^{13}C$ of respired CO_2 averaged 0.98‰ [*Buchmann et al.*, 1998].

4.3.3 Scaling Δ from leaf to ecosystem

Because canopy Δ_e measurements are time-consuming and require special apparatus, it has been recently proposed that leaf $\delta^{13}C$ measurements be used to approximate ecosystem discrimination [*Bonal et al.*, 2000; *Ehleringer*, 1997]. As BIOME4 scales from the leaf to the ecosystem level, we can test the premise that leaf carbon isotope composition should be related to Δ_e. We plotted PFT-average Δ_{leaf} against associated biome-average Δ_e for the 12 basic PFTs, and the single combination tree-grass PFT, in BIOME4 (Fig. 4.5). Reflecting the strong control of Δ_{leaf} on the carbon isotope composition of an ecosystem, Δ_{leaf} and Δ_e are highly correlated. A fit-line through the C_3 plant types has the equation $\Delta_e = 0.82\Delta_{leaf} + 2.16$ (n=24, r^2=0.67).

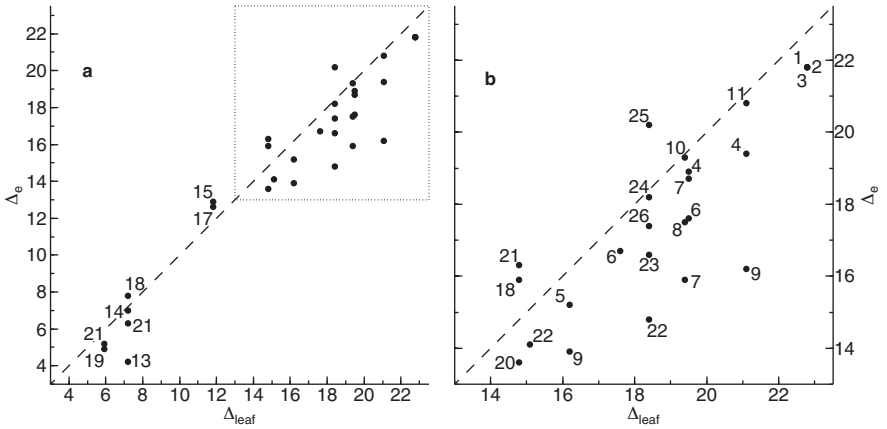

Fig. 4.5. Scaling from leaf to ecosystem. Modeled PFT-level mean Δ_{leaf} is plotted versus biome-level mean Δ_e for all PFTs **a** and for C_3 types **inset, b**. The number indicates the biome, see legend (Table 4.2).

Where modeled Δ_{leaf} is significantly greater than Δ_e, Δ_e is reduced by the long turnover time of C in the ecosystem. Cool mixed forests (7 and 9 in Fig. 4.5), and graminoid-forb tundra (22), have long residence times for ecosystem C because their ranges include cold, dry climates. BIOME4 integrates both climate and the structural resistance of the dominant PFT to decay (e.g. woody vs. herbaceous life-form) to approximate ecosystem turnover time. A single PFT may be dominant in several biomes, which also contributes to the differences between the means of Δ_{leaf} and Δ_e. In field studies where leaf and canopy measurements have been compared, Δ_e is typically 0-2‰ less than Δ_{leaf}; differential decomposition of isotopically distinct compounds in organic matter probably accounts for most of the variation [*Ehleringer et al.*, 2000; *Schmidt and Gleixner*, 1998]. Thus, scaling Δ from leaf to ecosystem is possible in most cases, except for those ecosystems with very long residence time for C, where additional isotopic fractionation is most likely to occur.

4.3.4 Agricultural land-use and global Δ_e

Δ_e simulated by BIOME4 with the agricultural land-use mask emphasizes the importance of C_4 crops in the temperate latitudes, especially in regions where the natural vegetation is forest (Fig. 4.6). The corn-growing regions of the central United States, northeastern China and the Western Mediterranean stand out. C_4 agriculture in sub-Saharan Africa also reduces the mean Δ_e relative to the natural vegetation. In high latitudes, the agricultural Δ_e is slightly higher than natural vegetation due to the influence of water-efficient and short-lived C_3 crops (Fig. 4.6). In the rest of the world, the agriculture-influenced Δ_e is lower than the value for natural vegetation from the widespread prevalence of C_4 crops. In all cases the agricul-

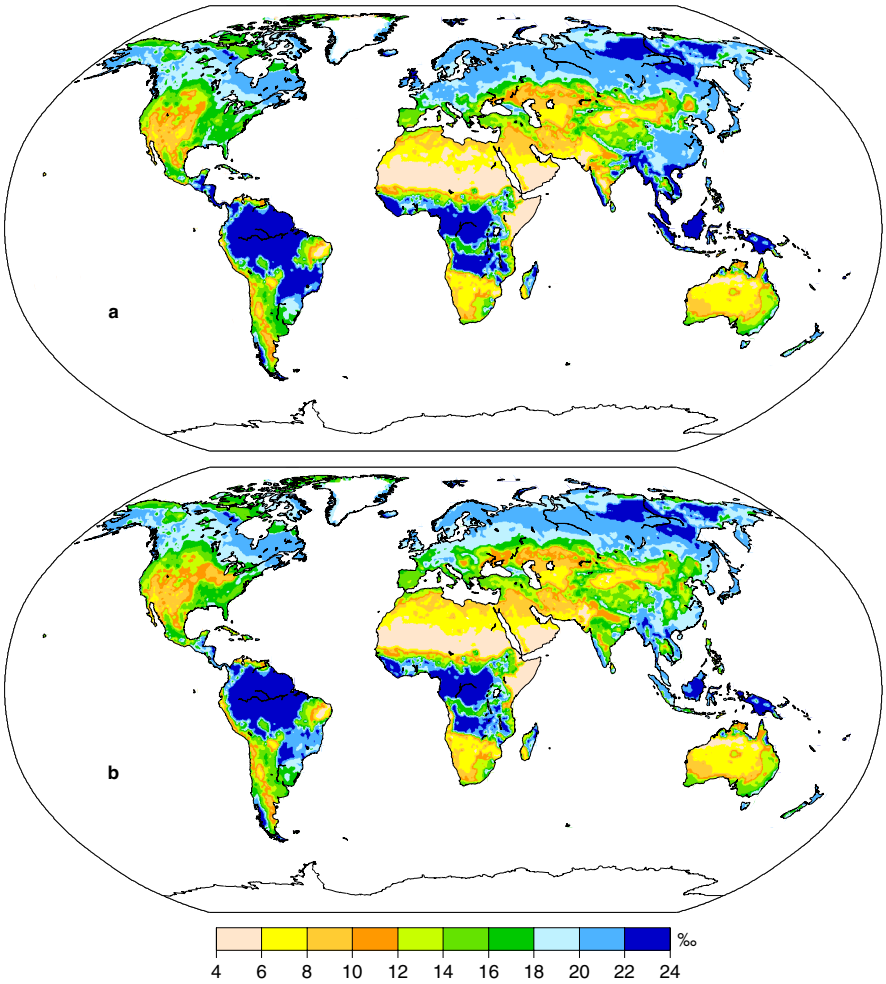

Fig. 4.6. Ecosystem discrimination simulated by BIOME4: **a** for potential natural vegetation, **b** including an agricultural land-use mask.

tural Δ_e is within 1 standard deviation around the mean value for Δ_e strictly from natural vegetation. Globally flux-weighted Δ_e decreased slightly with the addition of the agricultural land use mask, from 18.6‰ to 18.1‰.

Global (Fig. 4.6) and latitudinal (Fig. 4.7) patterns in Δ_e show that carbon isotope discrimination is heterogeneous and affected by agricultural land use. Other forms of land use, for example where forest has been converted to pasture in the tropics, may have a stronger effect on global Δ_e. Improved data sets on the nature and timing of land use and change are required before a more detailed assessment of land-use effects on Δ_e can be made.

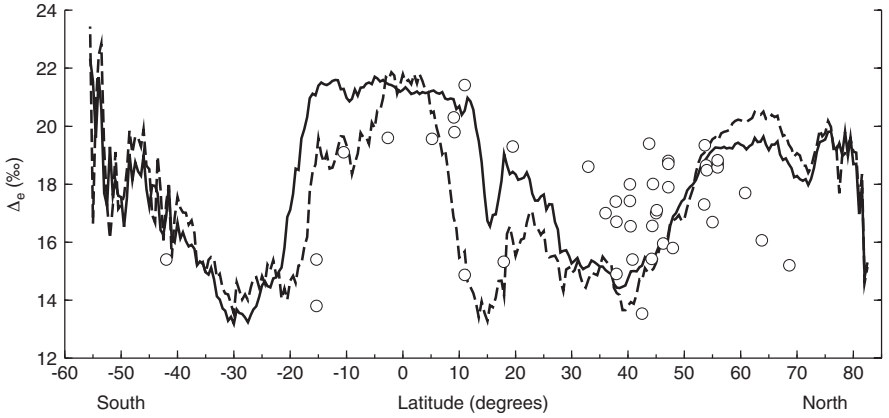

Fig. 4.7. Simulated flux-weighted latutidinal distribution of ecosystem discrimination with potential natural vegetation **solid line** and with the agricultural land-use mask **dashed line**. Open circles are measured canopy Δ_e values.

Bakwin et al. [1998], in their survey of mainly continental sampling locations, estimated a mean Δ_e for terrestrial ecosystems of 16.8‰. This value is smaller than the value of 18.1‰ we compute globally. The differences might be due to the influence of long-distance transport of CO_2 to the oceanic stations and to the omission of fossil fuel from our analysis. The modeled latitudinal gradient of $\delta^{13}C$ is somewhat steeper than that presented by Bakwin et al. [1998], but it is within the range both of canopy measurements and of the entire CMDL dataset. Our global flux-weighted model estimate of Δ_e is also 2-4‰ greater than values inferred from previous modeling studies by Fung et al. [1997] and Lloyd and Farquhar [1994]. Bakwin et al. [1998] suggested that these earlier modeling studies may not be supported by atmospheric observations. The Lloyd and Farquhar [1994] discrimination probably overemphasizes the importance of C_4 photosynthesis at mid-latitudes of the northern hemisphere, while the simulation of Fung et al. [1997] has a stronger latitudinal gradient than either this study or tropospheric measurements [*Bakwin et al.*, 1998].

4.3.5
^{13}C at the troposphere scale

Keeling plots for the six selected northern-hemisphere measuring stations show generally good agreement between modeled and measured CO_2 concentrations and ^{13}C ratios (Fig. 4.8). The y-intercept of the line fit to the Keeling plot data indicates the isotopic signature of the source CO_2; modeled and measured values compare reasonably well (Table 4.4). With decreasing latitude, the slope of the Keeling plot decreases and the inferred source $\delta^{13}C$ becomes slightly more positive. The influence of C_4 vegetation and increasing water stress cause the general enrichment with

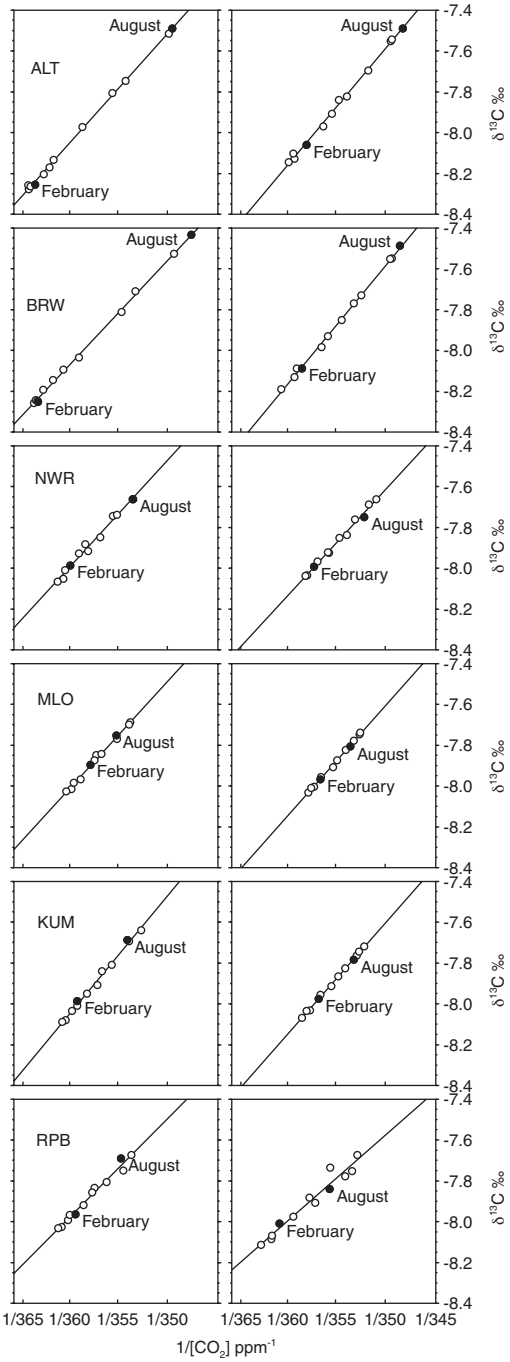

Fig. 4.8. Keeling plots of the measured **left column** and modeled **right column** CO_2 concentration and $\delta^{13}C$ at Northern Hemisphere free-troposphere measuring stations. See Table 4.1 for legend.

Table 4.4. Parameters for the best fit line used in Keeling plot analysis (Fig. 4.8)

Station	source	slope	SE of slope	intercept	SE of intercept	r^2
ALT	measured	6713	75.5	-26.70	0.21	0.999
	modeled	7170	123.6	-28.08	0.35	0.997
BRW	measured	6410	79.6	-25.87	0.22	0.998
	modeled	7275	107.5	-28.37	0.30	0.998
NWR	measured	6564	237.4	-26.23	0.66	0.987
	modeled	6536	190.4	-26.29	0.54	0.992
MLO	measured	6593	184.2	-26.32	0.52	0.992
	modeled	6779	112.5	-26.98	0.32	0.997
KUM	measured	7251	185.4	-28.19	0.52	0.993
	modeled	6834	108.3	-27.13	0.30	0.997
RPB	measured	6064	282.3	-24.82	0.79	0.979
	modeled	5283	363.1	-22.67	1.02	0.955

latitude. The seasonal cycle of CO_2 and $\delta^{13}C$ is less pronounced in lower latitudes, but for these stations (MLO, KUM, RPB) the fit of the trend line is still good as the stations integrate sources of CO_2 from wide regions [*Kaminski et al.*, 1996]. Niwot Ridge and Ragged Point have lower inferred $\delta^{13}C$ source signals compared to the other stations because their fetches integrate significant areas of C_4 vegetation from the interior plains of North America and the tropics, respectively. The seasonal trend is similar in the measured and modeled results for all stations.

At the highest latitudes (stations ALT and BRW), the intercepts of the Keeling plots are 2-3‰ more negative in the measurements than the model simulation indicates. At mid-latitudes the simulation fits the measured data more closely. Disagreement between the measured and modeled $\delta^{13}C$ may be caused by inaccuracies in the timing and magnitude of the modeled biosphere fluxes of both CO_2 and ^{13}C. However, the tracer transport and ocean models both add uncertainty to the final prediction of source $\delta^{13}C$. A sensitivity test suggests that the ocean $\delta^{13}C$, which is included in the modeled $\delta^{13}C$ and CO_2 of the troposphere, does not affect simulated y-intercept $\delta^{13}C$ at troposphere stations by more than ±0.5‰. Finally, in modeling $\delta^{13}C$ the impact of fossil fuel combustion was not included. Fossil fuel does not make a large contribution to the seasonal cycle of either CO_2 or $\delta^{13}C$ [*Heimann et al.*, 1998; *Heimann et al.*, 1989] but ignorning its seasonality could give rise to a small discrepancy between model and observations.

4.4 Conclusions

This study has provided a robust initial modeling platform for simulating the carbon isotopic composition of the biosphere. The model reproduces estimates of carbon isotope discrimination in a generally successful manner at three scales

representing processes from the leaf to the globe. More extensive information on the distribution and type of land use should add further power to such data-model comparisons. Future work will also incorporate the modeling framework into a dynamic global vegetation model (DGVM) [*Sitch*, 2000], capable of capturing the interannual variability in CO_2 and ^{13}C fluxes, which is central to current observationally-based analyses of the global C budget [*Bakwin et al.*, 1998; *Battle et al.*, 2000].

Acknowledgements. We thank M. Heimann for supplying the HAMOCC3 flux fields and W. Cramer for the 20th century climatology. S. Shafer, P.J. Bartlein, J.W. Williams and several others contributed to the development of BIOME4.

References

Bakwin, P.S., P.P. Tans, J.W.C. White, and R.J. Andres, Determination of the isotopic ($^{13}C/^{12}C$) discrimination by terrestrial biology from a global network of observations, *Global Biogeochemical Cycles*, *12* (3), 555-562, 1998.

Battle, M., M.L. Bender, P.P. Tans, J.W.C. White, J.T. Ellis, T. Conway, and R.J. Francey, Global carbon sinks and their variability inferred from atmospheric O_2 and $\delta^{13}C$, *Science*, *287* (5462), 2467-2470, 2000.

Bonal, D., D. Sabatier, P. Montpied, D. Tremeaux, and J.M. Guehl, Interspecific variability of $\delta^{13}C$ among trees in rainforests of French Guiana: functional groups and canopy integration, *Oecologia*, *124* (3), 454-468, 2000.

Bousquet, P., P. Peylin, P. Ciais, M. Ramonet, and P. Monfray, Inverse modeling of annual atmospheric CO_2 sources and sinks 2. Sensitivity study, *Journal of Geophysical Research-Atmospheres*, *104* (D21), 26179-26193, 1999.

Buchmann, N., R.J. Brooks, L.B. Flanagan, and J.R. Ehleringer, Carbon isotope discrimination of terrestrial ecosystems, in *Stable Isotopes*, edited by H. Griffiths, BIOS Scientific Publishers, Oxford, 1998.

Buchmann, N., and J.O. Kaplan, Carbon isotope discrimination of terrestrial ecosystems - how well do observed and modeled results match?, in *Global Biogeochemical Cycles in the Climate System*, edited by E.-D. Schulze, D.S. Schimel, and I.C. Prentice, Academic Press, in press.

Ciais, P., P.P. Tans, M. Trolier, J.W.C. White, and R.J. Francey, A large northern hemisphere terrestrial CO_2 sink indicated by the $^{13}C/^{12}C$ ratio of atmospheric CO_2, *Science*, *269* (5227), 1098-1102, 1995a.

Ciais, P., P.P. Tans, J.W.C. White, M. Trolier, R.J. Francey, J.A. Berry, D.R. Randall, P.J. Sellers, J.G. Collatz, and D.S. Schimel, Partitioning of ocean and land uptake of CO_2 as inferred by $\delta^{13}C$ measurements from the NOAA Climate Monitoring and Diagnostics Laboratory Global Air Sampling Network, *Journal of Geophysical Research-Atmospheres*, *100* (D3), 5051-5070, 1995b.

Conway, T.J., P.P. Tans, L.S. Waterman, K.W. Thoning, D.R. Kitzis, K.A. Masarie, and N. Zhang, Edivence for interannual variability of the carbon cycle from the National Oceanic and Atmospheric Administration/Climate Monitoring and Diagnostics Laboratory Global Air Sampling Network, *Journal of Geophysical Research-Atmospheres*, *99*, 22831-22855, 1994.

Ehleringer, J.R., Summary, in *Biosphere-Atmosphere Stable Isotope Network (BASIN) Workshop*, pp. 30, Snowbird, Utah, 1997.

Ehleringer, J.R., N. Buchmann, and L.B. Flanagan, Carbon and oxygen isotope ratios in belowground carbon-cycle processes, *Ecological Applications*, *10*, 412-422, 2000.

Ehleringer, J.R., Z.F. Lin, C.B. Field, G.C. Sun, and C.Y. Kuo, Leaf carbon isotope ratios of plants from a subtropical monsoon forest, *Oecologia*, *72*, 109-114, 1987.

FAO, Digital Soil Map of the World and Derived Soil Properties, Food and Agriculture Organization, Rome, 1995.

Farquhar, G.D., J.R. Ehleringer, and K.T. Hubick, Carbon isotope discrimination and photosynthesis, *Annual Review of Plant Physiology and Plant Molecular Biology*, *40*, 503-537, 1989.

Flanagan, L.B., and A.R. Ehleringer, Ecosystem-atmosphere CO_2 exchange: interpreting signals of change using stable isotope ratios, *Trends in Ecology & Evolution*, *13* (1), 10-14, 1998.

Foley, J.A., An equilibrium model of the terrestrial carbon budget, *Tellus Series B-Chemical and Physical Meteorology*, *47* (3), 310-319, 1995.

Francey, R.J., P.P. Tans, C.E. Allison, I.G. Enting, J.W.C. White, and M. Trolier, Changes in oceanic and terrestrial carbon uptake since 1982, *Nature*, *373*, 326-330, 1995.

Fung, I., C.B. Field, J.A. Berry, M.V. Thompson, J.T. Randerson, C.M. Malmstrom, P.M. Vitousek, G.J. Collatz, P.J. Sellers, D.A. Randall, A.S. Denning, F. Badeck, and J. John, Carbon 13 exchanges between the atmosphere and biosphere, *Global Biogeochemical Cycles*, *11* (4), 507-533, 1997.

Haxeltine, A., and I.C. Prentice, BIOME3: an equilibrium terrestrial biosphere model based on ecophysiological constraints, resource availability, and competition among plant functional types, *Global Biogeochemical Cycles*, *10* (4), 693-709, 1996.

Haxeltine, A., I.C. Prentice, and D.I. Creswell, A coupled carbon and water flux model to predict vegetation structure, *Journal of Vegetation Science*, *7* (5), 651-666, 1996.

Heimann, M., G. Esser, A. Haxeltine, J. Kaduk, D.W. Kicklighter, W. Knorr, G.H. Kohlmaier, A.D. McGuire, J. Melillo, B. Moore, III., R.D. Otto, I.C. Prentice, W. Sauf, A. Schloss, S. Sitch, U. Wittenberg, and G. WŸrth, Evaluation of terrestrial carbon cycle models through simulations of the cycle of atmospheric CO_2: first results of a model intercomparison study, *Global Biogeochemical Cycles*, *12* (1), 1 - 24, 1998.

Heimann, M., C.D. Keeling, and C.J. Tucker, A three dimensional model of atmospheric CO_2 transport based on observed winds: 3. Seasonal cycle and synoptic time scale variations, in *Aspects of Climate Variability in the Pacific and the Western Americas*, edited by D.H. Peterson, pp. 277-303, American Geophysical Union, Washington, D.C., 1989.

Jones, D.B., Oxford Economic Atlas of the World, pp. 239, Oxford University Press, Oxford, 1972.

Kaminski, T., R. Giering, and M. Heimann, Sensitivity of the seasonal cycle of CO_2 at remote monitoring stations with respect to seasonal surface exchange fluxes determined with the adjoint of an atmospheric transport model, *Physics and Chemistry of the Earth*, *21* (5-6), 457-462, 1996.

Kaplan, J.O., Geophysical Applications of Vegetation Modeling, Ph.D. Thesis, Lund University, Lund, 2001.

Keeling, C., The concentration and isotopic abundances of atmospheric carbon dioxide in rural areas, *Geochimicia Cosmochimicia Acta*, *13*, 322-334, 1958.

Keeling, C.D., The concentration and isotopic abundances of carbon dioxide in rural and marine air, *Geochimica et Cosmochimica Acta*, *24*, 277-298, 1961.

Keeling, C.D., W.G. Mook, and P.P. Tans, Recent Trends in the C-13-C-12 Ratio of Atmospheric Carbon- Dioxide, *Nature*, *277* (5692), 121-123, 1979.

Kloeppel, B.D., S.T. Gower, I.W. Treichel, and S. Kharuk, Foliar carbon isotope discrimination in *Larix* species and sympatric evergreen conifers: a global comparison, *Oecologia*, *114* (2), 153-159, 1998.

Körner, C., G.D. Farquhar, and Z. Roksandic, A global survey of carbon isotope discrimination in plants from high altitude, *Oecologia*, *74* (4), 623-632, 1988.

Körner, C., G.D. Farquhar, and S.C. Wong, Carbon isotope discrimination by plants follows latitudinal and altitudinal trends, *Oecologia*, *88* (1), 30-40, 1991.

Lavigne, M.B., M.G. Ryan, D.E. Anderson, D.D. Baldocchi, P.M. Crill, D.R. Fitzjarrald, M.L. Goulden, S.T. Gower, J.M. Massheder, J.H. McCaughey, M. Rayment, and R.G. Striegl, Comparing nocturnal eddy covariance measurements to estimates of ecosystem respiration made by scaling chamber measurements at six coniferous boreal sites, *Journal of Geophysical Research-Atmospheres*, *102* (D24), 28977-28985, 1997.

Leemans, R., and W.P. Cramer, The IIASA Database for Mean Monthly Values of Temperature, Precipitation, and Cloudiness on a Global Terrestrial Grid, pp. 62, International Institute for Applied Systems Analysis, Laxenberg, 1991.

Lloyd, J., and G.D. Farquhar, ^{13}C discrimination during CO_2 assimilation by the terrestrial biosphere, *Oecologia*, *99* (3-4), 201-215, 1994.

Lloyd, J., R.J. Francey, D. Mollicone, M.R. Raupach, A. Sogachev, A. Arneth, J.N. Byers, F.M. Kelliher, C. Rebmann, R. Valentini, S.-C. Wong, G. Bauer, and E.-D. Schulze, Vertical profiles, boundary layer budgets, and regional flux estimates for CO_2 and its $^{13}C/^{12}C$ ratio and for water

vapor above a forest/bog mosaic in central Siberia, *Global Biogeochemical Cycles*, in press.

Lloyd, J., and J.A. Taylor, On the temperature dependence of soil respiration, *Functional Ecology*, *8* (3), 315-323, 1994.

McGuire, A.D., S. Sitch, J.S. Clein, R. Dargaville, G. Esser, J. Foley, F. Joos, J.O. Kaplan, D.W. Kicklighter, R.A. Meier, J.M. Melillo, B. Moore, III., I.C. Prentice, R. Ramankutty, T. Reichenau, A. Schloss, H. Tian, L.J. Williams, and U. Wittenberg, Carbon balance of the terrestrial biosphere in the twentieth century: Analyses of CO_2, climate and land-use effects with four process-based ecosystem models, *Global Biogeochemical Cycles*, in press.

Ramankutty, N., and J.A. Foley, Estimating historical changes in global land cover: Croplands from 1700 to 1992, *Global Biogeochemical Cycles*, *13* (4), 997-1027, 1999.

Schmidt, H.-L., and G. Gleixner, Carbon isotope effects on key reactions in plant metabolism and ^{13}C-patterns in natural compounds, in *Stable Isotopes: Integration of Biological, Ecological and Geochemical Processes*, edited by H. Griffiths, pp. 13-26, BIOS Scientific Publishers, Oxford, 1998.

Sitch, S., The Role of Vegetation Dynamics in the Control of Atmospheric CO_2 Content, Ph.D. thesis, Lund University, Lund, 2000.

Six, K., and E. Maier-Reimer, Effects of plankton dynamics on seasonal carbon fluxes in an ocean general circulation model, *Global Biogeochemical Cycles*, *10* (4), 559-583, 1996.

Sternberg, L.S.L., A model to estimate carbon dioxide recycling in forests using $^{13}C/^{12}C$ ratios and concentrations of ambient carbion dioxide, *Agricultural and Forest Meteorology*, *48*, 163-173, 1989.

Tans, P.P., On Calculating the Transfer of C-13 in Reservoir Models of the Carbon-Cycle, *Tellus*, *32* (5), 464-469, 1980.

Tans, P.P., J.A. Berry, and R.F. Keeling, Oceanic C-13/C-12 Observations - a New Window on Ocean CO_2 Uptake, *Global Biogeochemical Cycles*, *7* (2), 353-368, 1993.

Trolier, M., J.W.C. White, P.P. Tans, K.A. Masarie, and P.A. Gemery, Monitoring the isotopic composition of atmospheric CO_2: measurements from the NOAA Global Air Sampling Network, *Journal of Geophysical Research-Atmospheres*, *101* (D20), 25897-25916, 1996.

Doctoral theses

published in the Department of Ecology, Plant Ecology, Lund University

1. Persson, Åke (1962). Mire and spring vegetation in an area north of lake Torneträsk, Torne Lappmark, Sweden.
2. Malmer, Nils (1962). Studies on mire vegetation in the archaean area of southwestern Götaland (South Sweden).
3. Mörnsjö, Tore (1969). Peatland studies in Scania, South Sweden.
4. Andersson, Folke (1970). An ecosystem approach to vegetation, environment and organic matter of a mixed woodland and meadow area.
5. Sonesson, Mats (1970). Ecological studies on poor mire vegetation in the Torneträsk area, Northern Sweden.
6. Nihlgård, Bengt (1970). Comparative studies on beech and planted spruce forest ecosystems in Southern Sweden.
7. Tyler, Germund (1971). Studies in the ecology of Baltic seashore meadows.
8. Olsson, Hans (1974). Studies on South Swedish sand vegetation.
9. Påhlsson, Lars (1974). Vegetation, microclimate and soil on slopes of some Scanian hills, southern Sweden.
10. Nylander, Carl-Erik (1975). Vegetationshistoria och vegetation i södra Bräkne-Hoby, Blekinge.
11. Nilsson, Ingvar (1977). Biogeochemical cycling and net primary production in forest ecosystems.
12. Kvillner, Ewa (1978). On the use of principal components and factor analysis in ecology.
13. Jensén, Sven (1978). Sampling methods and numerical treatments applied to a classification of lakes in Southern Sweden based on macrophyte composition.
14. Staaf, Håkan (1979). Decomposition and plant nutrient release from litter in two forest ecosystems.
15. Tyler, Carin (1979). Studies on Schoenus vegetation in South and Southeast Sweden.
16. Wallén, Bo (1980). Biomass, productivity and soil formation in early primary succession on sand dunes, S. Sweden.
17. Nicklasson, Allan (1980). Vattenståndets och markanvändningens inflytande på strand- och bottenvegetationen i sydsvenska oligotrofa sjöar.
18. Bringmark, Lage (1980). Processes controlling solutes in a pine forest soil.
19. Balsberg, Anna-Maj (1980). Studies in a *Filipendula ulmaria* L. meadow ecosystem and the effects of cadmium.
20. Magnusson, Magnus (1981). Composition and successions of bryophytes and lichens in a coastal dune area in southern Sweden.
21. Stjernquist, Ingrid (1982). Photosynthesis, growth and competitive ability of some coniferous forest mosses and the influence of herbicides and heavy metals (Cu, Zn).
22. Persson, Stefan (1982). Changes in vegetation, populations and environment during spontaneous successions in two plant communities in south Sweden.
23. Karlsson, Staffan (1982). Ecology of a deciduous and an evergreen dwarf shrub: *Vaccinium uliginosum* and *Vaccinium vitis-idaea* in subarctic Fennoscandia.
24. Folkeson, Lennart (1983). Heavy-metal pollution of forest ecosystems: effects on vegetation and mineralization of organic matter.
25. Olsson, Gunilla (1984). Old-field forest succession in the Swedish west coast archipelago.

26. Emanuelsson, Urban (1984). Ecological effects of grazing and trampling on mountain vegetation in northern Sweden.
27. Wiman, Bo (1985). Aerosol dynamics in coniferous forests - empirical and theoretical analyses.
28. Rörslett, Björn (1985). Regulation impact on submerged macrophyte communities in some Norwegian lakes.
29. Regnéll, Gösta (1986). Fen grassland in southern Sweden - the application of plant ecology to a problem of nature conservancy.
30. Wijk, Sture (1986). *Salix herbacea* and the alpine snow-bed environment.
31. Bergkvist, Bo (1986). Metal fluxes in spruce and beech forest ecosystems of South Sweden.
32. Svensson, Göran (1987). Studies on fossil plant communities, stratigraphy and development of peatlands in South Sweden.
33. Svensson, Brita (1987). Studies of the metapopulation dynamics of *Lycopodium annotium* and its microenvironment.
34. Hansen, Poul (1988). Statistical modeling of soil-macrofungal relationships in south Swedish beech forests.
35. Jonsdottir, Ingibjörg Svala (1989). The population dynamics, intraclonal physiology and grazing tolerance of *Carex bigelowii*.
36. Falkengren-Grerup, Ursula (1989). Soil acidification and vegetation changes in South Swedish forests.
37. Carlsson, Bengt Å. (1990). Controls on the growth and population dynamics of *Carex bigelowii*.
38. Berggren, Dan (1990). Species of Al, Cd, and Cu in forest soil solutions - analytical methods, mobilization mechanisms, and toxicity to plants.
39. Norden, Ullmar (1992). Soil acidification and element fluxes as related to tree species in deciduous forests of south Sweden.
40. Andersson, Maud E. (1993). Aluminium and hydrogen ions - limiting factors for growth and distribution of beech forest plants.
41. Bramryd, Torleif (1994). Effects on growth and nutrition of sewage sludge application in acid pine forests (Pinus sylvestris, L.) in a temperature gradient in Sweden.
42. Sonesson, L. Kerstin (1994). Regeneration ecology of oak, *Quercus robur* L. - influence of cotyledons and soil type on growth and nutrient uptake in seedlings.
43. Brunet, Jörg (1994). Importance of soil solution chemistry and land use to growth and distribution of four woodland grasses in south Sweden.
44. Magnusson, Sigurdur H. (1994). Plant colonization of eroded areas in Iceland.
45. Rosengren-Brinck, Ulrika (1994). The influence of nitrogen on the nutrient status of Norway spruce (*Picea abies* L. Karst).
46. Ljungström, Martin (1994). Beech (*Fagus sylvatica*) seedling growth and nutrition - effects of acid soils and liming.
47. Jonsson, Leif (1995). Effects of restoration on wooded meadows in southeastern Sweden.
48. Haxeltine, Alex (1996). Modelling the vegetation of the Earth.
49. Albinsson, Crister (1996). Vegetation structure and interactions on mires.
50. Thorén, Magnus (1998). Resource economy of carnivorous plants: Interactions between prey capture and plant performance in three subarctic *Pinguicula* species.
51. Berlin, Gudrun (1998). Semi-natural meadows in southern Sweden - changes over time and the relationship between nitrogen supply and management.
52. Gehrke, Carola (1998). Effects of enhanced ultraviolet-B radiation on subarctic ecosystems
53. Ström, Lena (1998). Organic acids in root exudates and soil solutions. Importance to calcicole and calcifuge behaviour of plants.

54. Linusson, Anna-Carin (1999). Changes in plant community diversity and management effects in semi-natural meadows in southern Sweden.
55. Williams, Lars-Erik (1999). Nutrient cycling in agroecosystems: nitrogen cycling in southern Sweden in the 1850s and two Tanzanian villages in the 1990s.
56. Kruuse af Verchou, Annika (1999). Reproductive strategies and liming responses in forest field-layer flora.
57. Fransson, Ann-Mari (2000). Soluble and plant available phosphorus in acid soils.
58. D'Hertefeldt, Tina (2000). Physiological integration and morphological plasticity in extensive clonal plants.
59. Zohlen, Angelika (2000). Iron nutrition dynamics. Differences between calcicole and calcifuge plants.
60. Sitch, Stephen (2000). The role of vegetation dynamics in the control of atmospheric CO_2 content.
61. Cowling, Sharon (2000). Plant-Climate interactions over historical and geological time.
62. Nilsson, Carin (2000). Hemiparasites in the Subarctic: Resource acquisition, growth and population dynamics.
63. Jönsson, Anna-Maria (2000). Bark lesions and sensitivity to frost in beech and Norway spruce.
64. Thelin, Gunnar (2000). Nutrient imbalance in Norway spruce.
65. Kaplan, Jed O. (2001). Geophysical applications of vegetation modeling.

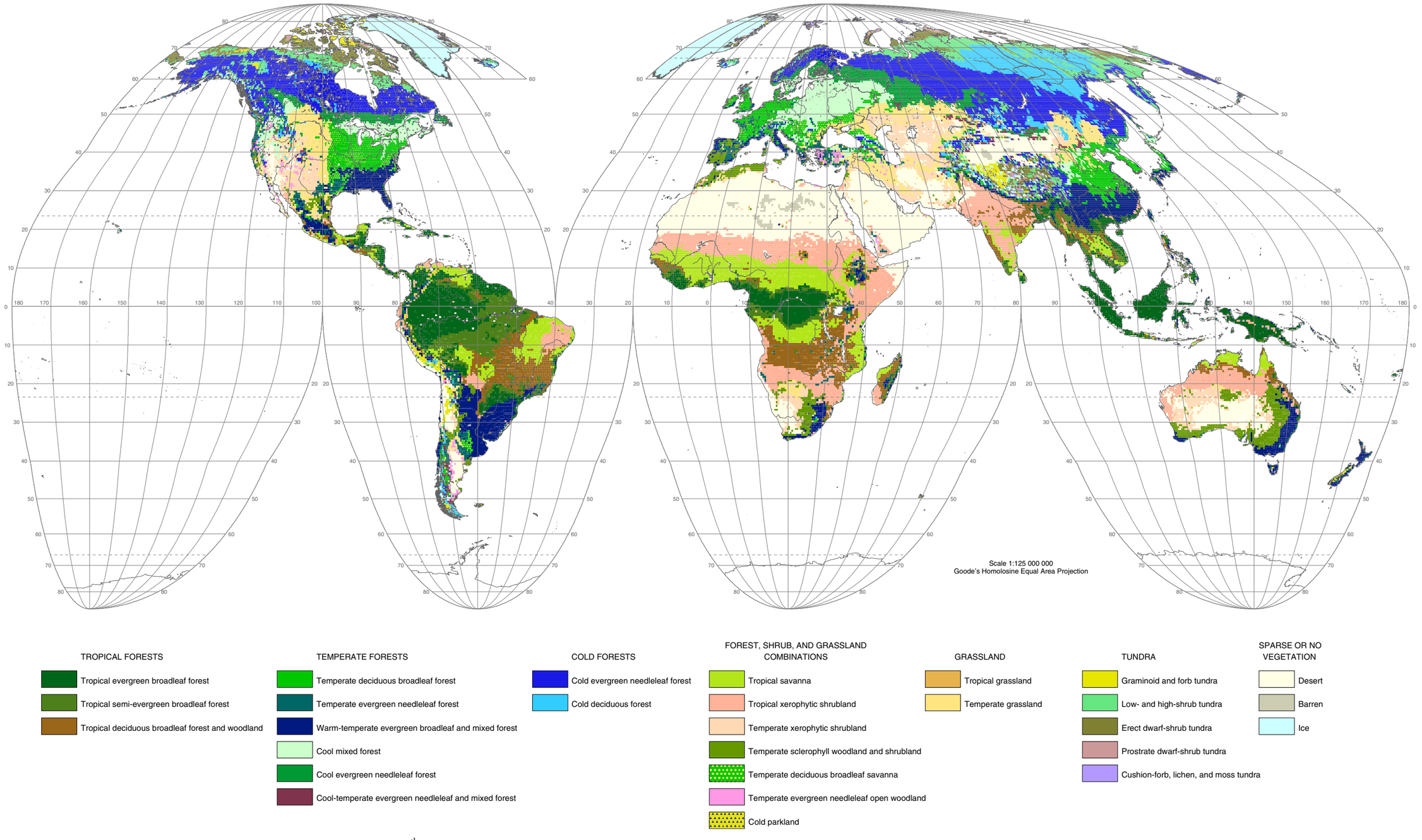

Fig. 1.2. Present-day potential natural vegetation simulated by BIOME4 using a late 20th century mean climatology [*W. Cramer* pers. comm.] and appropriate CO_2 concentration (324 ppm)